CR 166250

FINAL REPORT
ON THE
CALIBRATION OF THE AMES ANECHOIC FACILITY

PHASE 1: SHORT RANGE PLAN

DECEMBER 1980

CONTRACT NUMBER NASA 2215-4

PARTICIPATING JIAA STAFF

AMES RESEARCH CENTER
DAVID HICKEY
PAUL T. SODERMAN

STANFORD
K. KARAMCHETI
S. P. KOUTSOYANNIS
R. HOPKINS
B. MCLACHLAN

CONTENTS

ACKNOWLEDGEMENTS

Without the assistance of many people this project would have been difficult to accomplish. At AMES the support given by the electronic technician Mr. Art Silva and the aircraft mechanic Mr. Bill Douglas was greatly appreciated.

At Stanford appreciation goes to Mr. Vadim Matte and Mr. Gerry DeWerk of Stanford for their fabrication of mechanical components and other general assistance.

Thanks also go to Carolyn Edwards and Nikos Mourtos for their conscientious typing and putting together of this report.

Finally, a special thanks goes to electronic engineer of the J.I.A.A. Mr. Bill Janeway of Stanford. His help was crucial to the design and performance of the experiments.

INTRODUCTION AND FACILITY DESCRIPTION

This document summarizes and presents the results on a calibration of the NASA Ames open throat windtunnel facility. The scope of this project was outlined in the document "Proposed Calibration Studies of Ames Anechoic Facility" (December 5, 1978), which is included at the end of this progress report. Work was outlined there in terms of a Short Range Plan and a Long Range Plan. All work in this report pertains to the Short Range Plan, which includes six areas of research as follows:

I. Background Noise Levels
Measurements of 1/3 octave sound pressure levels have been made and the results are presented in Part A.

II. Determination Of Ideal Collector Position (acoustic)
For three different collector positions, 1/3 octave SPL measurements have been made at six different locations within the anechoic chamber. At each collector position, measurements were made for five different flow velocities. The results are presented in Part A.

III. Noise Contours In The Test Chamber
Testing has been completed and all data has been recorded on tape. Software for data analysis has been designed and tested, but need minor refinement prior to being used. The results are presented in Part A. The preliminary computer program is included in Part E.

IV. Hot Wire Calibration
A procedure for calibrating the DISA brand hot wire anemometer has been developed, and is presented in Part B.

V. Hot Wire Measurements
Measurements to determine the fluid properties of the jet have been made using a pitot tube and hot wire anenometer. The results are presented in Part B.

VI. Preliminary Selected Experiments With A Suitable Sound Source
Little work has been done in this area.

The facility being calibrated is an open throat acoustic windtunnel operated by the NASA Ames Research Center in Mountain View, California. It is located on the ground floor of the 40'x80' windtunnel building. FIGURE 1 shows the general configuration of the windtunnel components. The relationship between nozzle exit mach number and blower RPM is shown in FIGURE 2. Nozzle pressure ratio is also plotted as a function of blower RPM in FIGURE 3. The 4 inch diameter nozzle was used for all measurements discussed in this report.

The anechoic chamber surrounding the throat section is lined with foam wedges which are 8 inches across the base and 25 inches along the perpendicular. Inside room dimensions are 25 feet X 18 feet X 11 feet high (wedge tip to wedge tip). Metal grates have been installed above most of the floor wedges to support portable microphone stands, a microphone traversing mechanism, and personnel walking inside the chamber. Foam blankets 3 inches thick were laid on these grating to reduce their acoustic relections. Without the gratings and foam blankets, the lower cutoff frequency of the anechoic chamber has been found to be aorund 150 Hz.

The experiments were done during the period Summer 1978 to Fall 1979 and they were under the general guidance and supervision of Professor K. Karamcheti, Dept. of Aeronautics-Astronautics, Stanford University and Director of the Joint Institute for Aeronautics and Acoustics, and Mr. David Hickey of the Ames Research Center. The planning and day by day follow-up and decision making on the various phases of the work was espoused by Mr. Paul Soderman of the Ames Research Center and Professor S. P. Koutsoyannis of the Dept. of Aeronautics-Astronautics, Stanford University and member of the J.I.A.A. The experiments, data acquisiton and the write-up of the relevant results and conclusion with brief interpretations (wherever appropriate) has been the responsibility of Mr. Richard Hopkins (responsible for the Acoustic Measurements and the Preliminary Computer Programming for the DAS System at Ames) and Mr. Blair McLachlan, (responsible for the Aerodynamic Measurements both of which have been graduate students at the Department of Aeronautics-Astronautics, Stanford University and supported by the J.I.A.A. Finally from both the Ames Research Center as well as from Stanford and the J.I.A.A., there has been substantial help from supporting personnel (Mr. Vadim Matte, Mr. W. Janeway from the J.I.A.A. and Mr. Art Silva and Bill Douglas from Ames) and due credit is given in the acknowledgement section.

The present report on the studies performed under the Short Range Plan in summary contains the following parts:

A. ACOUSTIC MEASUREMENTS

I. BACKGROUND NOISE LEVELS

II. IDEAL COLLECTOR POSITION

III. ANECHOIC CHAMBER NOISE CONTOURS WITH THE 4" DIAMETER NOZZLE

LIST OF FIGURES

LIST OF FIGURES

LIST OF FIGURES

I. BACKGROUND NOISE LEVELS

Background noise levels inside the anechoic facility were measured at the two locations shown in FIGURE 4. FIGURES 6 and 7 show these levels for the following operating conditions:

1. with 40'X 80' windtunnel operating (91 dB linear)

2. with the nearby air compressor operating (72 dB linear)

3. with no noisy external equipment operating (67 dB linear)

The main path by which sound enters the chamber from ouside is through the 3 ft. diameter exhaust duct, shown in FIGURE 1. With no flow in the tunnel, conversations over the office paging system are clearly audible when standing near the jet's nozzle. Operation of the 40'X 80' windtunnel are felt (and heard) as a very low frequency vibration. Testing in the 40'X 80' of full scale jet engines caused noise levels inside the test chamber to increase considerably over those shown here.

Combining these observations with the spectra of FIGURES 6 and 7, the following conclusions can be drawn:

1. The anechoic chamber is fairly well insulated from exterior noise for frequencies above 150 Hz. Recall that this is the design cut-off frequency of this room.

2. Operation of the nearby shop air compressor will not effect jet noise measurements for frequencies above 100 Hz.

3. Operation of the 40' X80' windtunnel will significantly impact low velocity jet noise measurements at frequencies below 500 Hz. It is recommended that the acoustic windtunnel facility not be operated when the 40' X80' is in use.

Instrumentation used to measure overall and 1/3 octave sound pressure levels is listed in FIGURE 5. Measurements made with the portable sound level meter were found to be about 6-10 dB lower than those made using the main acoustic instrumentation system. As is shown in FIGURE 8, the B&K type 4133 microphone with type 2619 preamplifier is linear down to 45 dB. This suggests that the electrical noise floor of the instrumentation system is above the signal level of the microphone when measuring very low noise levels.

When the Gen-Rad real time analyzer was replaced with a B&K type 3347/3348 analyzer, nearly identical background levels were measured. This suggests that the electrical noise is from either the microphone conditioning amplifier, the differential amplifier, or both. All background noise levels reported here were made with the portable sound level meter. Note from FIGURE 8 that the specified minimum noise level for this meter is 37 dB.

II. DETERMINATION OF IDEAL COLLECTOR POSITION

The effect of different collector locations on far field sound levels was investigated at several jet velocities. This was done using the microphone array shown in FIGURE 9. All microphone heights were set to the horizontal plane of the nozzle centerline. For a fixed collector position, jet noise was recorded at several different jet velocities. The collector position was then changed, and the measurements repeated. The different test conditions are summarized below.

TEST 1. Collector is 4 feet from nozzle exit
RPM = 3000, 6000, 7000, 8000
Mach NO = 0.24, 0.48, 0.56, 0.64

TEST 2. Collector is 7 feet from nozzle exit
RPM = 3000, 6000, 8000, 10,000, 12,000
Mach No = 0.24, 0.48, 0.64, 0.80, 0.96

TEST 3. Collector is 10 feet from nozzle exit; fully retracted
RPM = 3000, 6000, 8000 10,000, 12,000
Mach No = 0.24, 0.48, 0.64, 0.80, 0.96

The instrumentation used for these measurements is listed in FIGURE 10 and diagramed in FIGURE 11. Because data was recorded on tape for later analysis, it is important to keep track of the amplifier gains used during recording. These are reported in FIGURE 12.

The contribution of low frequency jet noise to the overall sound pressure level is shown in FIGURE 13. This table compares the unfiltered SPL ($20 < f < 20,000$ Hz) to the level obtained by high pass filtering the measured signal at the 100 Hz 1/3 octave band ($100 < f < 20,000$ Hz). It is seen that the low frequencies can raise the overall sound level by as much as 20 dB at low mach numbers, but by only 0.5 dB at higher mach numbers. This is attributed to the decrease in anechoic performance of the chamber itself. That is, the absorption of sound inside the room is poor below the cut-off frequency of around 150 Hz. Because of this low freqeucy influence, all overall sound levels reported here have been calculated to include only 1/3 octave bands of 100 Hz and above. This will provide a better correlation between the SPL value and what the jet is really doing aerodynamically.

For the six microphone positions evaluated, the relationship between the jet's mean velocity and overall SPL is shown in FIGURE 14. To show effects of collector position and jet velocity on noise levels, average 1/3 octave band spectrums are shown in FIGURES 15 through 20 for each microphone location (8 sec. analyzer integration). A careful comparison of these figures reveals that both collector position and jet speed do influence far field sound levels. The details are summarized below:

EFFECTS OF COLLECTOR POSITION

1. For low and mid frequencies, changing collector position can have a small effect on both near and far field sound levels. This occurs at the closest collector position, 4 feet from the nozzle. Here a small decrease occurs (2.5 dB) in the 250-1250 Hz 1/3 octave band levels. Near field microphone #5 and far field microphone #4 show the effect most noticably. Recall that these two microphones are the farthest downstream. The effect is seen to decrease as one moves upstream, and at microphones #1 and #6, the change can not be seen. This difference in mid frequencies is attributed to the enclosing of part of the jet flow by the collector as it is moved closer to the nozzle. Consequently, noise generated by the large scale turbulent structures in the downstream portion of the jet are shielded by the collector, and prevented from reaching the downstream microphones. The postulate that noise from the downstream portion of the jet is predominately low frequency, while high frequency noise is generated near the nozzle, is supported by FIGURE 21. This figure compares the spectrum of the two nearfield microphones when the collector is fully retracted to avoid any shielding. This figure shows there is considerably more energy below 1000 Hz at downstream microphone position #5.

2. When the collector is moved to the fully retracted position (10 feet from nozzle), a 400 Hz spike is measured at the upstream microphones. This peak is most noticable at microphone position #1, and decreases in amplitude as one moves downstream. It is almost indistinguishable at microphone positions #3. The peak can not be detected with either of the near field microphones. One possible explaination is that this is a reflection off of the bell ending of the collector. However, insufficient data exists to verify or refute this postulate.

3. When the collector is moved to the fully retracted position, the far field microphones measure a considerable increase at the high frequencies. Althought this effect is less noticable at microphone #3, the increase begins at 4000 Hz and increases smoothly to 5-15 dB at 20,000 Hz. In the near field, the upstream microphone is completely uneffected by collector position. But the downstream near field microphone (#5) shows a slight increase in level above 12,500 Hz.

To get a better understanding of this phenomena, data from far field microphone #4 was analyzed with a narrow band spectrum analyzer. FIGURES 22 through 26 show spectrums at four different jet speeds with the collector fully retracted. One sees the same effect as with 1/3 octave band analysis. In all cases, the spectrum levels begin increasing smoothly above 4000 Hz. Also, there is no evidence of any pure tones between 1000-20,000 Hz. For the same microphone, but with the collector located 7 feet from the nozzle, a typical spectrum is shown in FIGURE 27. Here the sound level decreases constantly with increasing frequency. Narrow band spectrums for the two near field microphones are shown in FIGURES 28 and 29.

There is currently insuffecient data to determine the cause of this problem, but several possible mechanisms are: (1) new high frequency sound sources are being uncovered when the collector is moved to the fully retracted position; (2) the jet has grown enough to cause scrubbing against the collector's inner walls or bell; (3) the noise is associated with recirculating air currents along the bell, as discussed next.

4. While visiting several similiar commercial facilities, it was observed that large amounts of outside air are vented into their test chambers to prevent excessive air circulation. This movement is created as the jet entrains air from outside the boundry layer. To see if this condition existed in this faciltiy, a multitude of tufts were taped along the inside of the collector duct. Also, a probe with tufts attached along its length was used to explore the direction of air flow in the region of the collector. It was found that tufts along the wall indicated fluid flow upstream towards the nozzle. This occured even as far as 6 feet into the collector. This indicates that a recirculation region does exist for almost all jet speeds, and is especially prevalent at higher velocities. The flow of air back out of the collector can be easily felt by placing ones hand near the surface of the collector bell. A negative pressure was measured inside the room whenever the jet was operating, which also increased with jet speed. This is shown in FIGURE 30. Opening the main door to the test chamber allows additional air to vent into the room. This alleviates the condition only slightly, while degrading the acoustic

transmission loss of the chamber considerably. It is unknown if this problem exists at other collector positions.

EFFECTS OF JET FLOW VELOCITY

A relaionship between the mean fluid velocity and noise spectrum of the jet is given by the Strouhal number:

$$S = D\ fs\ /\ u$$

where D = nozzle diameter = 4 inches
fs = Strouhal frequency
u = mean jet velocity

Letting the Strouhal frequency correspond to the 1/3 octave band with the highest noise spectrum, one finds that the jet follows this relationship quite well. As the velocity is doubled from .24 to .48 to .96, the Strouhal frequency also doubles from 125 Hz to 250 Hz to 500 Hz. This is shown in FIGURE 21 for the two near field microphones.

Based on the above findings, it seems the best collector position is 7 feet from the nozzle exit. This position avoids the first 3 problems mentioned above. Correlation between near and far field spectrums for this position is also quite good. This is shown in FIGURE 31, which compares spectrums measured with near field microphone #6 and far field microphone #2. Both lie on a line perpendicular to the nozzle exit.

Not with standing the above comments, the collector was left in the fully retracted position for all further measurements. The distance between the nozzle and the collector is thus at its maximum. Although this position introduces several problems, it minimizes defraction and shielding effects by the collector while determining jet noise contours.

III. NOISE CONTOURS IN TEST CHAMBER

A major objective of this study is the mapping of jet noise contours inside the test chamber. Lines of constant sound pressure level are to be determined for jet velocities of mach number 0.24, 0.48, and 0.80 . Data has now been recorded for all three velocities and recorded on magnetic tape for later analysis. Measurements were made by traversing a microphone away from the jet while continually recording the acoustic signal. So that the position of the microphone along the traverse will always be known, the traversing mechanism has been designed to output a DC voltage which varies linearly with position from 0.1 to 1.0 volts. This voltage was recorded simultaneously on tape with the acoustic signal. Traverses were made perpendicular to the jet flow along the six different paths shown in FIGURE 32. The instrumentation used to record and analyze the acoustic data is listed in FIGURE 33 and diagramed in FIGURE 34.

Overall and 1/3 octave band sound pressure levels will be obtained by processing the recorded data on the Ames DAS computer. A software package to do this analysis has already been implemented. The output from the current revision of this program is a plot showing decay of SPL with distance along the traverse path. Sample outputs are shown in FIGURE 38 (overall SPL) and FIGURE 39 (500 Hz SPL). The complete output for a single microphone traverse consists of an overall and 23 1/3 octave band decay curves. The acoustic analyzer integration time was 1 second, which corresponds to integrating the acoustic signal along 3.2 inches of traverse. Noise contours inside the test chamber can be mapped using the decay curves from all six traverses to plot lines of constant SPL. FIGURES 35-37 show contours for the overall, 500 Hz, and 5000 Hz 1/3 octave bands. These contours are for a jet velocity of mach number 0.80 .

The current revision of the software package has several deficiencies. Problems associated with the sampling logic result in decay curves that differ, depending on which direction the microphone is traversing. That is, the maximum and minimum levels measured are different when the traverse is from near to far field than vise-versa. This difference can be seen by comparing FIGURES 39 and 40. To correct this problem, the following improvements are offered:

1. Turn on the General Radio analyzer immediately, but save only the current sample until a change in the DC voltage threshold is detected. This sample would then become the first one in the storage array. The array would begin filling, starting with I=2, once the change has been detected.

2. Continue sampling the [illegible] voltage, but now use a 0.3 second sampling time until three consequitive samples of the opposite threshold voltage are measured. The last acoustic sample obtained would then be stored, and sampling stopped. This would replace the current method of taking 51 samples corresponding to the 63 second traverse time.

3. Before executing the routine which determines a distance for each integer SPL value, the decay curve should be smoothed twice with a 3 point moving smoother. This would correspond to flairing a smooth curve through the data before trying to assign a location to a specified level. The present method results in bad values due to small deviations in the decay curve. This jitter is associated with the random characteristic of the jet noise. This second curve could also be plotted, say 10 dB above the unsmoothed curve.

It is expected that these modifications to the current program will provide results of suffecient accuracy. However, another checkout of the program should be performed to verify this. Once corrected, processing of the data and plotting of the contours would be able to proceed rapidy. Once these contours are plotted, work in the Long Term Plan could be addressed.

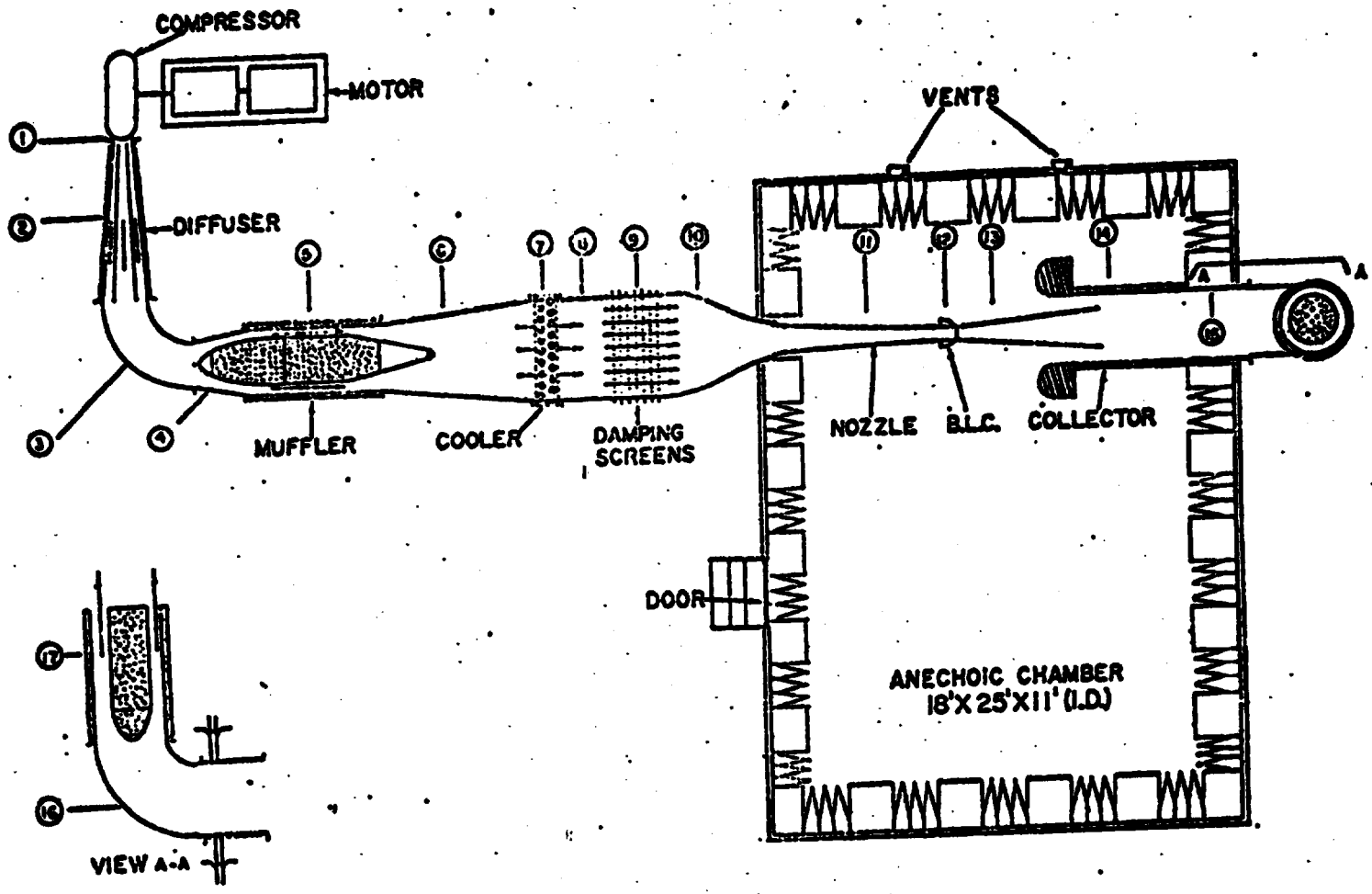

Figure A-1 - General arrangement of anechoic open-throat wind tunnel.

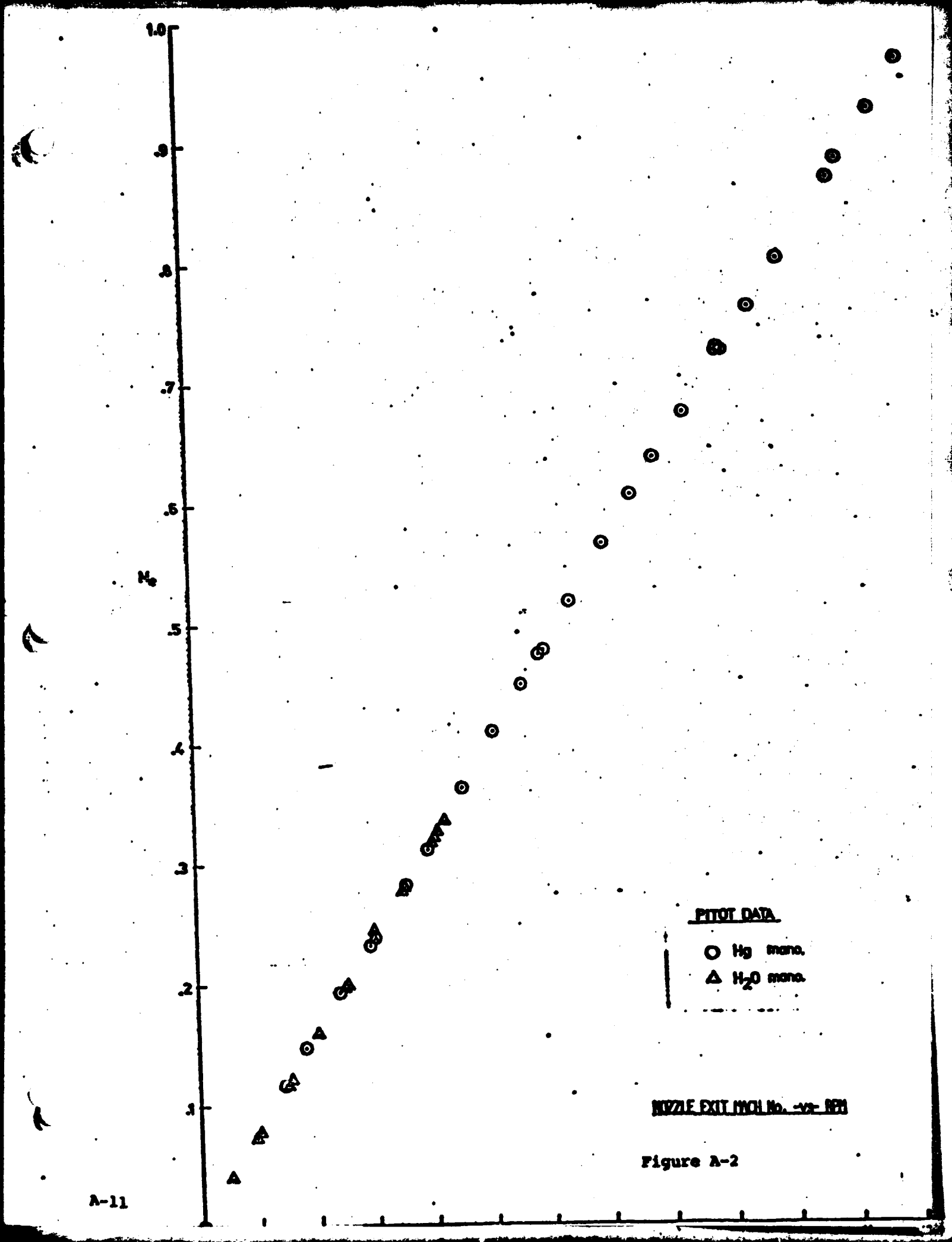
1.0
.9
.8
.7
.6
.5
.4
.3
.2
.1
M_e
PITOT DATA
Hg mano.
H_2O mano.
NOZZLE EXIT MACH No. -vs- RPM

Figure A-2

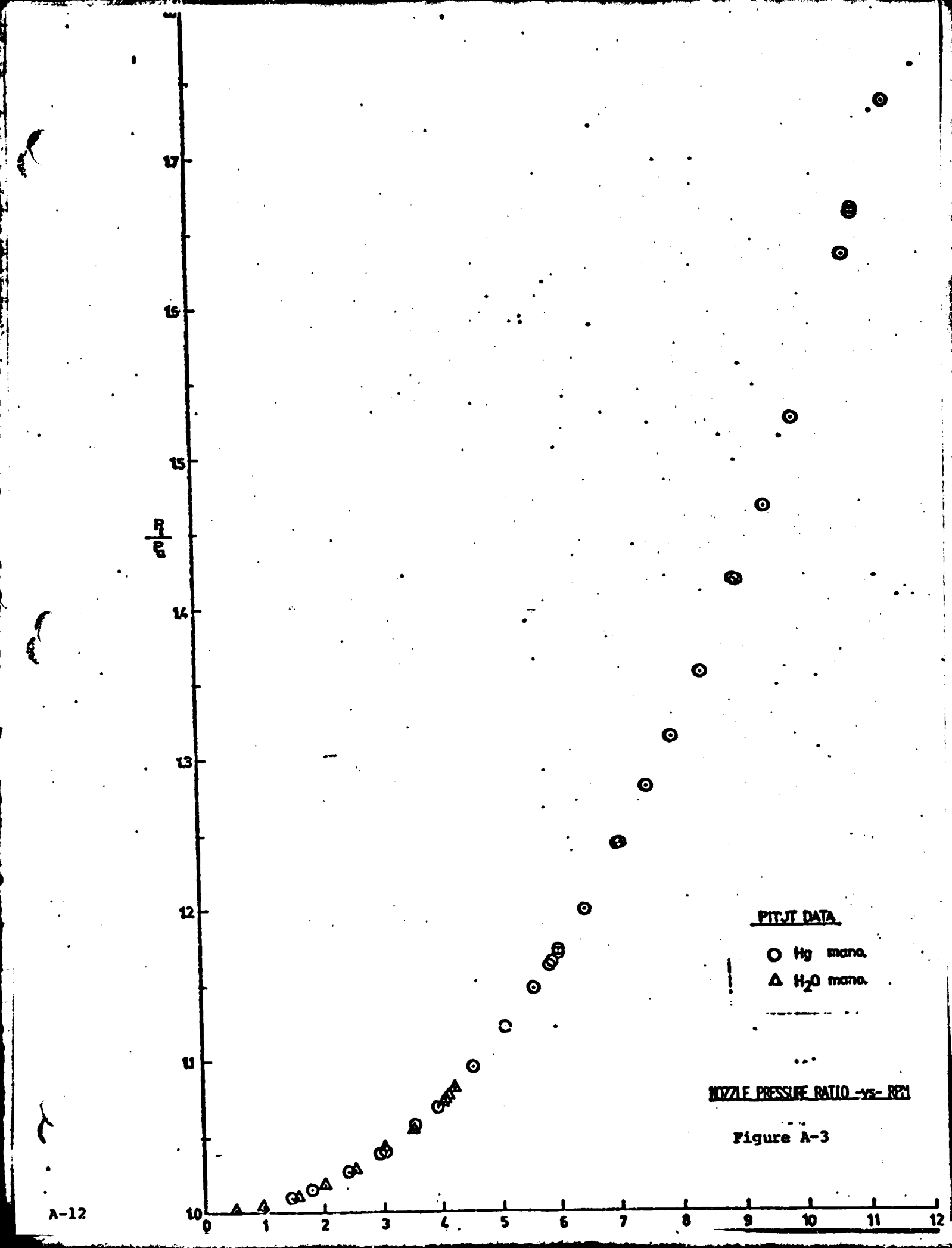
17
16
15
$\frac{P_1}{P_0}$
14
13
12
11
10
0
1
2
3
4
5
6
7
8
9
10
11
12
PITOT DATA
Hg mano.
H_2O mano.
NOZZLE PRESSURE RATIO -vs- RPM

Figure A-3

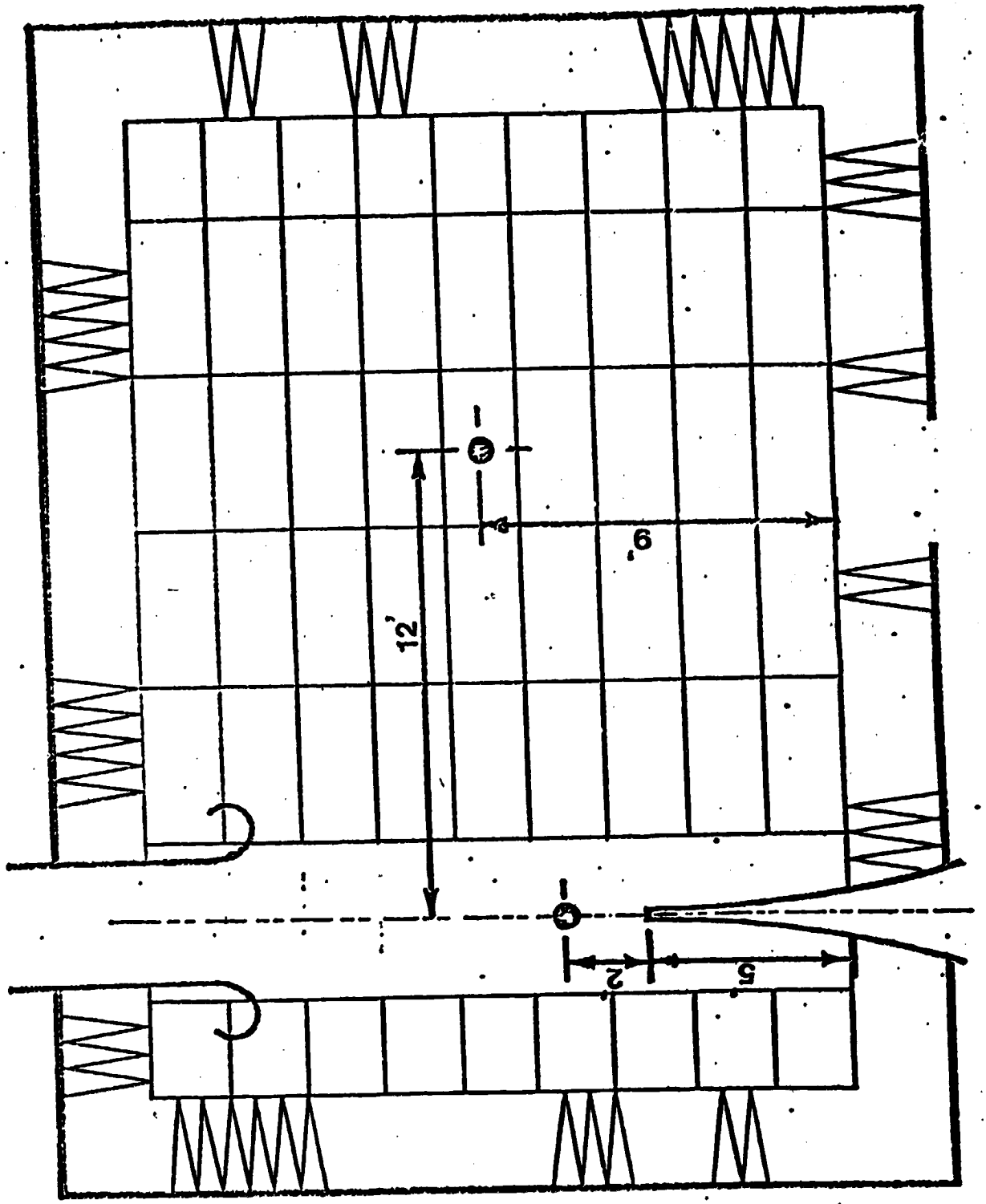

MICROPHONE LOCATIONS FOR MEASURING

INSTRUMENTATION LIST FOR MEASURING BACKGROUND NOISE LEVELS

	(NASA NO.)
1/2" microphone; B&K type 4133	
microphone conditioner; B&K type 222-2	(26479)
microphone conditioner multiplexer; B&K 221-3	(26479)
differential amplifier; Textronics AM502	(52476)
Real Time Specturm Analyzers:	
Gen-Rad model 1995 1/3 octave bands	(57330)
Portable sound level meter; B&K type 2209 w/ 1/2" microphone; B&K type 4133	(90479)
Portable 1/3 octave band filter set; B&K type 1616	(90456)

Figure A-5

BACKGROUND NOISE LEVEL ON JET AXIS

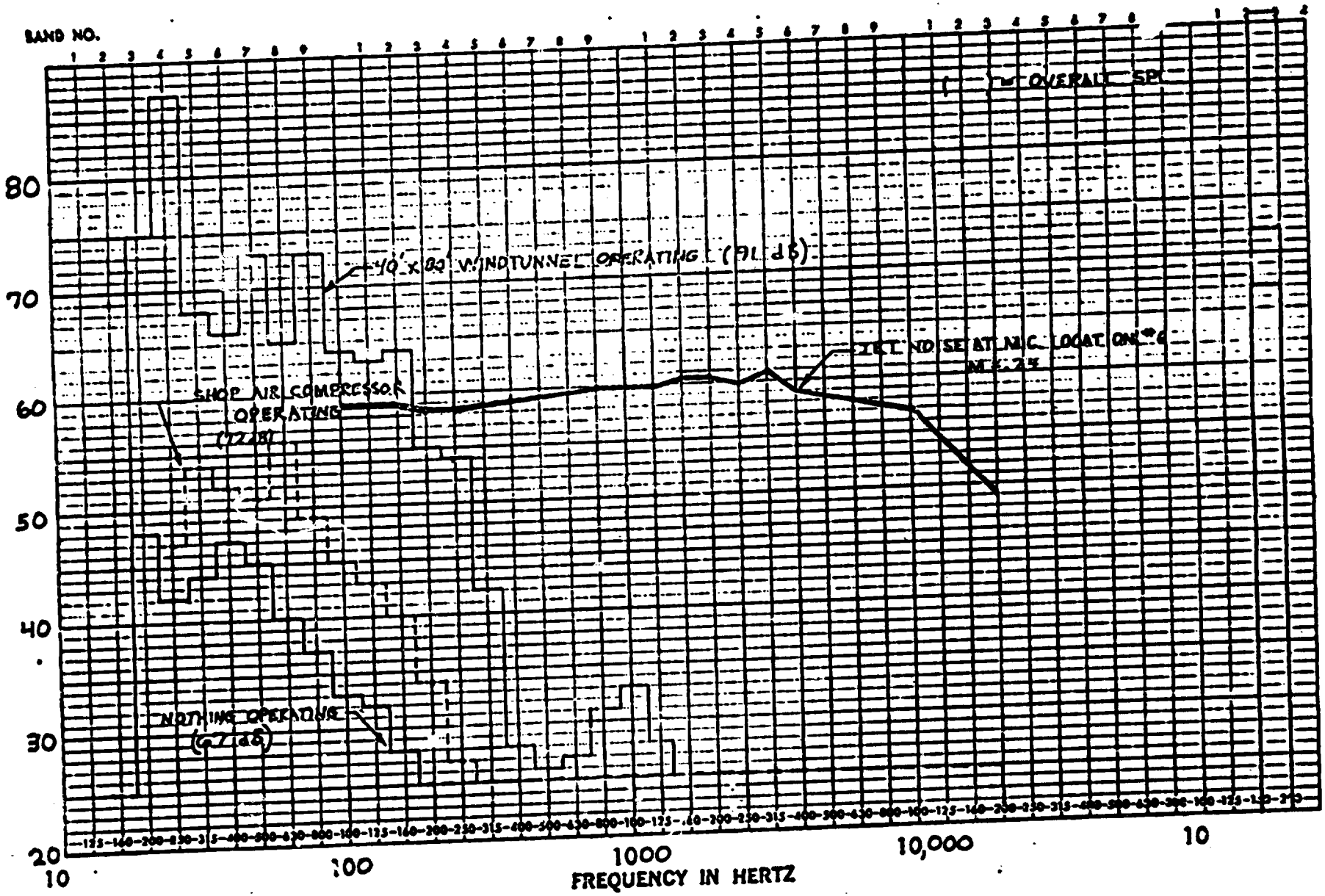

Figure A-6

BACKGROUND NOISE LEVEL AT ROOM CENTER

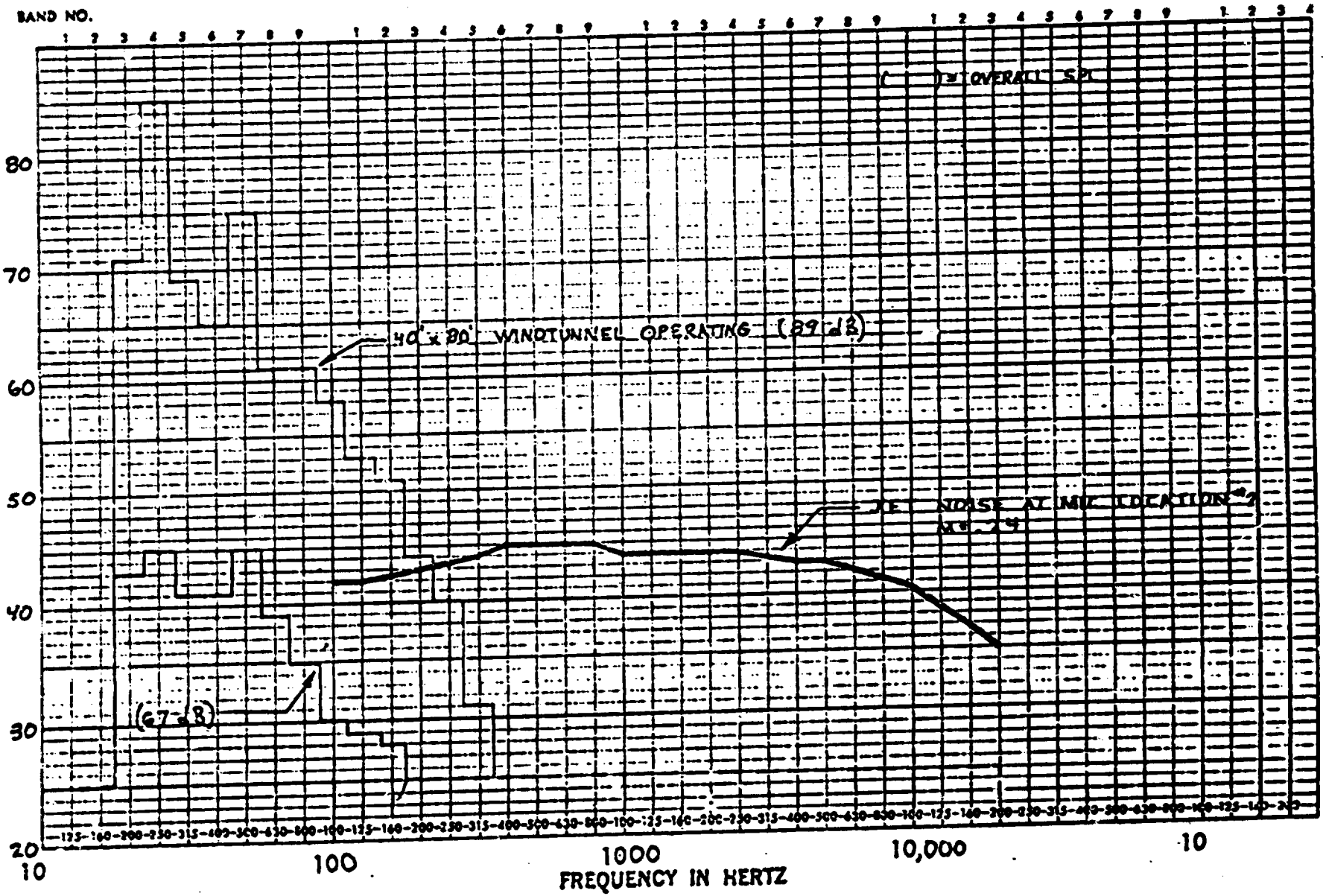

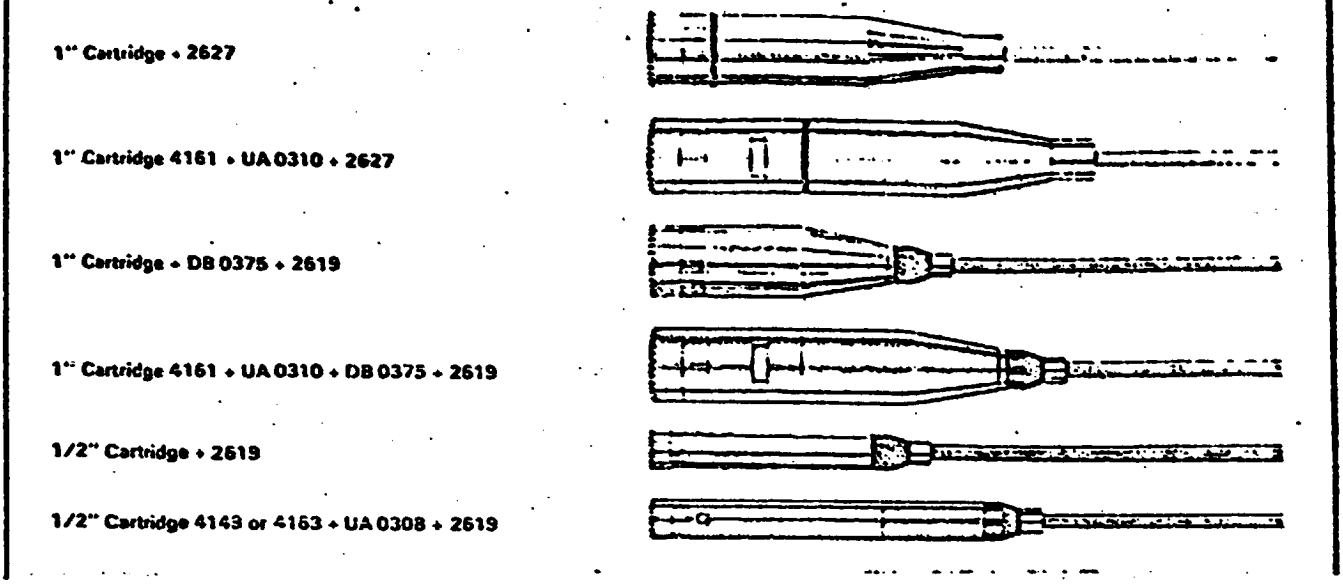

Specifications 2209

(Specifications refer to 2209 with Extension Rod UA 0196 and Microphone 4165, unless otherwise stated)

Measuring Ranges:

Microphone Type No.	Max. Level (dB)	Minimum Level (dB)										
		Weighting Network					External Filter Type No.					
							1613 (Octave)			1616 (1/3 Octave)		
		D	A	B	C	Lin	31.5 — 63 Hz	125 — 250 Hz	0.5 — 16 (31.5) kHz	20 — 400 Hz	0.5 — 16 (40) kHz	Lin
1/2"	4144 — 4145	140	25	18	22	24	36	23	18	15	17	17	28
1/2"	4165* — 4166	140	34	24	28	34	42	33	28	22	25	19	32
1/2"	4133 — 4134	150	45	35	40	46	55	45	40	34	37	31	44

* Included in 2209

Frequency Response: (Microphone)*
(zero degree incidence, free-field)
±1 dB: 4 Hz to 12.5 kHz
±2 dB: 3 Hz to 20 kHz
*) individually calibrated
(see also curves Figs. 7 and 8)

Frequency Response: (Amplifier)
±0.5 dB: 5 Hz (20 Hz) to 30 kHz
±1 dB: 2 Hz (10 Hz) to 70 kHz
(Figures in parantheses obtainable by switch in input stage)

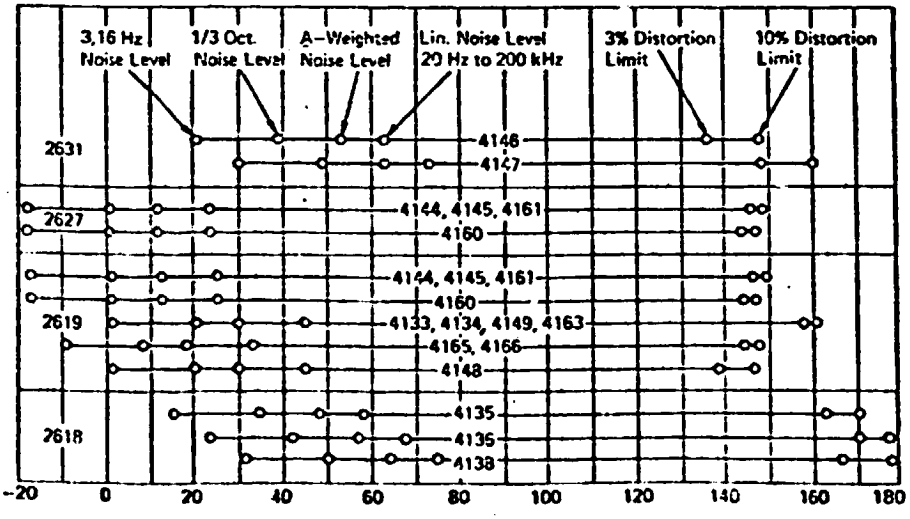

Fig. 13. Dynamic ranges of B & K Microphone Preamplifiers (except 2642) and the Carrier System 2631 with different microphones. The upper limit is indicated for two degrees of distortion while the lower limit is given for various bandwidths of the measuring equipment. The limits for 3,16 Hz and 1/3 octave bandwidth is valid at 1000 Hz only

to the Western Electric condenser microphone WE 640A. The front cavity of the microphone is tested for hydrogen leakage. The 4160 is included with the Reciprocity Calibration Apparatus Type 4143.

Preamplifiers

The microphones are designed for use with a DC polarization voltage of 200V (28V for 4148) or with a 10 MHz carrier frequency. A microphone assembly will consist of a microphone cartridge and a preamplifier, when using the DC polarization voltage, and of the 10 MHz Carrier Frequency System Type 2631 and a cartridge when using the carrier frequency.

The cartridges screw directly onto the preamplifier housing or the

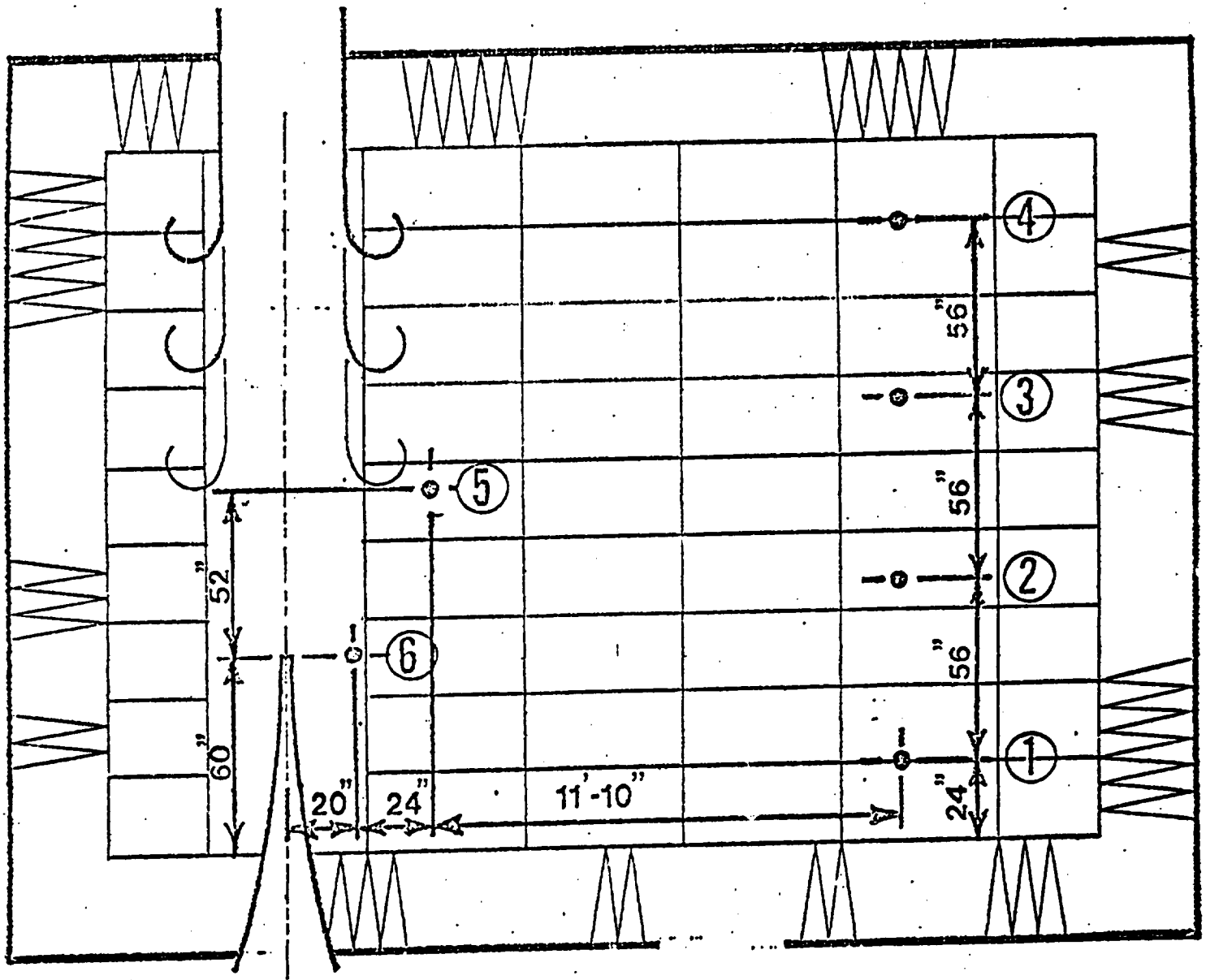

○ = MICROPHONE POSITION NO.

MICROPHONE LOCATIONS FOR DETERMINING EFFECT OF COLLECTOR LENGTH ON SOUND PRESSURE FIELD

Figure A-9

INSTRUMENTATION LIST FOR DETERMINING EFFECTS OF COLLECTOR LENGTH ON THE SOUND PRESSURE FIELD

	(NASA NO.)
1/2" microphone; B&K type 4133	
microphone conditioner; B&K type 222-2	(26479)
microphone conditioner multiplexer; B&K type 221-3	(26479)
differential amplifier; Textronics AM502	(52476)
multichannel tape recorder; Ampex FR1300	(44583) (90386)
RMS volt meter, Hewlett-Packard	(45554)
Oscilloscope; Textronics type 551 with type 1A7A amplifiers	(Stanford)
Real Time Spectrum Analyzers:	
B&K type 3347/3348 1/3 octave bands	(49808 & 49809)
Gen-Rad model 1995 1/3 octave bands	(57330)
Gen-Rad model 2512 narrow band	

Figure A-10

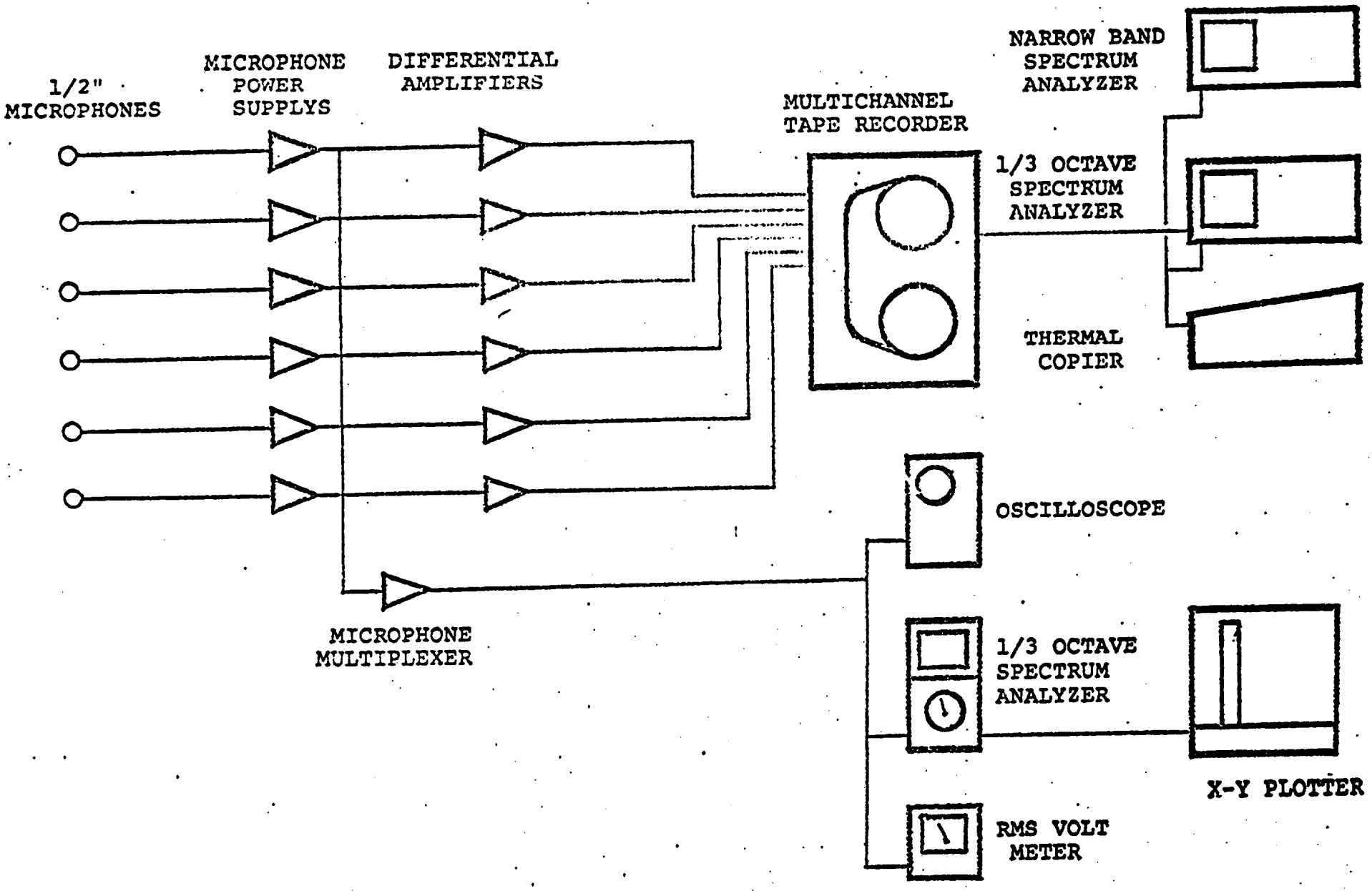

INSTRUMENTATION FOR DETERMINING EFFECTS OF COLLECTOR LENGTH ON SOUND PRESSURE FIELD

Figure A-11

SUMMARY OF OPERATING CONDITIONS WHEN DETERMINING EFFECTS OF COLLECTOR LENGTH ON THE SOUND PRESSURE FIELD

RPM = speed of windtunnel blower
Pplem = static pressure measured in windtunnel plenum
Gain = amplification gain used in tape recording acoustic dat

TEST #1 (collector is 4 ft from nozzle exit)

RUN NO.	RPM	Pplen(in. Hg.)	GAIN(dB)
cal.	-	-	0
1	3000	1.2	+40
2	6000	5.2	+20
3	8000	9.8	+20
4	7000	7.4	+20

TEST #2 (collector is 7 ft from nozzle exit)

RUN NO.	RPM	Pplen(in. Hg.)	GAIN(dB)
cal.	-	-	0
1	3000	1.2	+40
2	6000	5.2	+20
3	8000	9.6	+10
4	10000	16.0	0
5	12000	?	0

TEST #3 (collector is 10 ft from nozzle exi

RUN NO.	RPM	Pplen(in. Hg.)	GAIN(dB)
cal.	-	-	0
1	3000	1.2	+30
2	6000	5.3	+10
3	8000	9.7	-10
4	10000	16.2	-10
5	12000	24.8	-20

Figure A-12

COMPARISON OF HIGH-PASS FILTERED AND UNFILTERED OVERALL SOUND PRESSURE LEVELS FOR 3 DIFFERE. . COLLECTOR LENGHTS

TEST #1 (collector is 4ft from nozzle exit)

Mach No.	Blower RPM	MIC #1		MIC #2		MIC #3		MIC #4		MIC #5		MIC #6	
		f>100	f>20	f>100	f>20	f>100	f>20	f>100	f>20	f>100	f>20	f>100	f>20
.24	3000	56.3	76.8	56.9	74.2	57.0	76.2	55.0	76.5	67.4	77.9	73.0	79.2
.48	6000	78.5	85.5	79.7	83.8	80.4	85.5	78.7	85.2	92.0	94.2	93.7	95.0
.64	8000	87.7	90.5	89.3	90.8	90.3	92.0	89.0	91.2	102.3	103.8	100.9	101.5

TEST #2 (collector is 7ft from nozzle exit)

Mach No.	Blower RPM	MIC #1		MIC #2		MIC #3		MIC #4		MIC #5		MIC #6	
		f>100	f>20	f>100	f>20	f>100	f>20	f>100	f>20	f>100	f>20	f>100	f>20
.24	3000	56.3	77.0	57.0	73.2	57.3	74.5	56.4	74.2	67.9	77.5	72.4	79.5
.48	6000	78.2	92.0	79.8	88.8	80.6	89.0	80.3	88.0	92.2	94.5	93.0	95.2
.64	8000	87.7	96.0	89.6	94.2	90.6	94.0	90.6	93.5	102.7	103.5	101.4	102.2
.80	10000	94.8	98.8	96.9	98.5	98.1	99.2	98.7	99.8	110.2	110.8	108.6	109.0
.96	12000	100.4	102.5	103.1	103.8	104.4	105.0	105.3	105.8	116.0	116.5	114.2	114.8

TEST #3 (collector is 10ft from nozzle exit)

Mach No.	Blower RPM	MIC #1		MIC #2		MIC #3		MIC #4		MIC #5		MIC #6	
		f>100	f>20	f>100	f>20	f>100	f>20	f>100	f>20	f>100	f>20	f>100	f>20
.24	3000	59.8	76.5	59.6	69.0	59.9	75.2	57.6	76.5	68.9	79.5	73.0	80.0
.48	6000	78.7	90.0	80.1	86.0	80.9	86.8	80.7	87.5	92.9	94.8	93.0	95.0
.64	8000	90.3	97.8	91.0	94.5	90.7	93.5	92.8	96.0	103.3	104.0	101.6	102.8
.80	10000	95.7	102.0	97.1	99.2	98.3	100.0	99.1	101.5	111.3	112.0	108.1	108.8
.96	12000	101.9	105.2	103.3	104.5	104.7	105.5	105.9	107.0	117.4	117.8	114.3	114.8

UNFILTERED OVERALL LEVEL INCLUDES 1/3 OCTAVE BANDS FROM 20 - 20,000 Hz

HIGH PASS FILTERED OVERALL LEVEL INCLUDES 1/3 OCTAVE BANDS FROM 100 - 20,000 Hz

Figure A-13

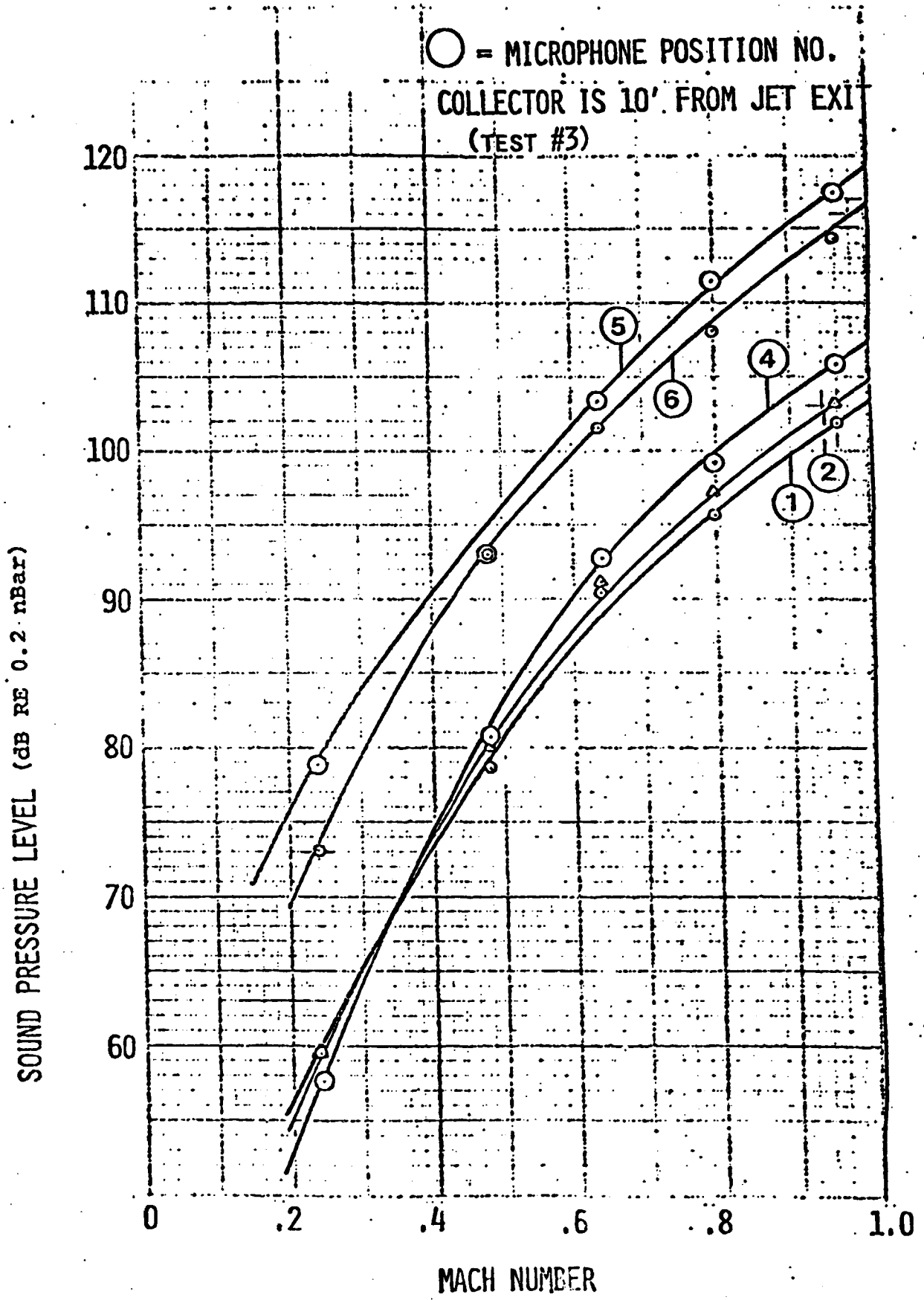

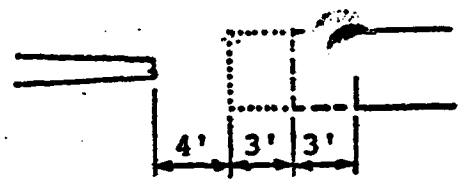

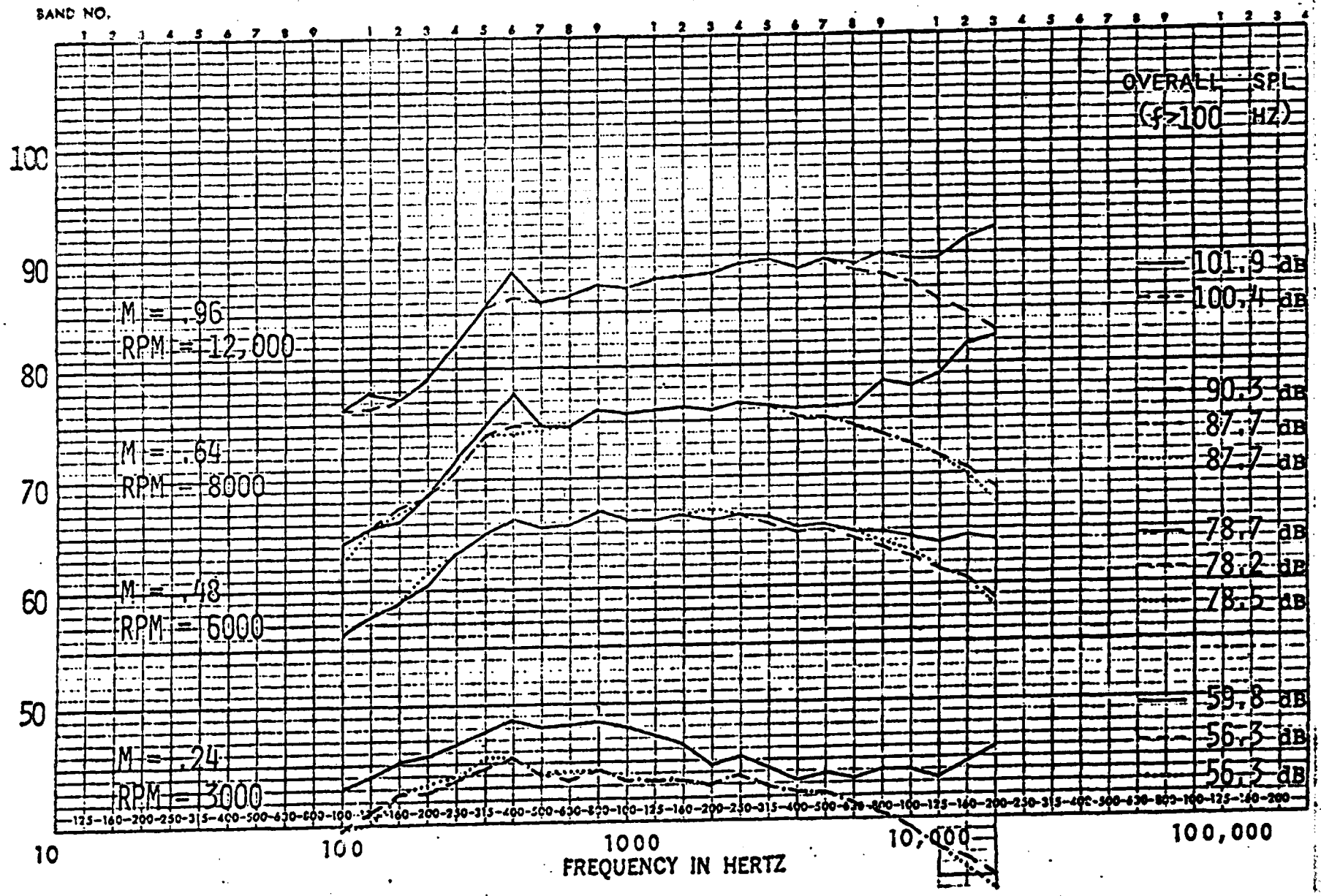

EFFECTS OF COLLECTOR LENGTH ON SOUND PRESSURE FIELD
MICROPHONE POSITION #1

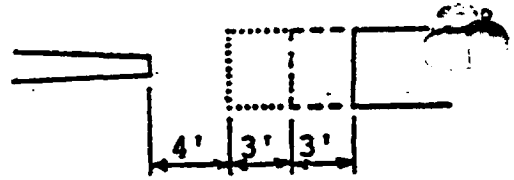

BAND NO.

SOUND PRESSURE LEVEL (dB RE 0.2 nBar)

100
90
80
70
60
50

M = .96
RPM = 12,000

M = .80
RPM = 10,000

M = .64
RPM = 8000

M = .48
RPM = 6000

M = .24
RPM = 3000

OVERALL SPL
(f > 100 HZ)

103.3 dB
103.1 dB
97.1 dB
96.9 dB
91.0 dB
89.6 dB
89.3 dB
80.1 dB
79.8 dB
79.7 dB
59.6 dB
57.0 dB
56.9 dB

10
100
1000
10,000
FREQUENCY IN HERTZ

EFFECTS OF COLLECTOR LENGTH ON SOUND PRESSURE FIELD
MICROPHONE POSITION #2

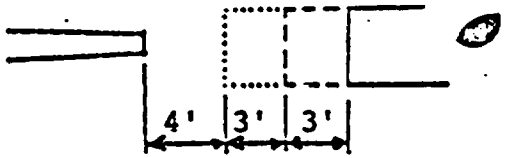

BAND NO.

SOUND PRESSURE LEVEL (dB RE 0.2 nBar)

100
90
80
70
60
50

M = .96
RPM = 12,000

M = .64
RPM = 8000

M = .48
RPM = 6000

M = .24
RPM = 3000

OVERALL SPL
(f > 100 HZ)

104.7
104.4
90.7
90.6
90.3
80.9
80.6
80.4
59.9
57.3
57.0

10
100
1000
10,000
FREQUENCY IN HERTZ

EFFECTS OF COLLECTOR LENGTH ON SOUND PRESSURE FIELD
MICROPHONE POSITION #3

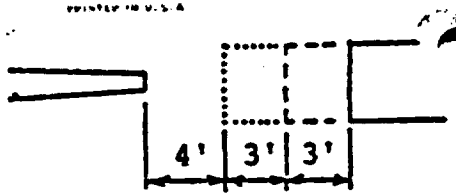

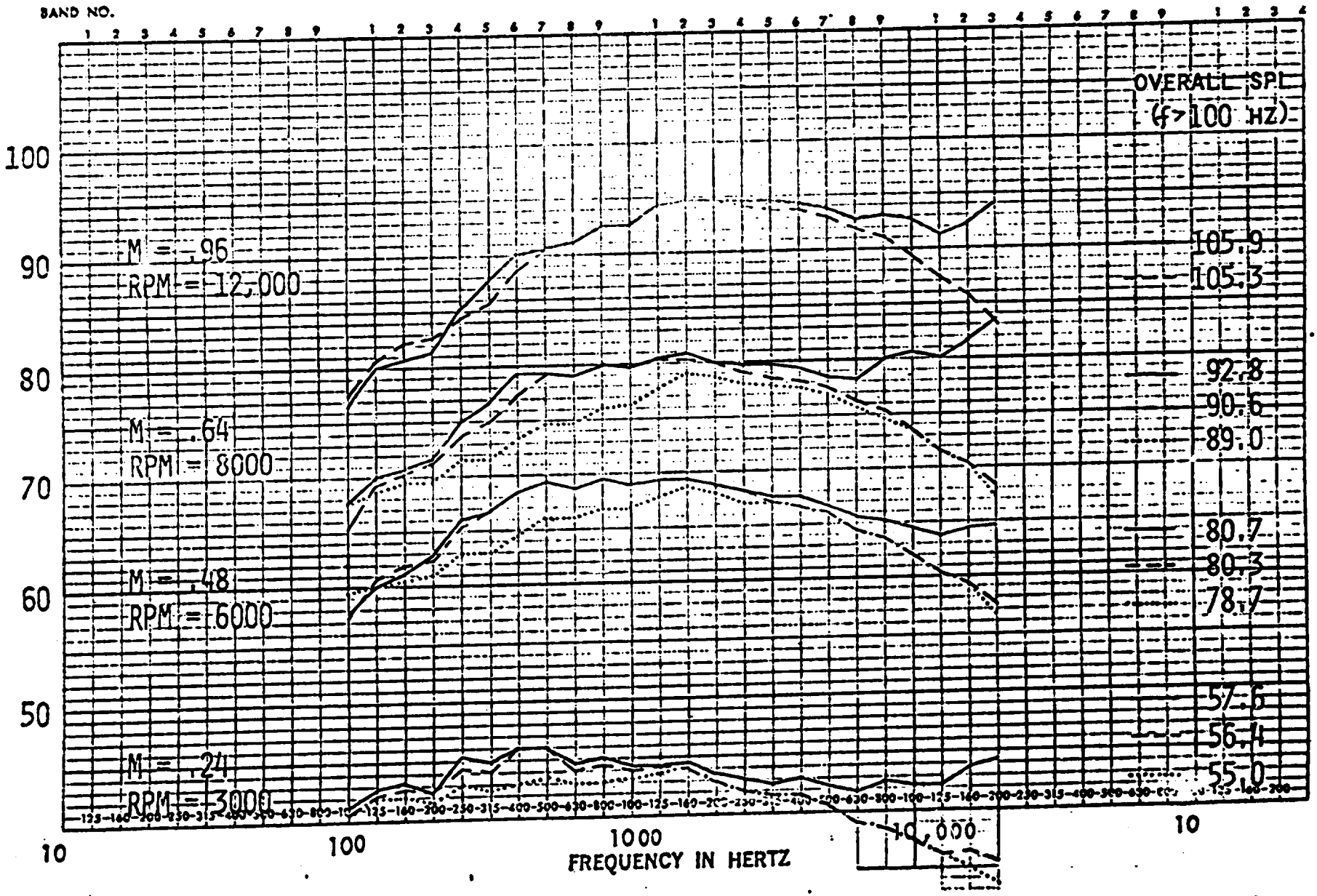

EFFECTS OF COLLECTOR LENGTH ON SOUND PRESSURE FIELD
MICROPHONE POSITION #4

ORIGINAL PAGE IS
OF POOR QUALITY

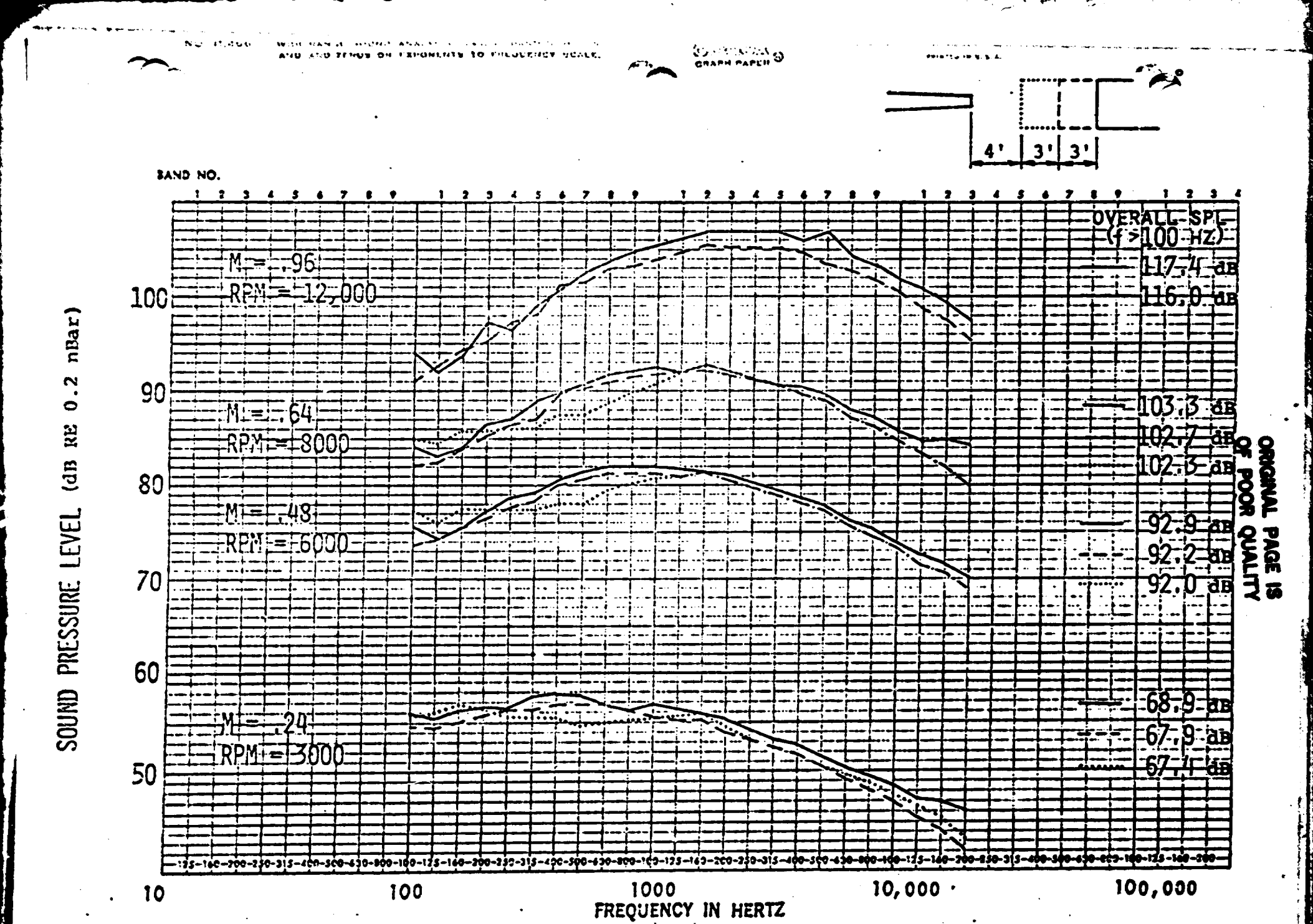

ORIGINAL PAGE IS OF POOR QUALITY

EFFECTS OF COLLECTOR LENGTH ON SOUND PRESSURE FIELD
MICROPHONE POSITION #5

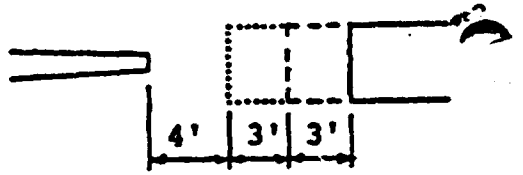

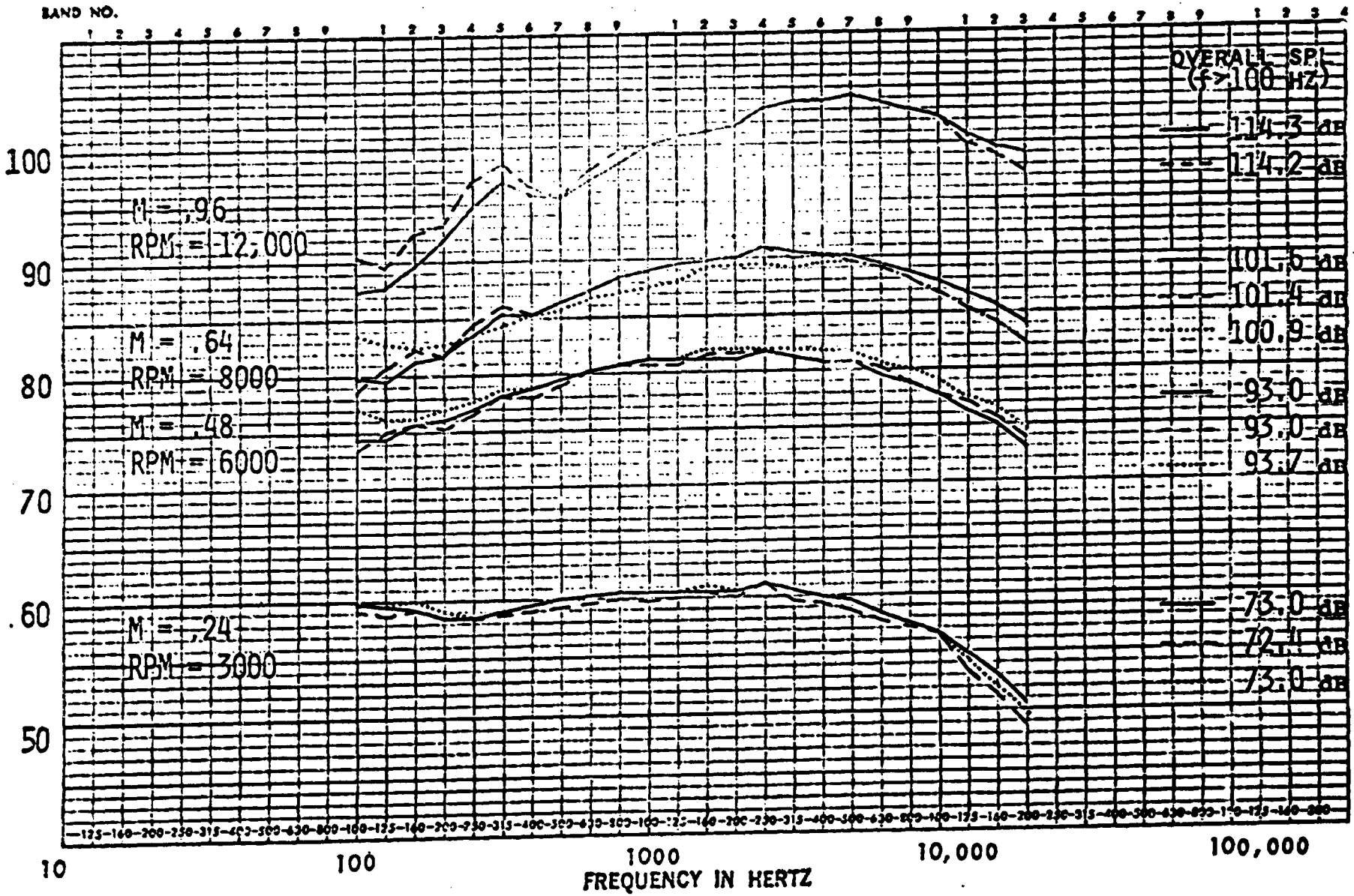

EFFECTS OF COLLECTOR LENGTH ON SOUND PRESSURE FIELD

MICROPHONE POSITION # 6

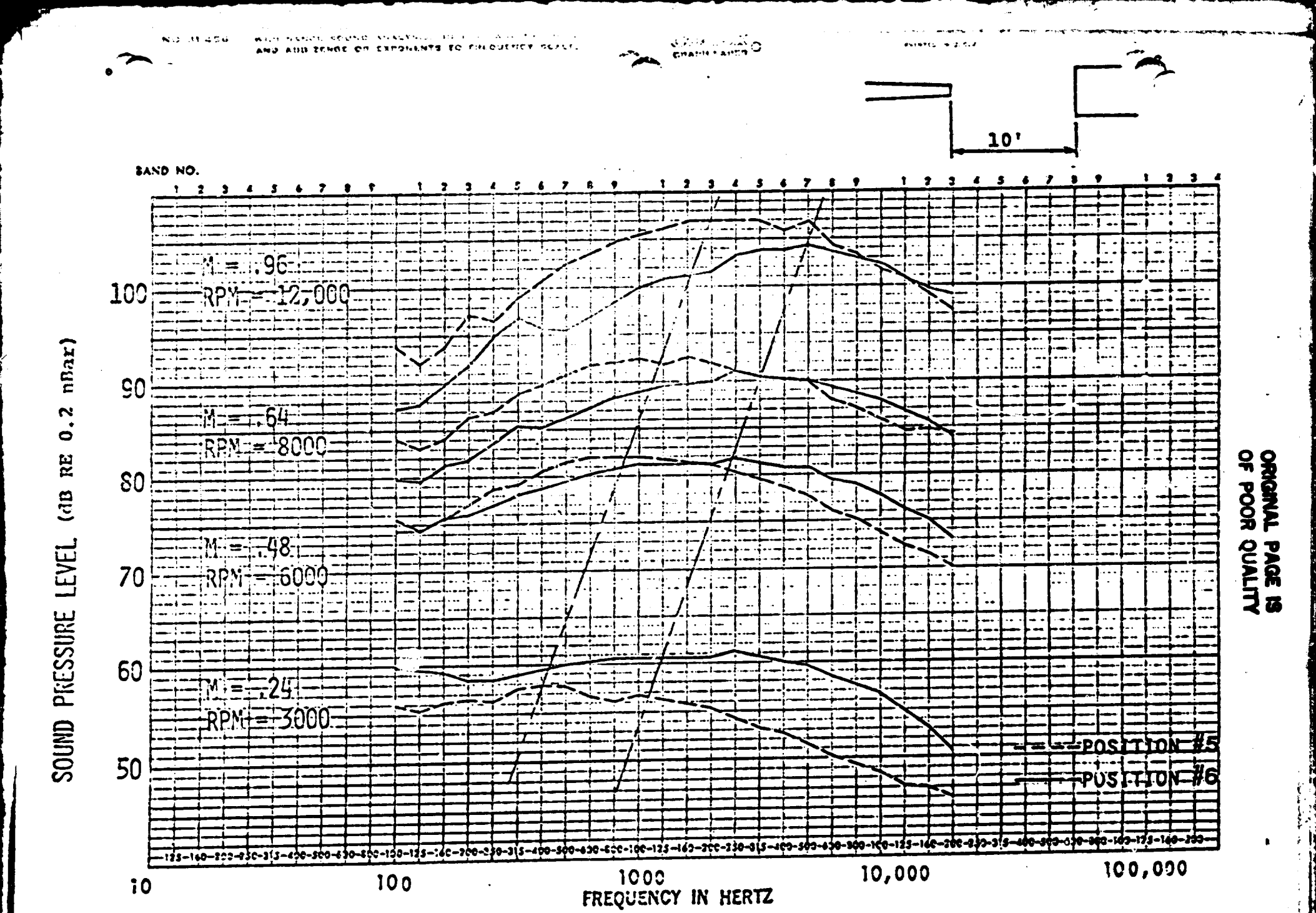

ORIGINAL PAGE IS
OF POOR QUALITY

COMPARISON OF NEAR FIELD MICROPHONE
POSITIONS #5 AND #6

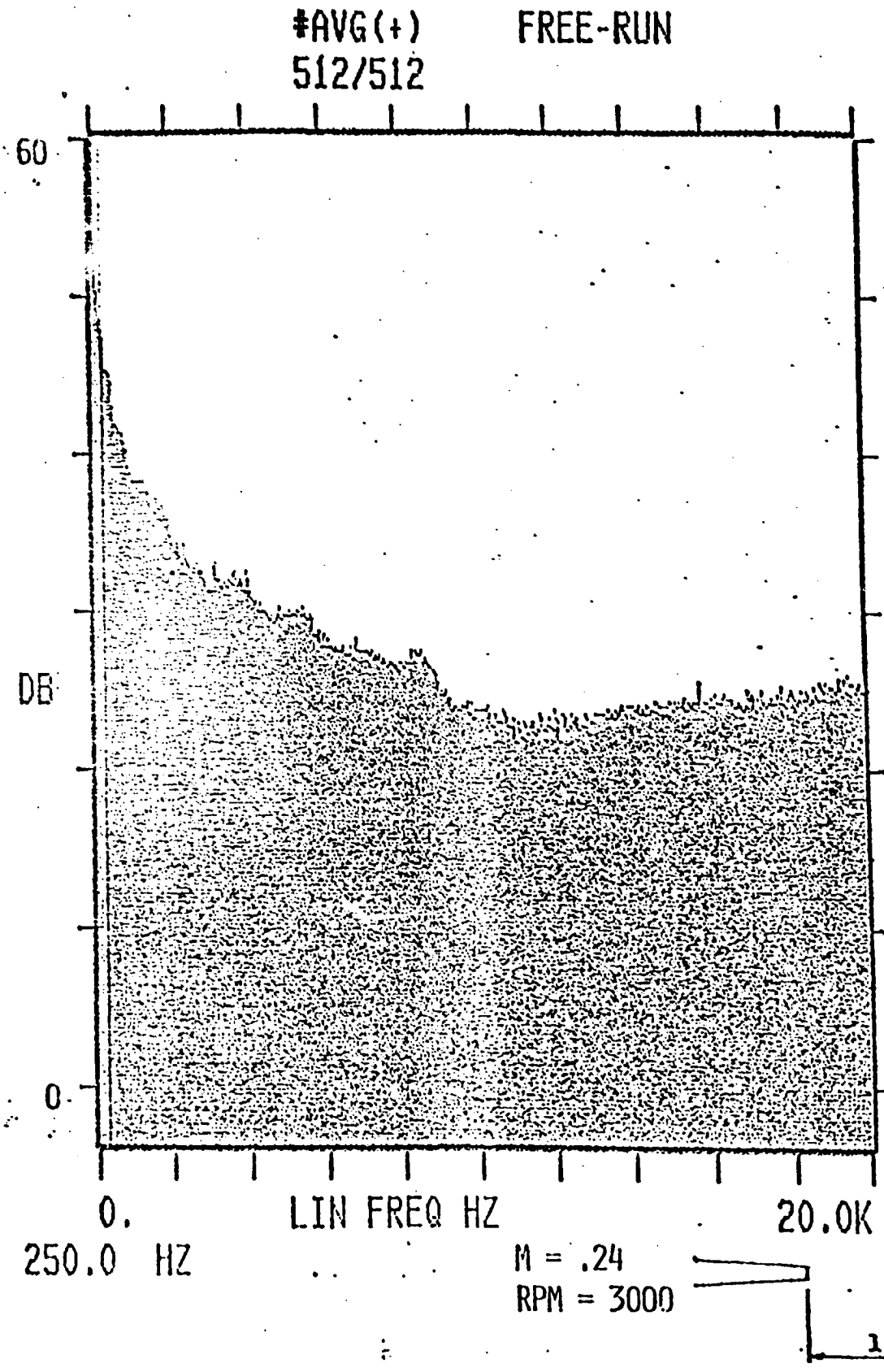

MICROPHONE POSITION #1

ORIGINAL PAGE IS
OF POOR QUALITY

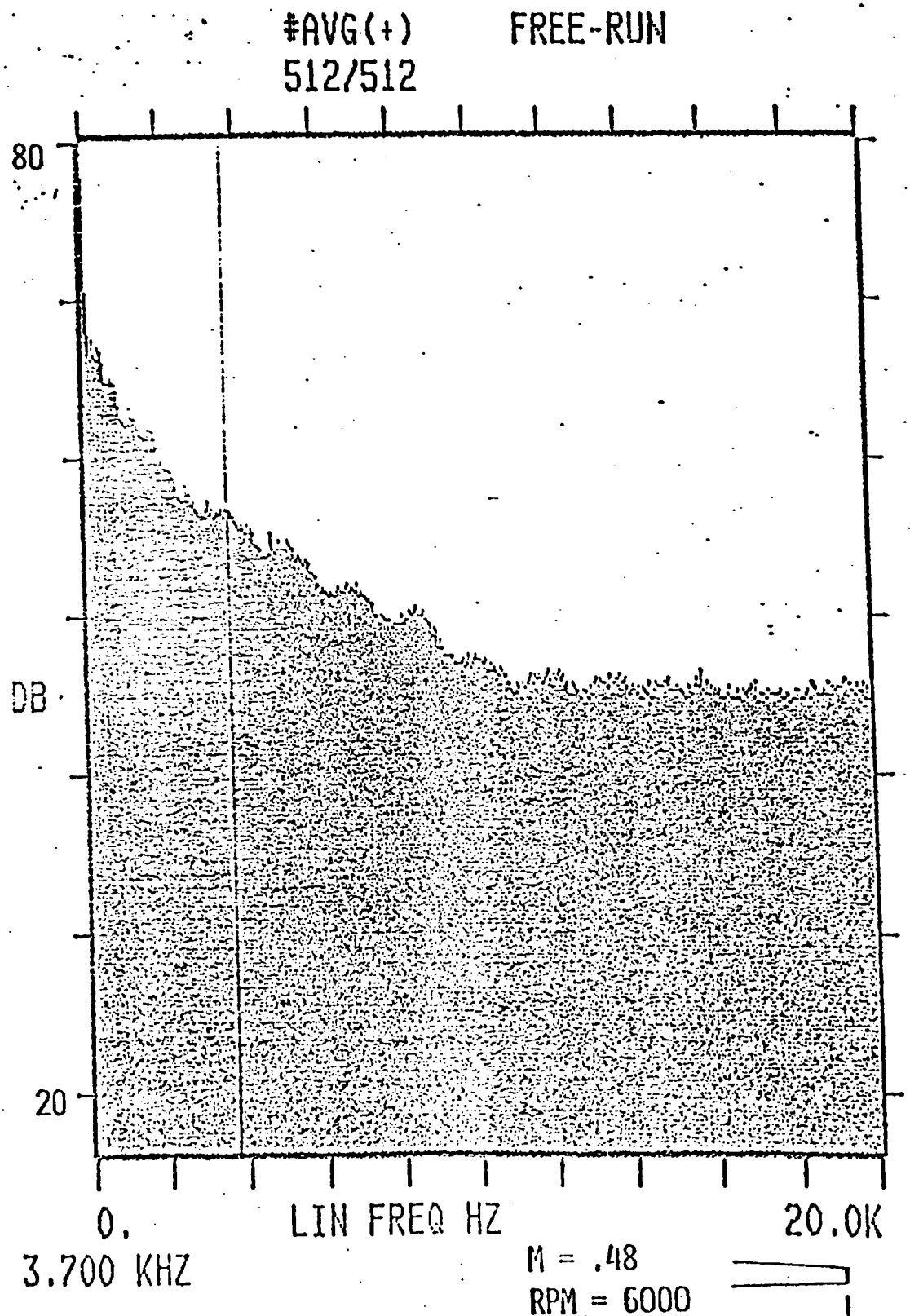

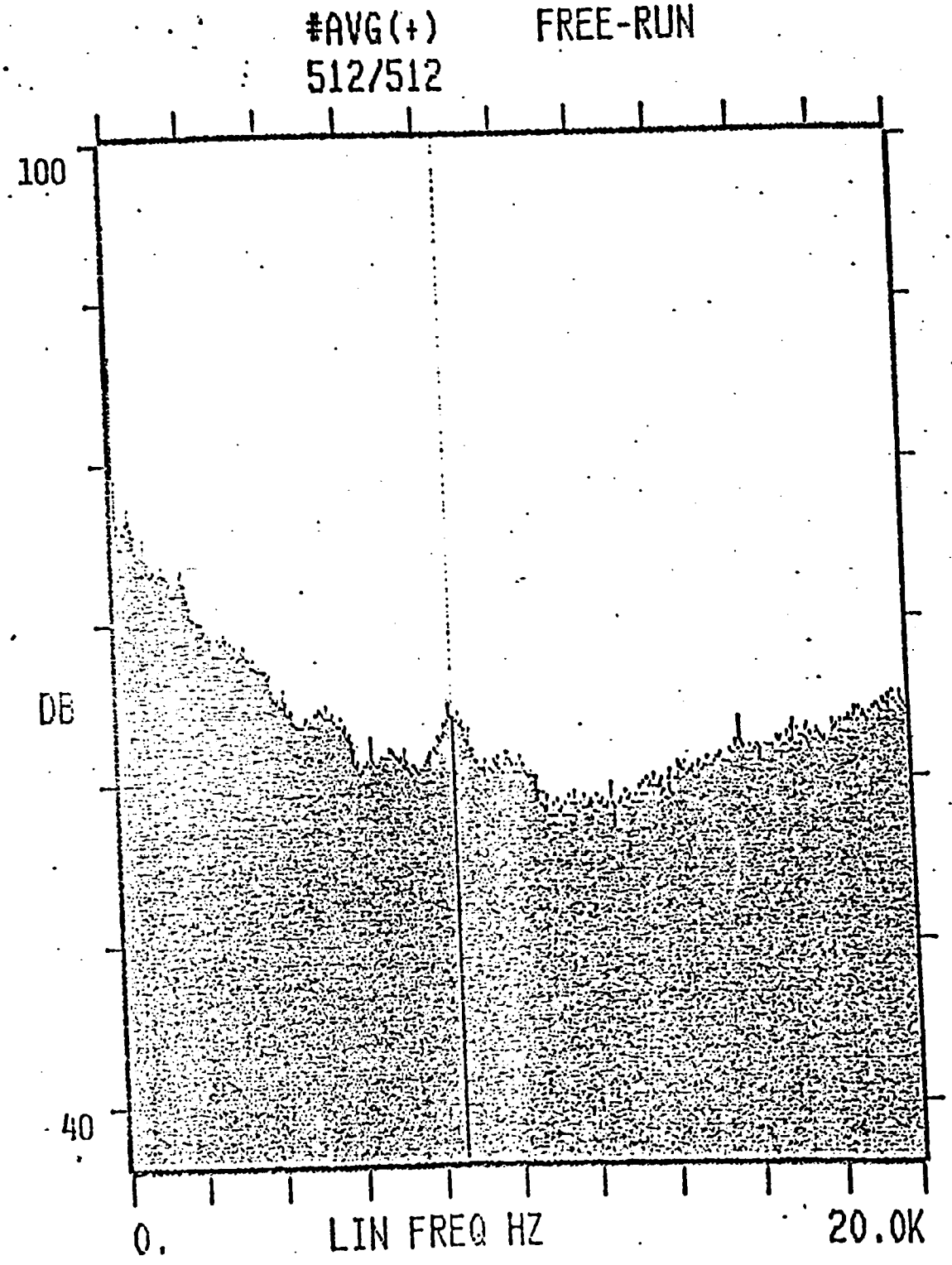

MICROPHONE POSITION #4

ORIGINAL PAGE IS
OF POOR QUALITY

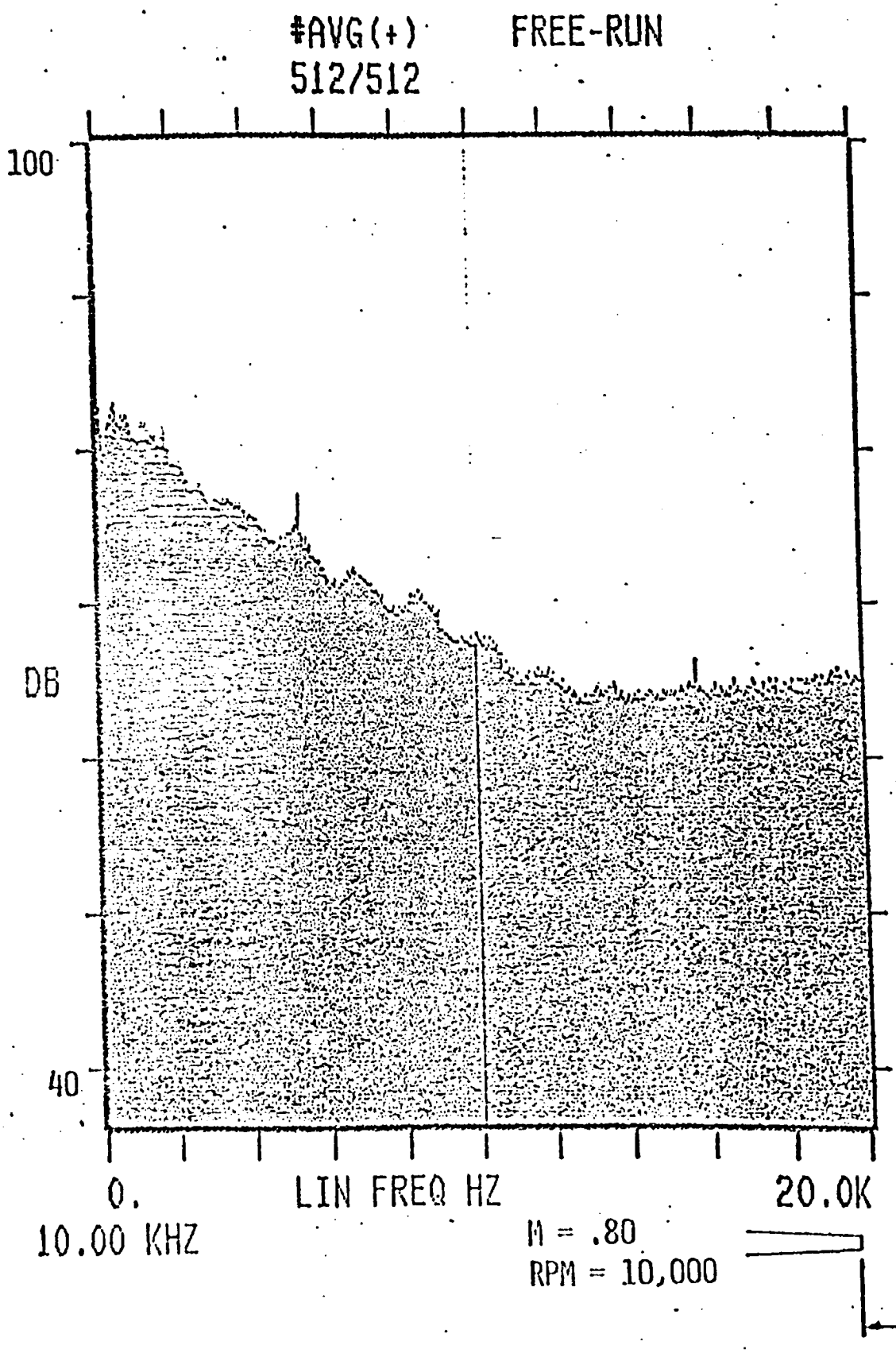

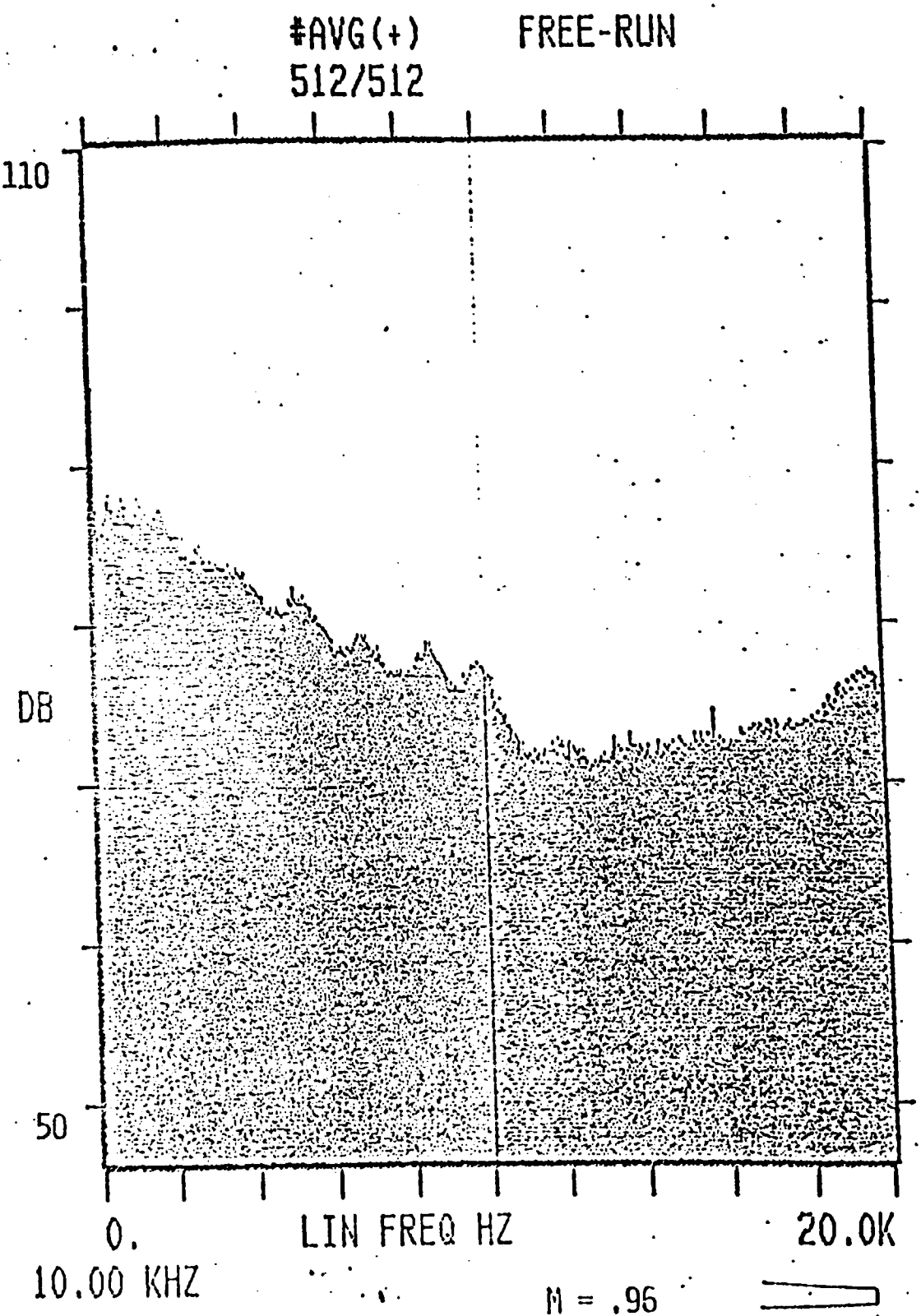

MICROPHONE POSITION #4

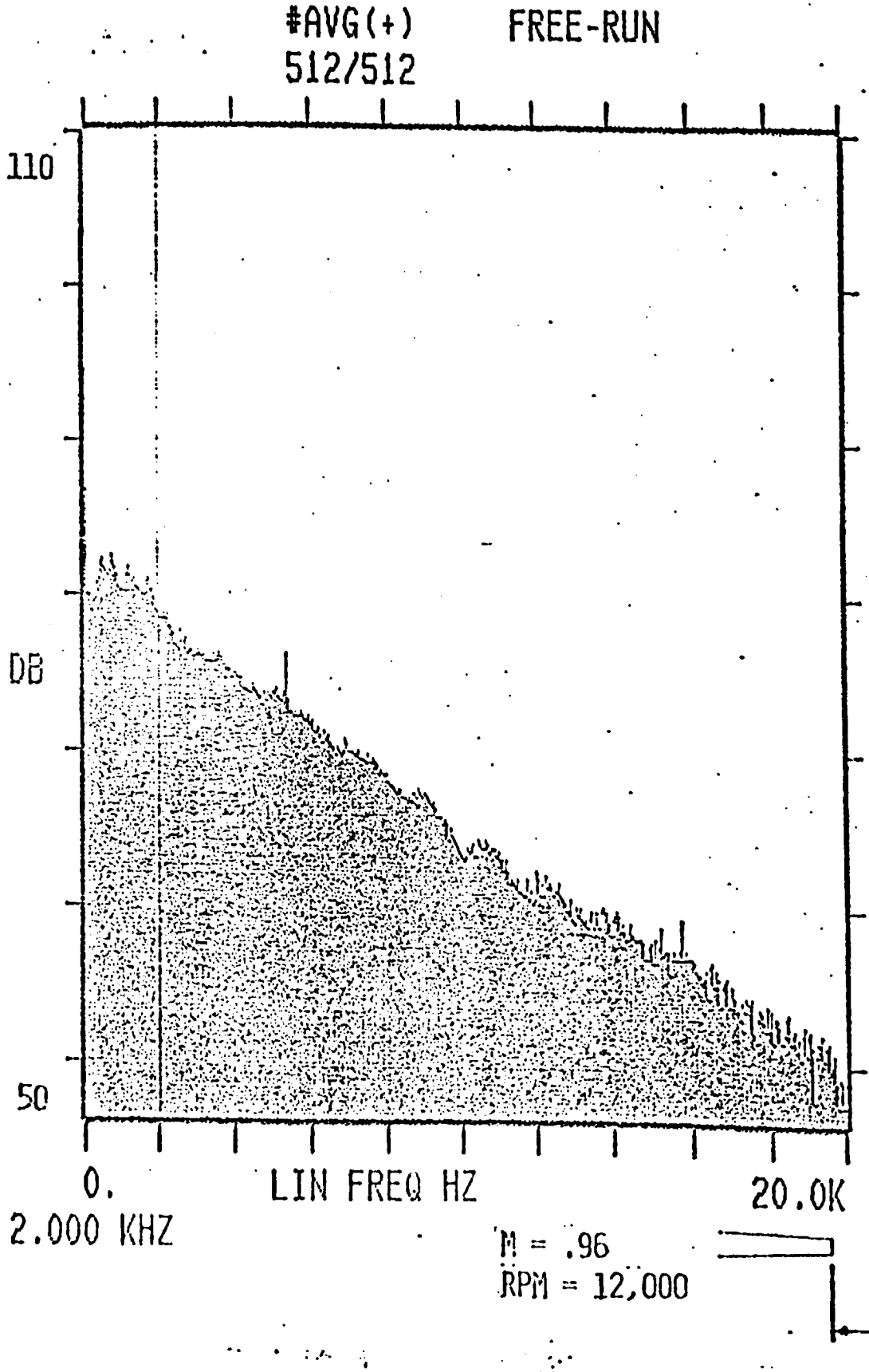

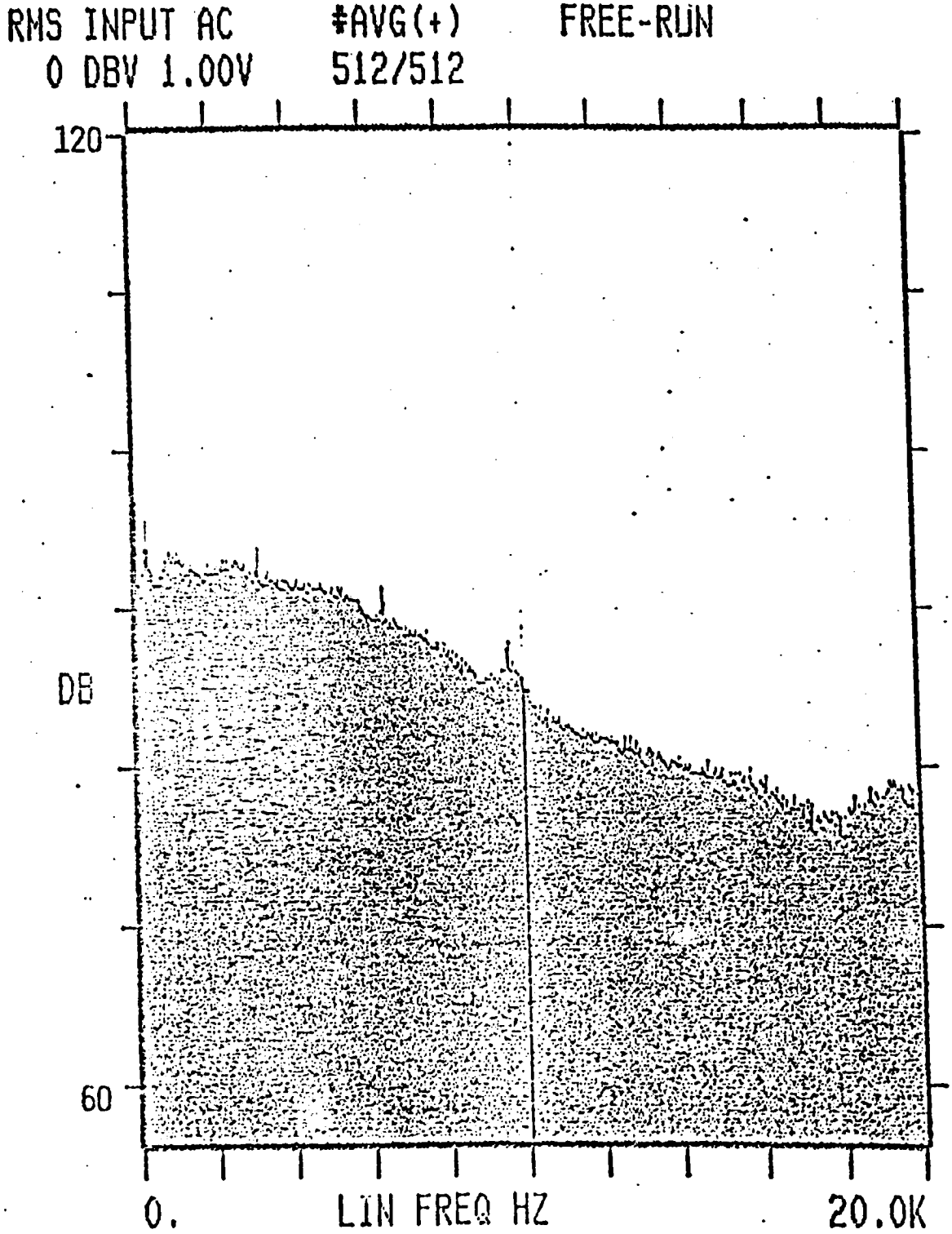

MICROPHONE POSITION #6

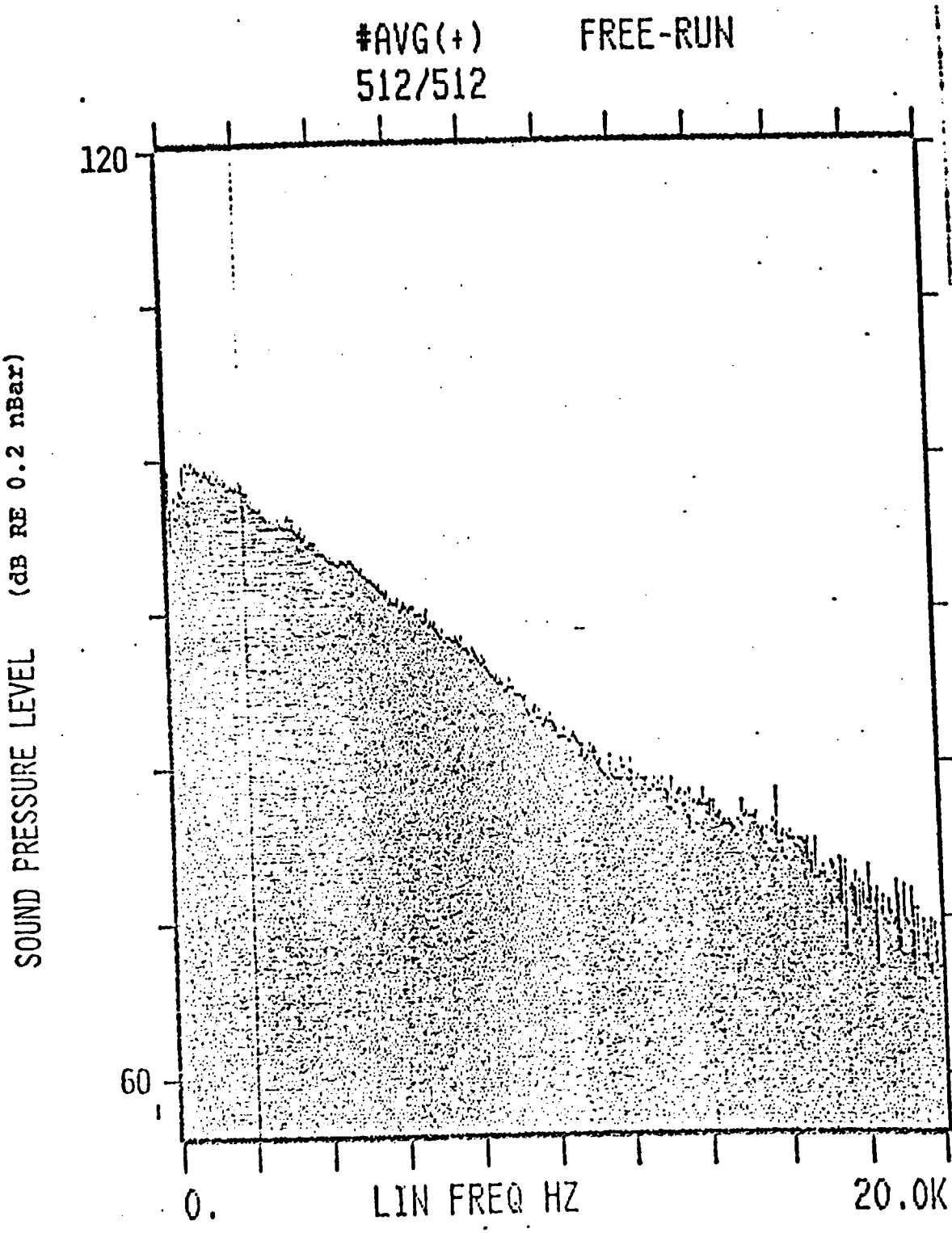

MICROPHONE POSITION #5

Figure A-29

P_a (Atmospheric Pressure)= 992.5 mb

$\Delta P_{rm} = P_a - P_{rm}$

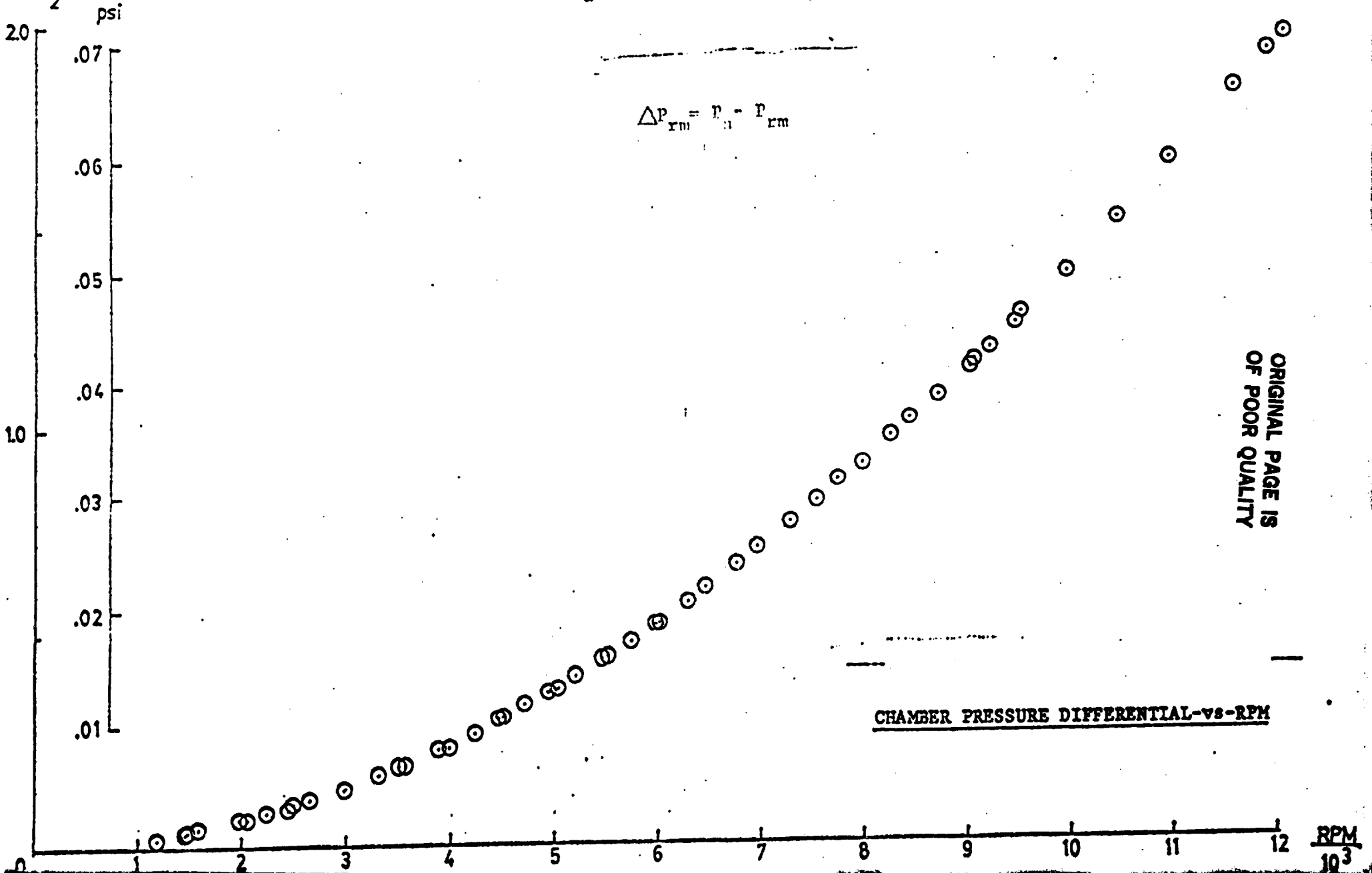

CHAMBER PRESSURE DIFFERENTIAL-vs-RPM

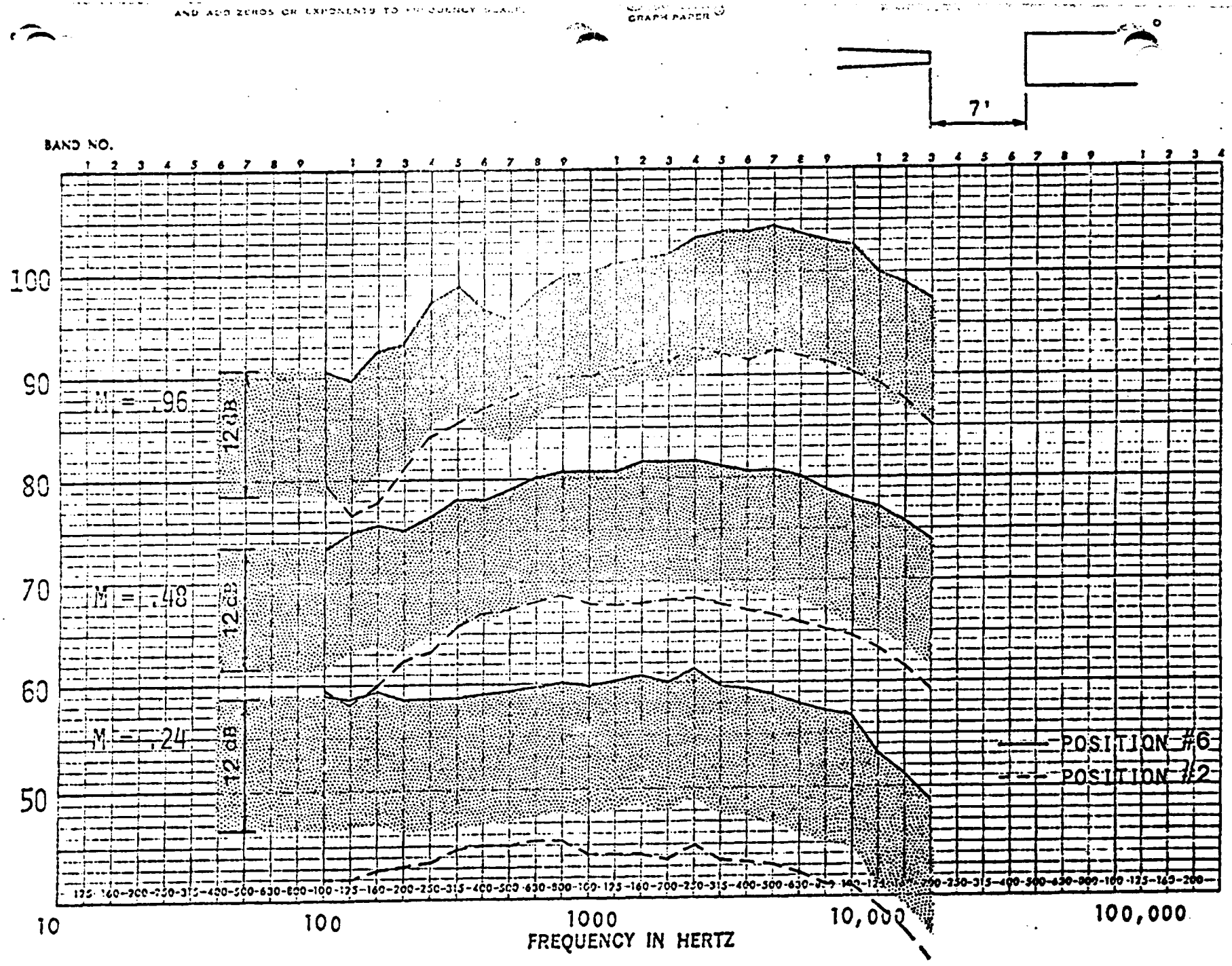

ORIGINAL PAGE IS
OF POOR QUALITY

COMPARISON OF NEAR FIELD MICROPHONE POSITION #6
AND FAR FIELD MICROPHONE POSITION #2

Figure A-31

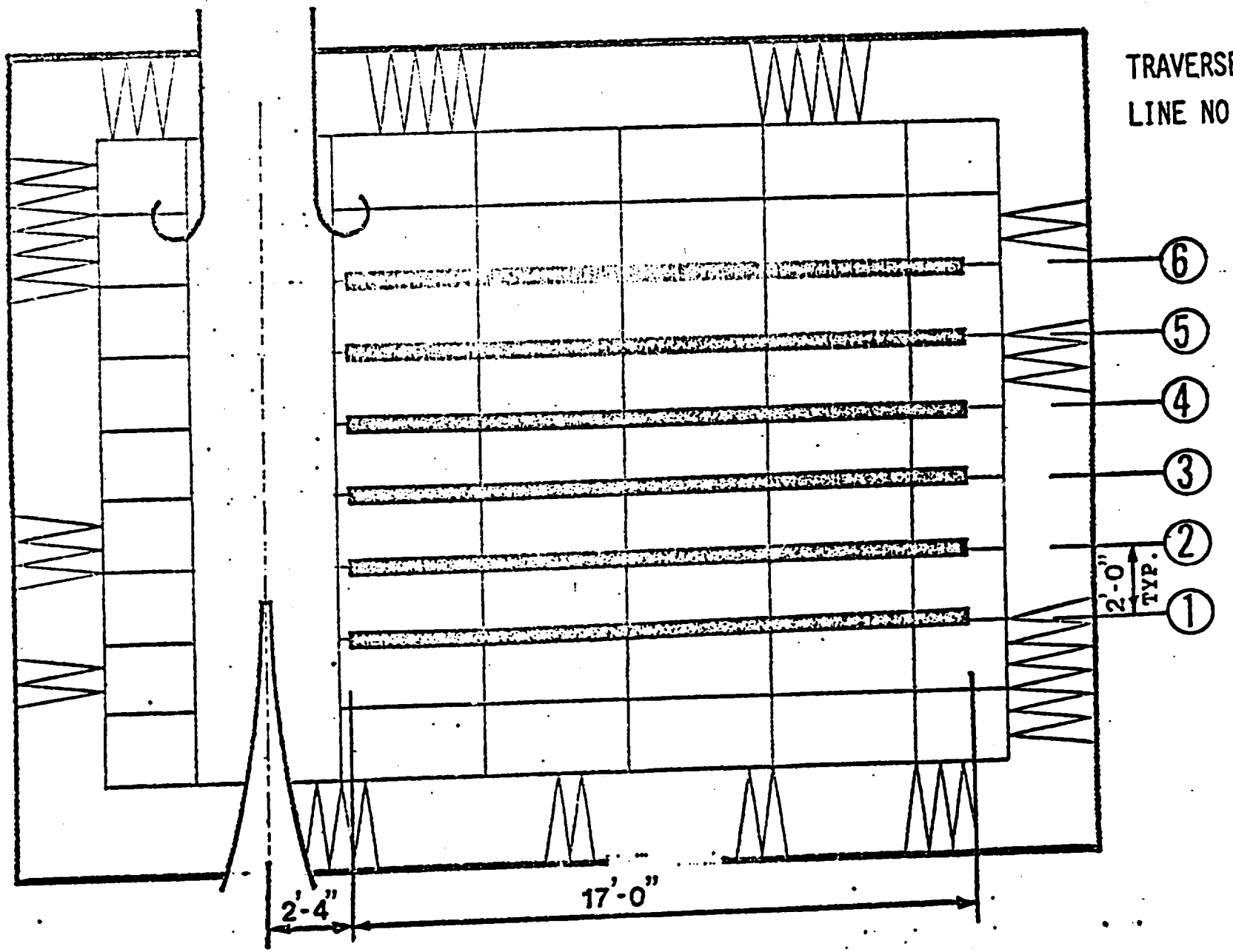

MICROPHONE TRAVERSE LOCATIONS FOR
DETERMINING JET NOISE CONTOURS

INSTRUMENTATION LIST FOR DETERMINING JET NOISE CONTOURS (4" NOZZLE)

	(NASA NO.)
1/2" microphone; B&K type 4122	
microphone power supply; B&K type 2807	(41966)
differential amplifier; Textronics AM502	(52477)
multichannel tape recorder; Ampex FR1300	
RMS voltmeter; DISA type 55D35	(40338)
1/3 octave band real time analyzer; Gen-Rad model 1995	(57330)
X-Y plotter; Hewlett-Packard model 7004B	(45008)
DAS computer system	
PDP/1145 minicomputer	
General Radio model 1925 parallel filter set	
General Radio model 1926 multichannel RMS detector	
Textronics termanal	
Textronics thermal printer	

Figure A-33

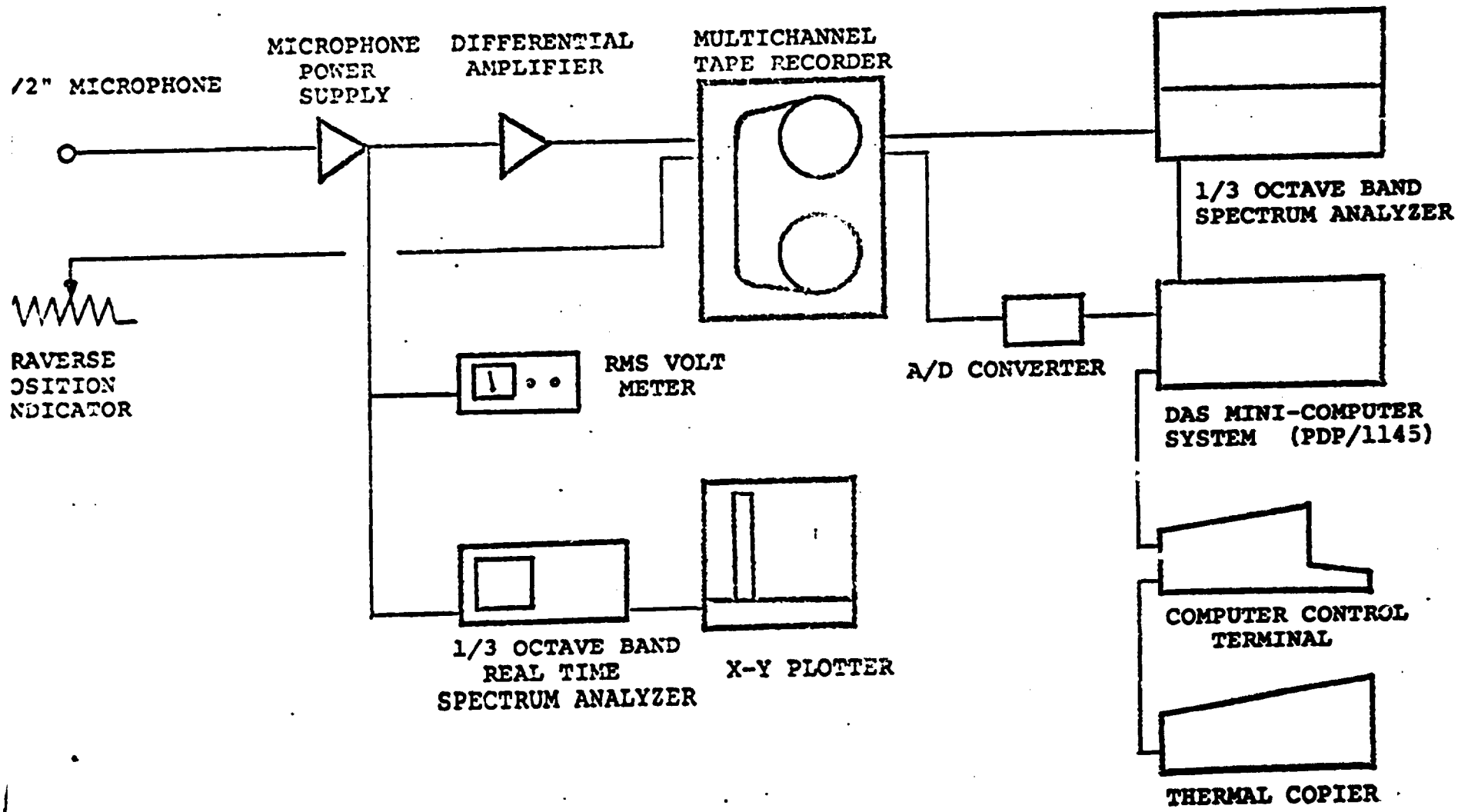

INSTRUMENTATION FOR DETERMINING JET NOISE CONTOURS

Figure A-34

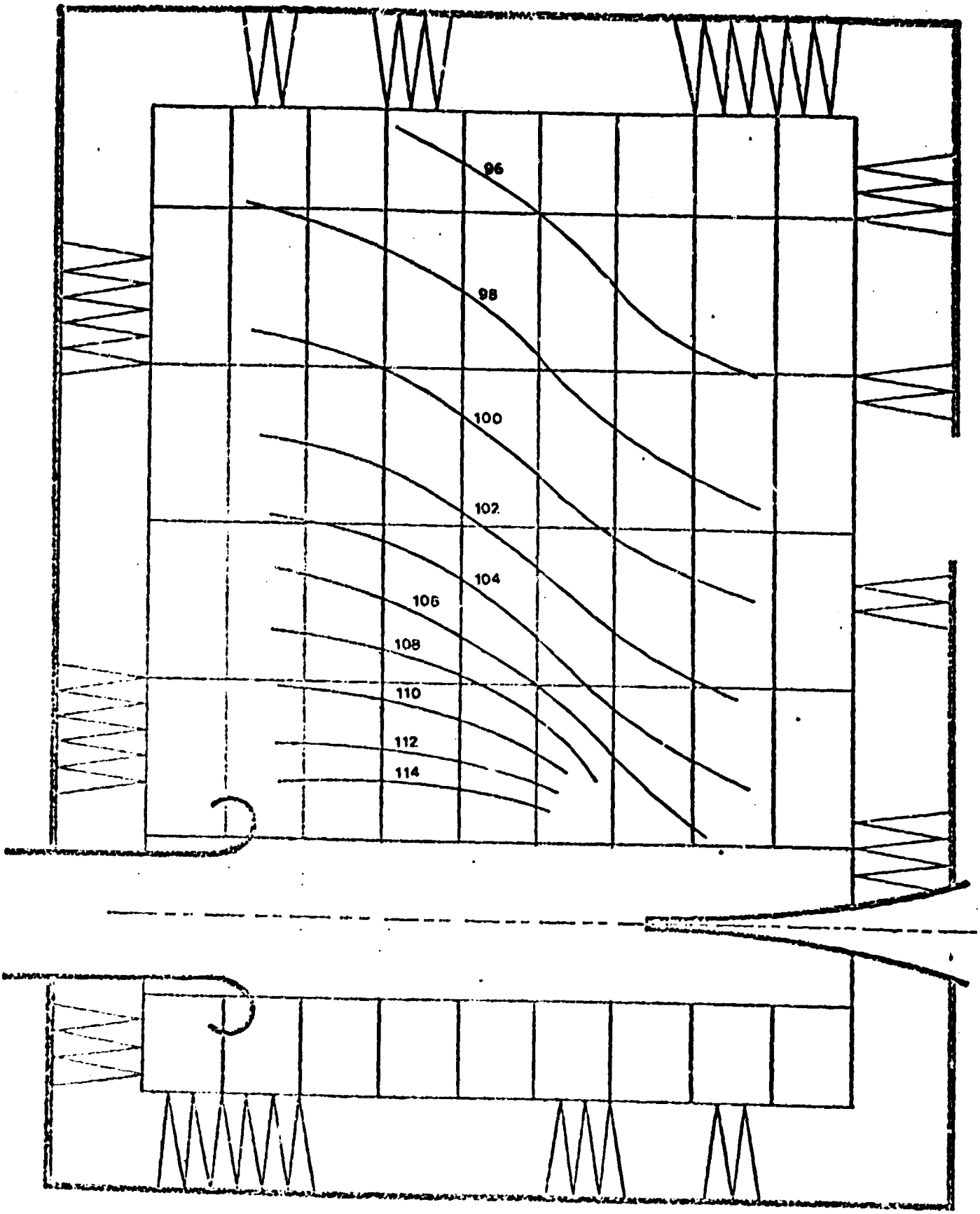

NOISE CONTOURS - OVERALL LEVEL M = 0.80

Figure A-35

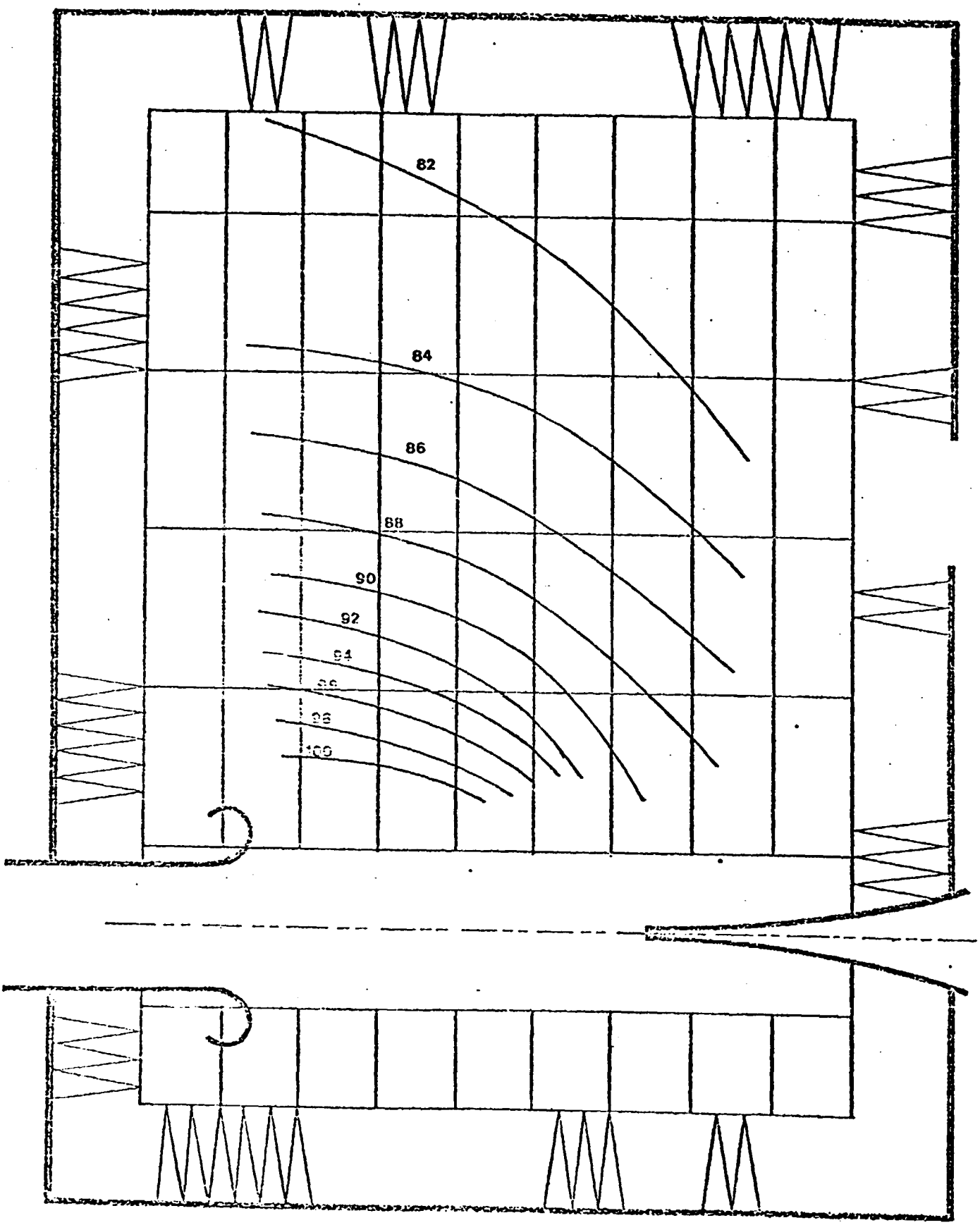

NOISE CONTOURS - 500 Hz.

M = 0.80

Figure A-36

ORIGINAL PAGE IS
OF POOR QUALITY

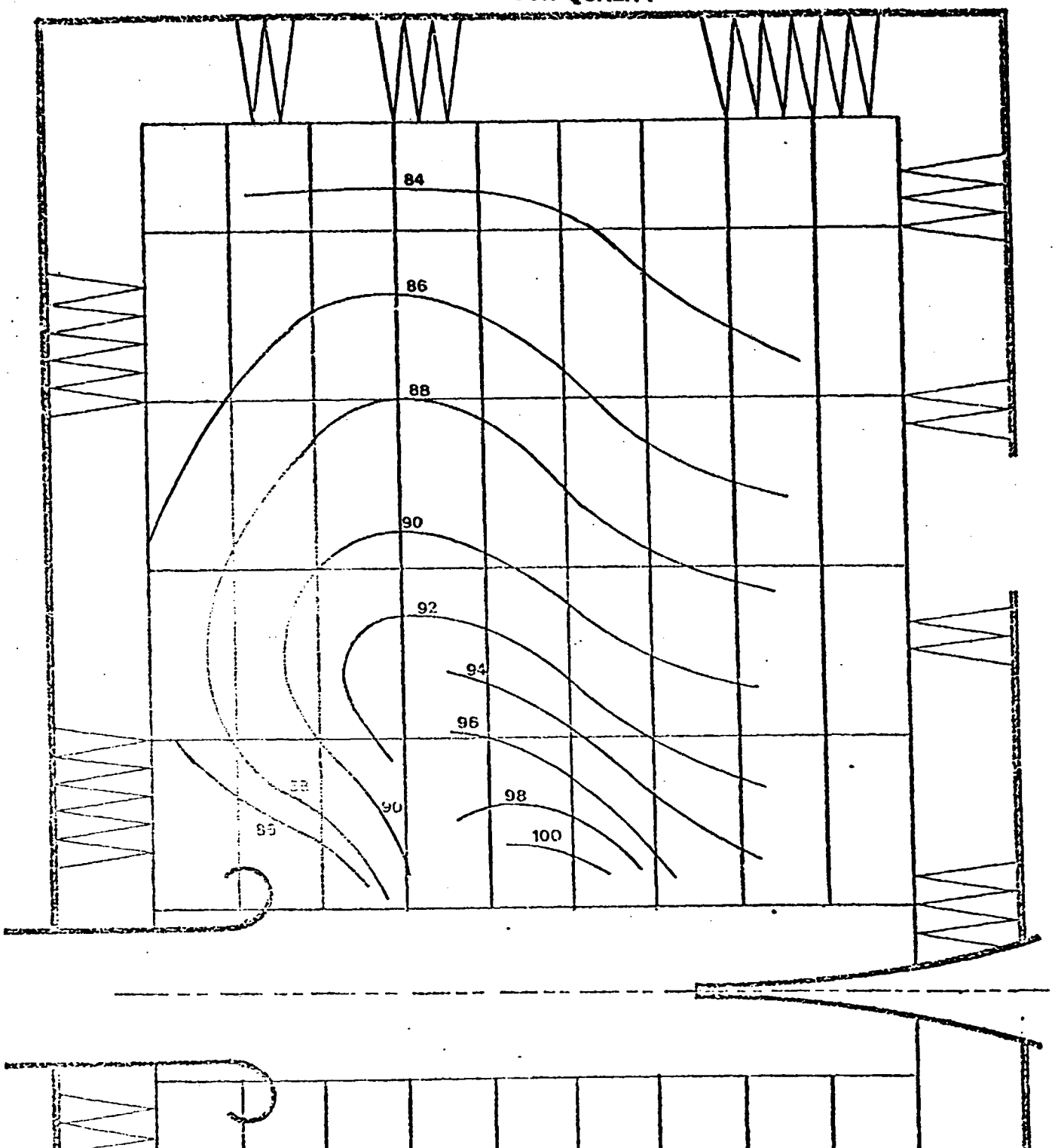

NOISE CONTOURS - 5000 Hz.

M = 0.80

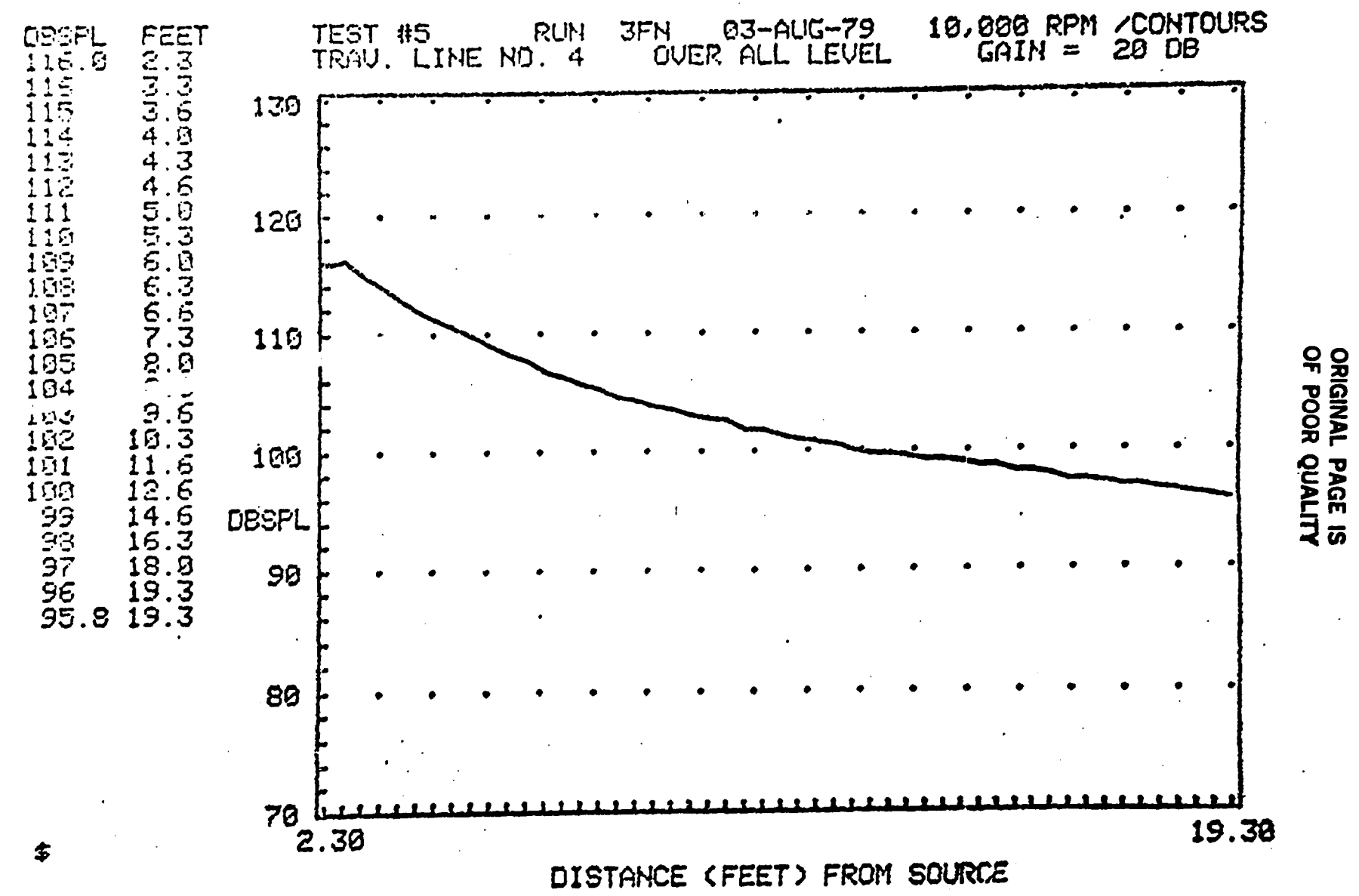

ORIGINAL PAGE IS
OF POOR QUALITY

Figure A-38

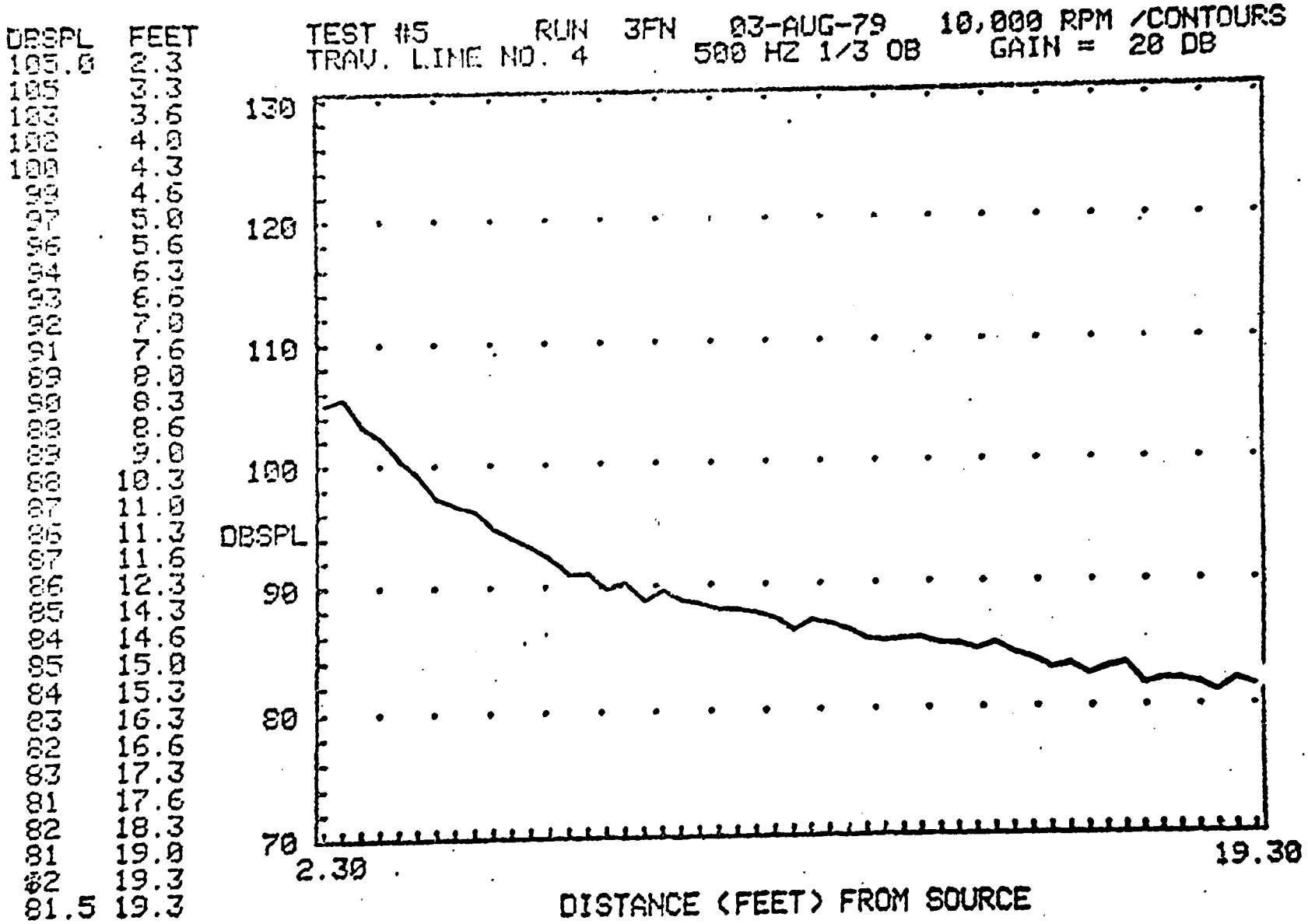

ORIGINAL PAGE IS
OF POOR QUALITY

Figure A-39

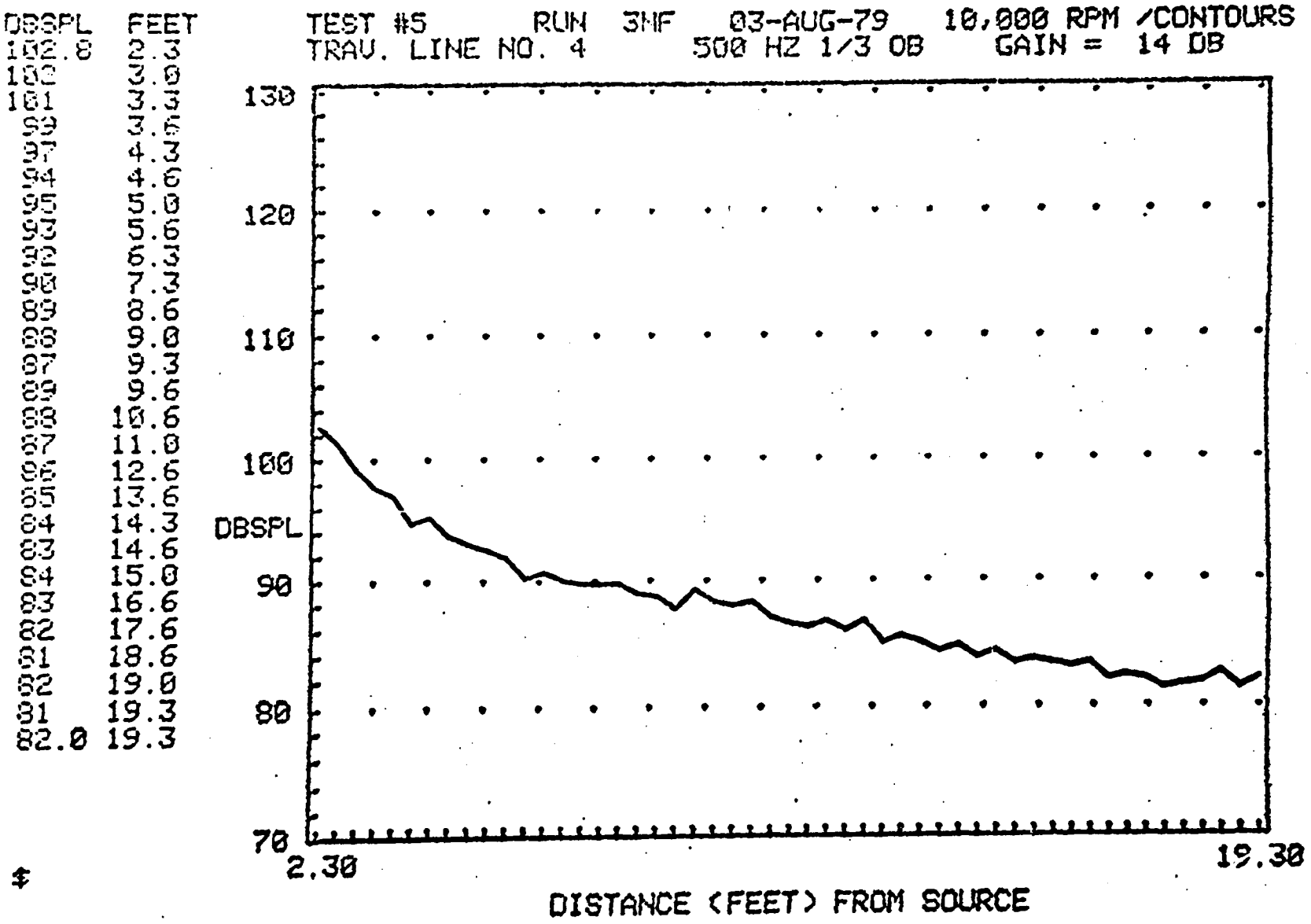

Figure A-40

B. FLUID FLOW MEASUREMENTS

IV. HOT WIRE MEASUREMENTS

V. VELOCITY FLUCTUATION SPECTRA

TABLE OF CONTENTS

LIST OF FIGURES

Nomenclature

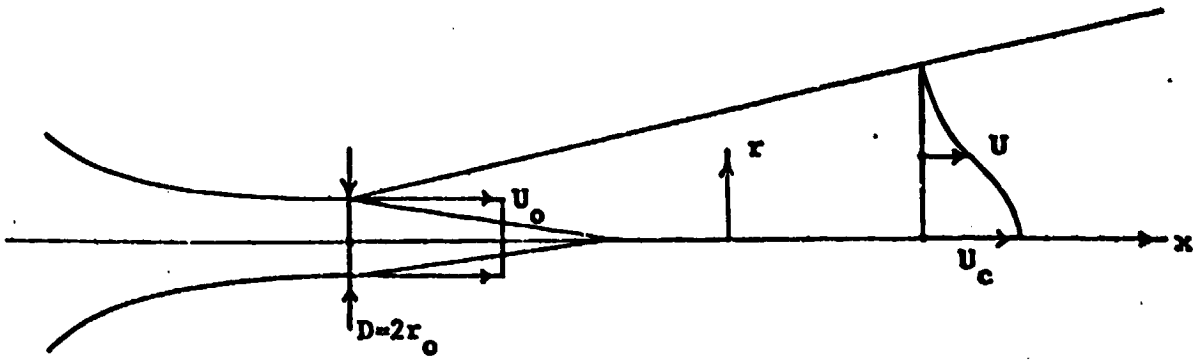

D	=	Nozzle Diameter (D=4in.)
M_E	=	Nozzle Exit Mach Number
P_a	=	Atmospheric Pressure
P_{rm}	=	Pressure in the Anechoic Chamber
P_t	=	Total Pressure in the Jet (Nozzle Exit Centerline)
r	=	Coordinate in the Radial Direction
r_o	=	Nozzle Exit Radius
$\bar{r}$	=	r/r_o
U	=	Velocity Measured with Single Wire Probe
U_c	=	Maximum Velocity in a Velocity Profile
U_o	=	Maximum Velocity at the Nozzle Exit
X	=	Coordinate in the Streamwise Direction

1. INTRODUCTION

The purpose of this part of the experiment is to evaluate some basic aerodynamic characteristics of the AMES anechoic open throat wind tunnel facility. The characteristics we have concen-concentrated our experiments upon are:

1. The nature of the nozzle (jet) flow.
2. The mean and fluctuating velocity profiles of the jet.
3. Anechoic chamber pressure variation.

For these experiments the configuration of the facility chosen was fixed making use of only the 4" diameter (round) nozzle, one collector position, fully retracted, and without making making use of either the heat exchanger or the jet boundary layer control device.

2. FACILITY DESCRIPTION

The facility under study, the anechoic open throat wind tunnel, is located in the 40' x 80' wind tunnel building. The general configuration of the facility is shown in Figure 1. As studied the facility had only the 4" diameter (round) nozzle in place and the collector was in the fully retracted position (10 feet from the nozzle exit). The heat exchanger for flow temperature control and the boundary layer control devices have been removed from the facility.

The air compressor is of the centrifugal type with sixteen blades. It's operating range is from 0 to 12000 rpm corresponding to a nozzle exit Mach number* range of 0 to .96.

A more detailed description can be found in the NEAR Design Report (Reference 1).

3. EXPERIMENTAL APPARATUS AND PROCEDURE

For the aerodynamic investigation only the 4" diameter (round) nozzle was used. Neither the boundary layer control nor the heat exchanger devices were in place during the tests.

The collector was kept in a fully retracted position, 10' from the nozzle exit, throughout the test (see part A).

Total pressure was measured at the center of the nozzle exit cross-section. The static pressure was measured in the plenum chamber, as shown in Figure 1. Measurements of the static pressure in the anechoic chamber were made at a point located a suitable distance from the jet, as shown in Figure 1.

Velocity profiles in the jet were obtained for only two compressor speeds, 3000 and 6000 rpm, corresponding to exit Mach numbers of .24 and .48 respectively. The velocity profiles in the jet were made at six axial locations from the nozzle exit plane, i.e. at X/D = 0, 1.5, 3.0, 6.0, 9.0, and 12.0. They were

*From now on the terminology "Exit Mach number" will be used with the understanding that it refers to the (measured) Mach number at the center of the nozzle exit cross-section.

obtained utilizing a single wire probe. Traverses across the jet diameter were made along two orthogonal axes; one vertical and one horizontal. At all times the single wire was kept perpendicular to the flow direction and the axis of traverse. The single wire probe was rotated 90° when going from one axis of traverse to the other.

A traverse was made along the centerline of the jet at more than the above six axial locations using a pitot-static probe. This was done at one compressor speed only, 3000 rpm (M_E = .24).

Total pressure in the jet was measured utilizing a 1/8 inch diameter pitot-static probe mounted at the nozzle exit centerline. The pitot-static probe was mounted onto the traversing mechanism used for the hot-wire measurements, see Figure 2. The static and total pressure taps from the pitot-static probe were connected via plastic tubing to manometers. The total pressure was read from a reservoir type water or mercury manometer depending on the jet exit velocity. Static pressure was always connected to a reservoir type water manometer.

The static pressure in the plenum chamber was measured at three locations at the side of the plenum chamber, see Figure 2. All static pressure data from the plenum chamber was taken utilizing a U-tube type water manometer.

Static pressure in the anechoic chamber was obtained by an inclined manometer, using red gage oil (S.G. = .826), connected to the inside of the anechoic chamber via a plastic tube. The free end of the tube was located near the chamber door, see Figure 1.

Atmospheric pressure during the tests was recorded using a barometer that is part of the DISA type 55D90 calibrator.

Hot wire measurements of the mean and fluctuating velocities in the jet were made using a single wire probe with a DISA anemometer and linearizer as shown in figure 3. The type of probe and anemometer bridge circuit used provided for temperature compensation. This was to eliminate any affects due to the temperature differences in the jet from those during calibration of the hot-wire. Calibration of the circuit was performed using a DISA type 55D90 calibrator.

The signal coming from the linearizer was read from DISA D.C. and R.M.S. voltmeters, see Figure 4.

The hot-wire was mounted on a traversing mechanism providing three axis position control and is shown in Figure 2.

The output voltage of the linearizer was fed into a narrow-band spectrum analyzer. (Unfortunately the spectrum analyzer was was available only during the test run with a compressor speed of 3000 rpm (M_E = .24) and only for a few measurements at certain locations in the jet.)

Some of the data was taped. But only for a compressor speed of 3000 rpm and at selected locations in the jet. For the taped data the signal from a microphone at microphone position 3 (see description of acoustic calibration, Part A) was included along with the signal from the hot-wire, see Figure 3.

Particulate matter was found to be present in the jet. Most probably it is oil originating from the compressor. The presence

of such a material contaminated the hot-wire changing the calibration curve. Thus it was not possible to obtain absolute velocity profiles using the hot-wire although it was possible to measure velocity profiles normalized with respect to the jet centerline velocity at the axial location of the profile from the nozzle exit.

The presence of oil particles in the jet destroyed the calibration of the hot-wire as soon as the hot-wire entered the jet. Without knowing the calibration curve of the hot-wire at the time of measurement it is impossible to obtain absolute velocity using the hot-wire.

With the hot-wire positioned in the potential core of the jet it was possible to see the hot-wire being struck by an oil particle by monitoring the hot-wire output voltage. Upon being hit the D.C. output voltage would shift and the R.M.S. voltage would jump appreciably.

By assuming that the calibration curve, at any instant of time, of the hot-wire changed slowly with time it was possible to still obtain velocity profiles in the jet. With this assumption the D.C. voltages of points away from the centerline were normalized using the centerline D.C. voltage. Only a few points were taken away from the centerline and then a reading at the centerline itself. Repeating this procedure it was possible to build up a normalized velocity profile. The D.C. reading at the centerline, at the axial location of the profile, was used to normalize the other readings. The turbulence intensity profiles were contructed

in the same way. Except the R.M.S. readings were normalized utilizing the centerline D.C. voltage.

4. RESULTS AND DISCUSSION

4A. Nature of Nozzle Flow

It was found that the total pressure measured at the center of the nozzle exit cross-section and the static pressure measured at the wall of the plenum chamber are equal. This allows the jet exit quantities, such as velocity, to be determined assuming 1-D inviscid compressible flow for isentropic conditions.

With isentropic flow through the nozzle the exit Mach number can be calculated directly knowing just the plenum pressure and the nozzle exit static pressure assuming 1-D inviscid compressible flow. The ratio of the plenum static pressure to the nozzle exit static pressure is referred to as the nozzle pressure ratio. This parameter determines the nozzle exit Mach number (see Appendix).

The additional knowledge of another plenum flow quantity, total temperature, allows the nozzle exit velocity to be calculated directly (see Appendix). But the significant parameter for both calculations of nozzle exit conditions, such as Mach number and velocity is the nozzle pressure ratio. For the control of nozzle exit conditions the compressor rpm has been used exclusively. It is therefore suggested that a more accurate measure of establishing a flow with specific characteristics, such as a required jet exit velocity for instance, would be the pressure ratio (P_T/P_A).

The nozzle pressure ratio versus compressor rpm is shown in Figure 5.

For the nozzle pressure ratio the total pressure (P_T) is normalized using the atmospheric pressure (P_A) instead of the nozzle exit static pressure. The nozzle exit static pressure is the room pressure and is slightly less than atmospheric depending on the compressor rpm. But the difference in the nozzle pressure ratio is negligible by using the atmospheric pressure as the normalizing factor rather than the room pressure. The affect on the calculation of the exit Mach number or velocity is small.

Utilizing the nozzle pressure ratio it is possible to calculate the exit Mach number (M_E) directly (see Appendix). The result of this calculation is shown in Figure 6. It was found that the exit Mach number varies linearly with compressor rpm. At 12000 rpm the exit Mach number is .96. This is larger than the exit Mach number of .85 at 12000 rpm predicted by the NEAR Design Report (Reference 1). Figure 7 is a comparison of the design reports prediction with the exit Mach number as determined by these tests. The exit Mach number determined by these measurements is always larger at any compressor rpm than the one predicted by the NEAR Design Report.

At present the heat exchanger (see Figure 1) is not in place. It was removed after it was found to generate acoustic disturbances. The calculations in the design report for the exit Mach number included the pressure loss due to the heat exchanger. Thus the measured values of the exit Mach numbers over the ones

in the NEAR Design Report may possibly be due to the absence of the heat exchanger from the flow path.

4B. Anechoic Chamber Pressure Variation

Due to inadequate chamber ventilation jet entrainment causes a pressure drop in the chamber. Figure 8 shows the pressure difference across the walls of the chamber versus compressor rpm. The affect of this inadequate chamber ventilation on the flow around the collector is reported in part A (Acoustic Measurements).

This pressure difference can pose a personnel hazard, not necessarily in itself, but by making it difficult to open the chamber door, which opens outwards. When operating at high compressor rpm, above 6000 rpm, it is difficult for even two men to get the chamber door open. This poses a hazard to personnel inside the chamber during jet operation if for some reason (such as fire) exiting the chamber quickly becomes necessary.

It is recommended that contact between the control room and personnel in the chamber be maintained at all times when running at high compressor rpm. In case a quick exit becomes necessary the compressor rpm can then be lowered expeditiously. A better solution would be to install a compressor cut-off switch inside the chamber near the door.

4C. Nozzle Exit Mean Flow Velocity

The mean velocities at the nozzle exit for the two compressor speeds, 3000 and 6000 rpm, used in the hot-wire measurements

are shown in Figure 9. The velocities as measured by the hot-wire are compared to those calculated (see Appendix) using the nozzle pressure ratio. Also included is a calculation based on using the nozzle exit Mach number and multiplying it by the speed of sound at standard conditions. All of the values agree well. The values based on the nozzle pressure ratio are probably more accurate. Since that data was taken utilizing a pitot-static probe which is probably unaffected by the oil mist in the jet, unlike the hot-wire acquired data.

4D. Normalized Mean Velocity Profiles

From the mean velocity data obtained utilizing the hot-wire and a pitot-static probe it is possible to make the following observations about the jet characteristics.

1. The jet is symmetric.
2. The spreading of the jet is independent of the nozzle exit velocity (or Reynolds number).
3. The length of the potential core is 4.5 nozzle exit diameters downstream from the exit plane.

As explained previously, even though the hot-wire was contaminated it was possible to construct normalized mean velocity profiles. The mean velocity data at each profile location was normalized using the jet centerline mean velocity at the axial location of each profile. Normalized velocity profiles are shown for axial locations X/D = 1.5, 3, 6, 9, and 12. No normalized

velocity profile is shown for the nozzle exit, X/D = 0. At the nozzle exit the jet exhibits a tophat mean velocity profile.

The normalized velocity profiles for a compressor speed of 3000 rpm (M_E = .24) are shown in Figures 10-14. The scatter in the data is due to the limitations of the facility conditions and method of measurement. (The data was taken by hot-wire which was contaminated.)

Overlaying the normalized velocity profiles obtained at a compressor speed of 6000 rpm (M_E = .48) on those obtained at 3000 rpm (M_E = .24) results in Figures 15-19. Again scatter is evident in the data. But the scatter at 6000 rpm appears to be smaller (5%) while that at 3000 rpm shows larger variations (5 - 8%). However, the profiles at both speeds show fair agreement.

This general agreement indicates that the jet spreading is independent of the nozzle exit velocity (or jet Reynolds number based on nozzle exit diameter). Which is as it should be for Reynolds numbers above a few thousand based on nozzle exit diameter. At a compressor speed of 6000 rpm (M_E = .48) the jet Reynolds number, based on diameter, is 10^6. The jet Reynolds number at 3000 rpm (M_E = .24) is just half that at 6000 rpm.

To within the scatter present in the normalized velocity profiles it can be stated that the jet is symmetric. The profiles were contructed using data from both axes of traverse, horizontal and vertical. Data taken from both axes falls within the band of scatter for the profiles. This indicates that the profiles are symmetric at least to the order of error in the data (5 - 8%).

The utilization of a measurement method not affected by the oil mist contamination, such as pitot-static pressure survey or laser anemometry, in the jet will allow accurate measurement of the mean velocity profiles.

Mean velocity measurements were taken along the centerline of the jet at a number of axial locations utilizing a pitot-static probe at a compressor speed of 3000 rpm (M_E = .24). The mean velocity along the jet centerline was normalized using the nozzle exit velocity. Figure 24 shows the normalized velocity along the jet centerline. The data indicates that the potential core ends at X/D = 4.5. This is a typical value for a round jet (Reference 2). Approximate calculations using the normalized velocity profile data result in a potential core length in the range of X/D = 4 to 5. At a compressor speed of 6000 rpm (M_E = .48) the potential core should be the same as that at 3000 rpm since the jet spreading is independant of nozzle exit velocity. Unfortunately no pitot-static data was taken at a compressor speed of 6000 rpm.

In the fully developed region of a round jet the jet centerline velocity decreases linearly with distance from the end of the potential core. The data in Figure 24 shows this linear decrease after the potential core. At X/D = 12 it appears that the slope of the curve is changing. It is not clear if the jet is fully developed yet by X/D = 12. More than likely the transition region occupies the majority of the range X/D = 4.5 to 12.

Figure 25 shows a comparison of the normalized jet centerline velocity obtained using the hot-wire to the pitot-static

data. Only at X/D = 12 does the hot-wire data from both jet speeds agree with the pitot-static data. The agreement is not so good over the rest of the curve. But due to the problems of contamination, as already stressed, of the hot-wire this is not unexpected. This comparison is ment to indicate the errors in using hot-wire anemometry for aerodynamic measurements of the jet in its present condition. All the hot-wire data shown in Figure 25 was taken immediately after calibration with minimum time in the jet. Still differences are large. The conclusion is again that one cannot escape the effects of contamination possibly due to the presence of oil mist in the jet flow.

4E. Turbulence Intensity Profiles

Turbulence intensity profiles at compressor speeds of 3000 and 6000 rpm (M_E = .24 and .48) are shown in Figures 20 and 21. Due to the method of measurement, utilizing the hot-wire in the oil contaminated environment of the jet, the profiles should be viewed with caution. There is substantial scatter in the profiles, on the order of 10% in each profile. Although the profiles do not correspond to absolute measurements they do show the trends expected.

It is interesting that when the profiles from both speeds are overlayed that those profiles at X/D = 9 and 12 show fair agreement. For the fully developed region this is what is expected, i.e. the turbulence intensity profiles should be independent of the nozzle exit velocity.

Taking just the turbulence intensities along the centerline and plotting them versus X/D, results in Figures 22 and 23. When overlaying these curves the turbulence intensities at X/D = 6, 9, and 12 for both speeds show fair agreement. For X/D less than 6 the centerline turbulence intensities at 3000 rpm are less than those at 6000 rpm. This seems to indicate that the turbulence intensity in the potential core increases with nozzle exit velocity.

Accurate measurements of the turbulent fluctuations in the jet will have to presuppose the elimination of the present problem of hot-wire contamination, or the use of a measurement method which is not affected by the oil mist contamination such as laser anemometry for instance.

4F. Spectra of Velocity Fluctuations

The frequency spectra of the velocity fluctuations are shown in Figures 26-40. They are only for a compressor speed of 3000 rpm (M_E = .24) and at axial locations of X/D = 6, 9, and 12. (The narrowband spectrum analyzer was available only at that speed and at those locations.)

Except for a spike observed in each spectra at 7.3 kHz nothing unusual is observed. The cause for the 7.3 kHz spike is not known at the moment (originally it was thought to be due to the compressor, but calculation shows the blade passage frequency of the compressor at 3000 rpm to be .8 kHz). The instrumentation being the source of the spike is not likely since when the jet was turned off the spike disappeared.

SOME COMPARISONS
OF THE MEASURED AERODYNAMIC QUANTITIES
WITH THE THEORETICAL
RESULTS OF TOLLMIEN AND GOERTLER
AND SOME OTHER RELEVENT EXPERIMENTS

4G. Comparisons With Theories and Other Experiments

An effort was made to assess the measured aerodynamic quantities in light of the theoretical work of Tollmien and Goertler and other relevant experimental work. The results are shown in Figures 41 to 45 and are briefly discussed below.

From Fig. 41 it is seen that the measured mean jet centerline velocities fall within the range predicted by both the Tollmien and Goertler theories for about $\frac{x}{d} \geq 7$, i.e within the fully developed region and beyond the potential core. The measured results agree much better with Tollmien's predictions than those of Goertlers. It is also seen from the Fig. 41 that the virtual origin of the jet is about 0.35d behind the nozzle exit and a straight line fit to the (straight line - type part of the data) yielded the equation:

$$\frac{U_m}{U_o} = \frac{6.97}{\frac{x}{d} + 0.35}$$

The above equation compares reasonably well with the experimental results of Hinze and Zijnen (1949) who obtained the numerical relation:

$$\frac{U_m}{U_o} = \frac{6.39}{\frac{x}{d} + 0.6}$$

Figures 42 and 43 show again comparisons of the measured axial component of the jet speed with that predicted by the Tollruien and Goertler theories. As have been observed by others the predictions of Tollmien's theory fit much better the experimental values for the larger values of r/b (≥ 1), i.e away from the centerline, whereas

close to the centerline Goertler's theory seems to apply better ($r/b \leq 1$).

Figure 44 shows the variations of the turbulent intensity associated with the x-fluctuating velocity component. Most data available from previous work are for $\frac{x}{d} = 50$ or higher with one or two exceptions for a value of $\frac{x}{d} = 20$. In the range of our experiments, i.e. for $1.5 \leq \frac{x}{d} \leq 12$ probably the only other comparable data are those of Sami et al., (1967), who examined the region $1 \leq \frac{x}{d} \leq 10$. Their results are reproduced in Fig. 45. Comparing Figs. 44 and 45 we see that the two sets of data are remarkably similar not only with respect to the general trend of the curves for the same $\frac{x}{d}$ values but even as to specific numerical values, such as the tendency for peaks at $\frac{r}{r_o} \sim 1$, the range of values at $\frac{r}{r_o} = 0$, i.e. on the jet axis, etc. Note that the conditions of Sami et al. in Fig. 45 (1ft. diameter nozzle; exit speed 35ft/sec) are tottally different from those pertaining to ours in Fig. 44 (4" diameter nozzle; exit speed $\sim$ 270 ft/sec) these results probably indicate that self preservation of the mean quantities of a turbulent jet, which is known to exist some few diameters downstream of the nozzle exit, may also be true for the fluctuating quantities and not only for large distances downstream. From numerous experiments and the theory of self preserving axisymmetric turbulent jets, one expects that the fluctuating (turbulent) quantities should be self-preserving for very large $\frac{x}{d}$ (far enough downstream of the nozzle exit). But for $\frac{x}{d}$ not large the initial conditions at the nozzle exit, where the annular shear layer starts, neither adequate, let alone extensive, experiments,

nor an appropriate analytical model exist. In view of our preliminary deductions above in comparing our results of Figure 44 to those of Sami et al. (Fig. 45) we suggest that an investigation conserving the nature or possible existence of self-similarity for the turbulent intensities close to the nozzle exit be undertaken.

Finally on the basis of the measured velocity profiles we have made an estimate of the entrainement velocity for various $\frac{x}{d}$ for the case of 3000 r.p.m. compressor speed. These are given below, where the following nomenclature has been used:

$Q(x)$ = Flow rate of the jet out the location x from the nozzle exit.

$\bar{b}$ = Radius where the axial velocity is negligibly small

v_e = Entrainment velocity

Q, $\bar{b}$ and v_e are related by

$$\frac{dQ}{dx} = 2\pi \bar{b} v_e$$

	v_e (m/sec)	$\bar{b}$ (m)	dQ/dx (m^2/sec)
$\frac{x}{d} = 1.5$	1.09	0.0875	0.60
$\frac{x}{d} = 3.0$	1.70	0.1125	1.20
$\frac{x}{d} = 6.0$	1.00	0.1500	0.97
$\frac{x}{d} = 9.0$	0.80	0.2000	1.000

5. SUMMARY

Flow through the 4" diameter round nozzle is isentropic. This enables the exit Mach number to be fixed by utilizing the pressure in the plenum chamber. If the total temperature of the flow in the plenum chamber were known then it would be possible to calculate the nozzle exit velocity.

The jet is symmetric and displays no unusual characteristics. The potential core length of the jet is approximately 4.5 nozzle exit diameters. Jet spreading was found to be independent of nozzle exit velocity.

Particulate matter, most probably in the form of oil mist probably emanating from the compressor, is present in the jet. This matter contaminates the hot-wire making the interpretation of any hot-wire measurements extremely difficult. Until the contamination is eliminated or properly accounted for it will not be possible to make any accurate absolute hot-wire measurements in the jet.

There is inadequate mass flow provided by chamber ventilation for jet entrainment. This results in a pressure drop in the chamber which although it does not affect the aerodynamic characteristics of the jet it does pose a possible personnel hazard by preventing people inside the anechoic chamber operating with closed door to open the door. The problem is particularly severe at compressor speeds above 6000 rpm.

REFERENCES

1. Wooley, J. P., Karamcheti, K. and Mendenall, M. R.: The Design of an Open-Throat Wind Tunnel. Nielsen Engineering and Research (NEAR) Technical Report 66, March 1974.

2. Rajaratnam, N.: Turbulent Jets. Chapters 2 and 6, Elsevier Publishing Company, 1976.

3. Soderman, P. T.: Acoustic Calibration of the Large-Scale Aerodynamics Branch Anechoic Chamber. FSA Technical Memorandum, No. 15, November 1975.

APPENDIX

1. NOZZLE EXIT MACH NUMBER CALCULATION

For 1-D inviscid compressible isentropic flow the energy equation may be written in the form

$$(1) \quad \frac{P_T}{P_E} = \left(1 + \frac{\gamma - 1}{2} M_E^2\right)^{\frac{\gamma}{\gamma - 1}}$$

where; P_T = Total pressure in the plenum chamber (or at the nozzle exit centerline)

P_E = Static pressure at the nozzle exit centerline

γ = Ratio of specific heats (for air) 1.4

M_E = Mach number at the nozzle exit centerline

From the experimental results it can be assumed that $P_E = P_A$, for a wide variety of conditions*

where; P_A = atmospheric pressure

Rewriting (1) yields the relation for calculating nozzle exit Mach number knowing the plenum chamber pressure.

$$M_E = \left\{\left(\frac{2}{\gamma - 1}\right)\left[\left(\frac{P_T}{P_A}\right)^{\frac{\gamma - 1}{\gamma}} - 1\right]\right\}^{\frac{1}{2}}$$

*It is not possible from the method of measurement to know if $P_E = P_A$ or is equal to the chamber pressure which is less than P_A. All indications are that $P_E = P_{rm}$, the chamber pressure. The difference between P_A and P_{rm} is negligible on the calculation of M_E or U_E.

2. NOZZLE EXIT VELOCITY CALCULATION

For 1-D inviscid compressible isentropic flow the energy equation may be written in the form

$$(2) \quad \frac{1}{2} U_E^2 + \frac{\gamma}{\gamma - 1} \frac{P_T}{\rho_T} \left(\frac{P_E}{P_T} \right)^{\frac{\gamma - 1}{\gamma}} = \frac{\gamma}{\gamma - 1} \frac{P_T}{\rho_T}$$

where; U_E = Velocity at the nozzle exit centerline

ρ_T = Flow density in the plenum chamber

Allowing, as before, $P_E = P_A$ and rewriting (2) results in

$$U_E = \left\{ \left(\frac{2\gamma}{\gamma - 1} \right) \left(\frac{P_T}{\rho_T} \right) \left[1 - \left(\frac{P_T}{P_A} \right)^{\frac{\gamma - 1}{\gamma}} \right] \right\}^{\frac{1}{2}}$$

This relation could be used to calculate the nozzle exit velocity (U_E) if only the flow density (ρ_T) were known in the plenum. For the calculations in Figure 9 the density (ρ_T) was assumed to be that of air at standard conditions ρ_T = .00234 slugs/ft^3 (.00121 gm/cm^3).

In order to calculate the density accurately it would be necessary to know the temperature of the flow in the plenum chamber.

Since flow velocity in the plenum is probably quite low there is effectively no difference between the total and static temperature in the plenum.

NOTE: At present temperature sensors (thermocouples) have been installed in the plenum chamber. They are located at the wall of the plenum chamber. All indications are that they are not measuring the total temperature of the flow in the interior of the plenum. But are measuring the temperature of the walls of the plenum chamber. So these temperature sensors should not be relied upon for measurements of flow temperature.

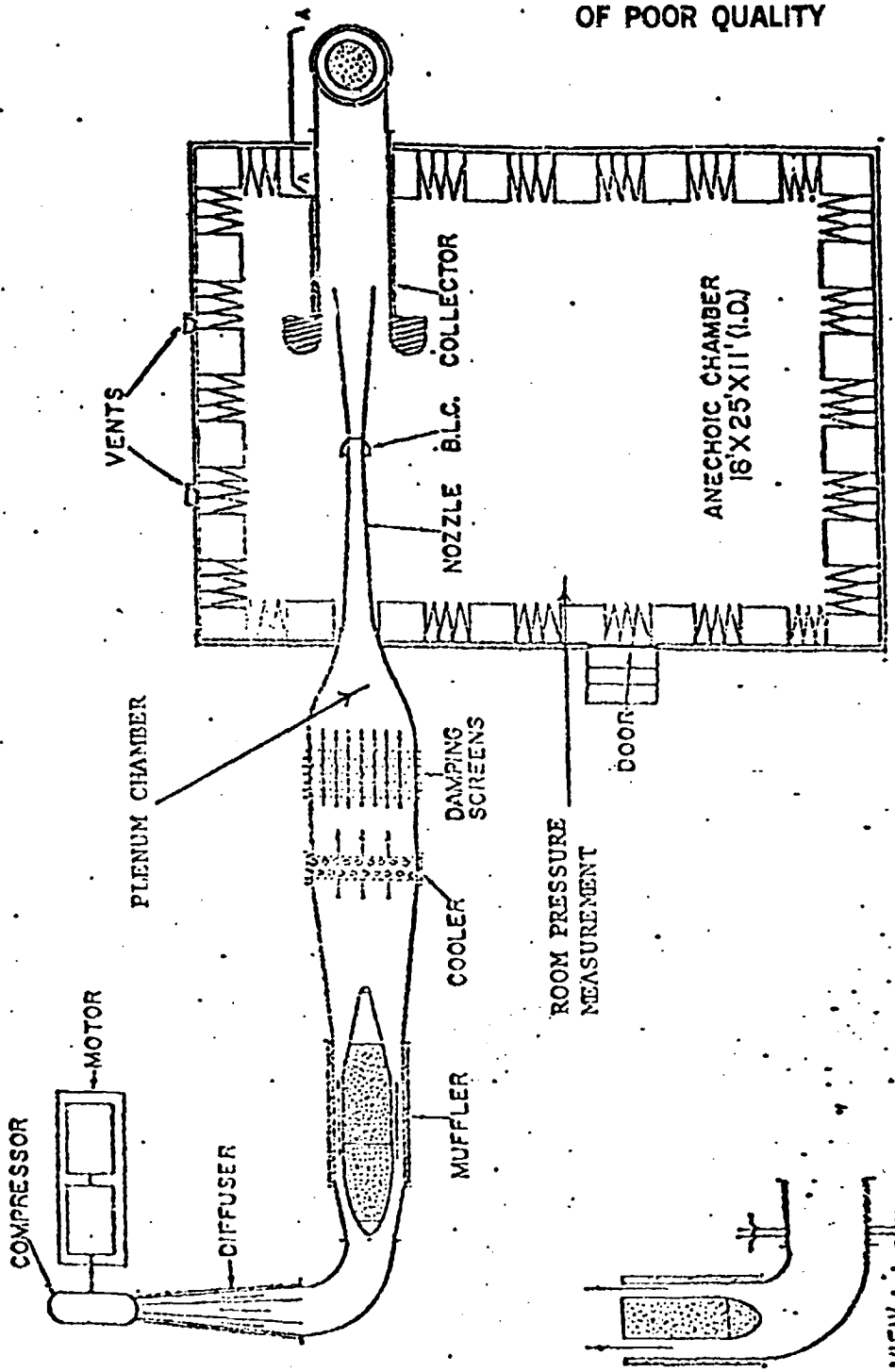

Figure 1.- General arrangement of anechoic open-throat wind tunnel.

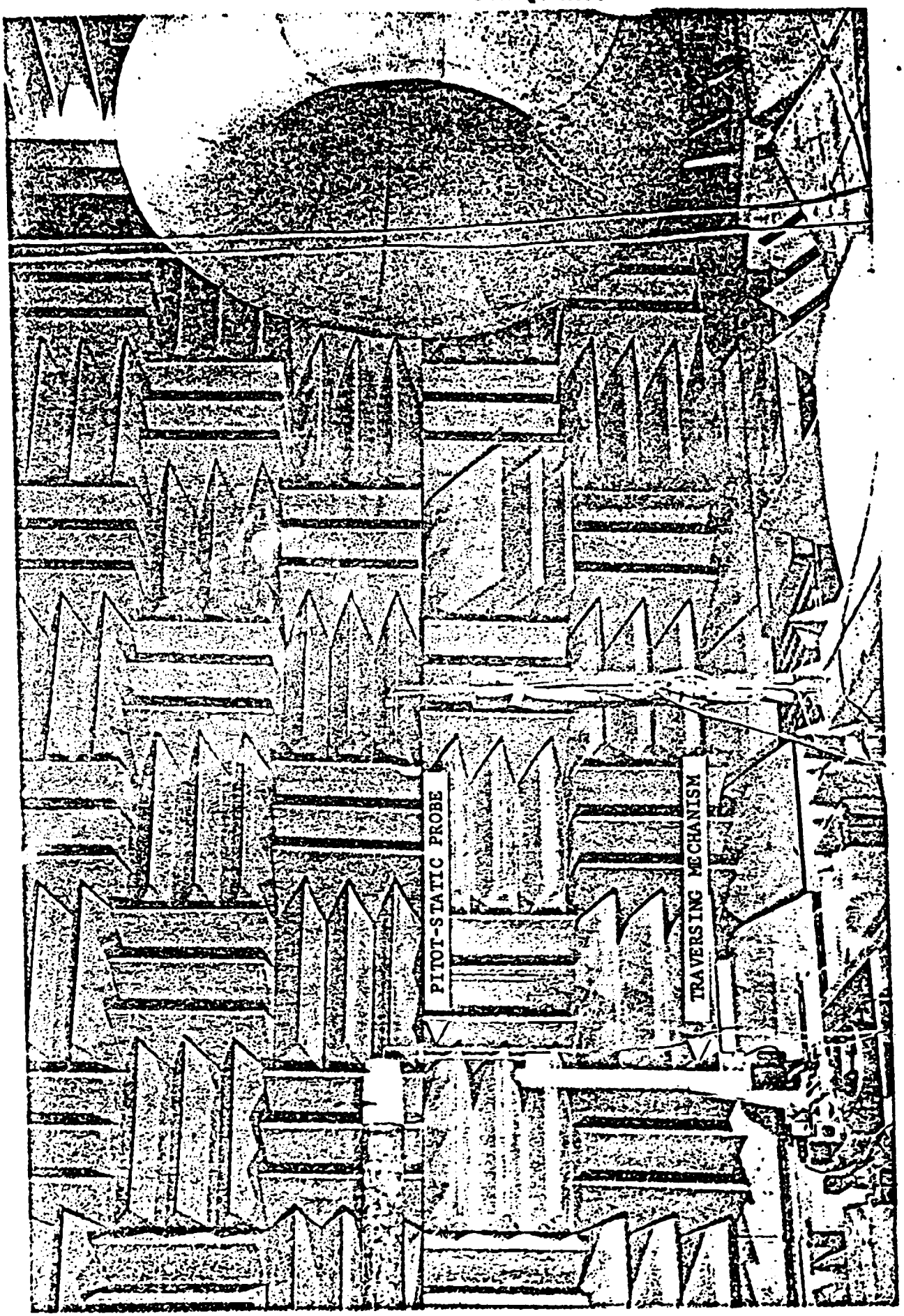

FIGURE 2

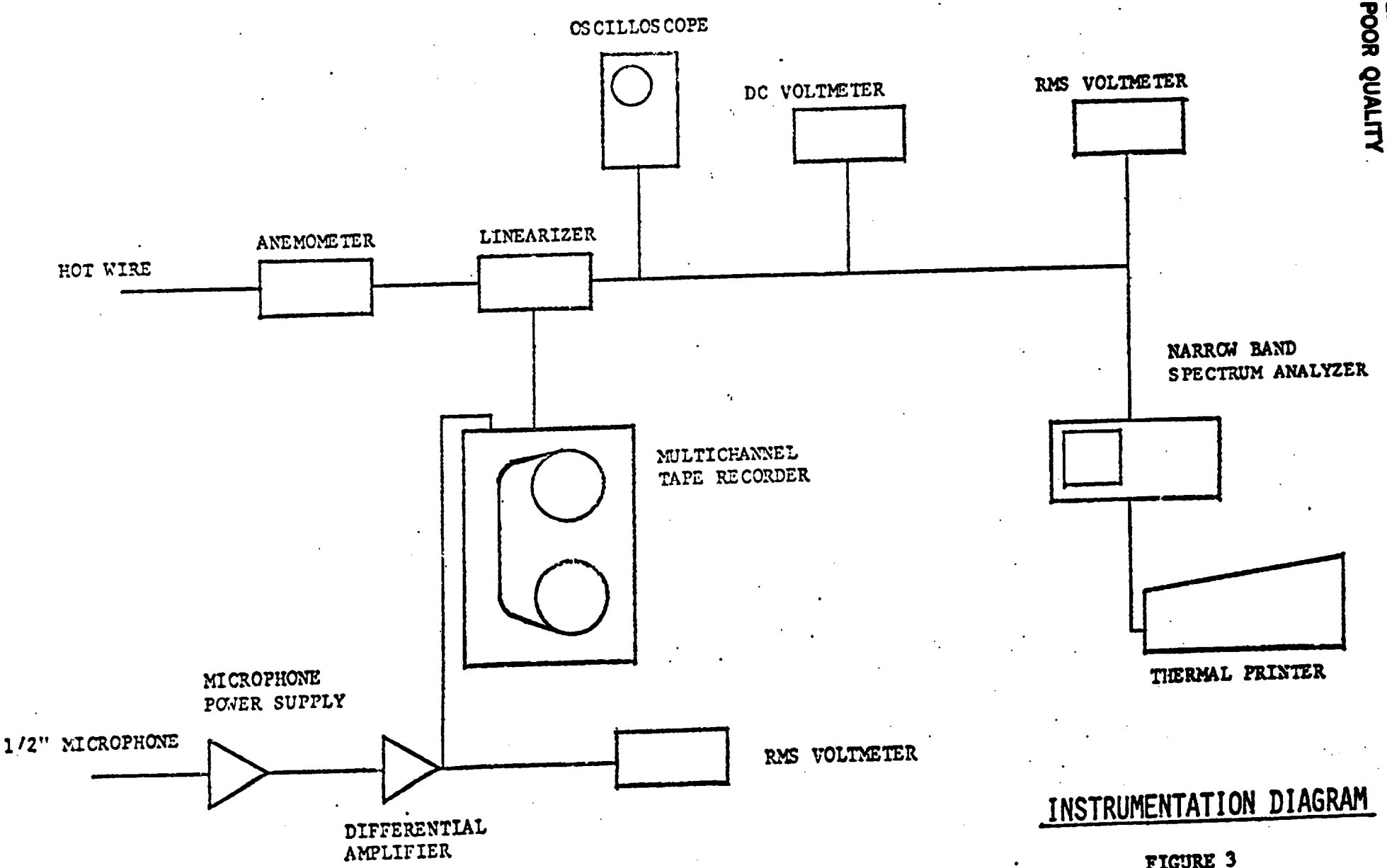

INSTRUMENTATION DIAGRAM

FIGURE 3

INSTRUMENTATION LIST

	NASA No.
Hot Wire (DISA, Type 55P86)	
Main Unit (DISA, Type 55M01)	52142-79
Temperature Compensating Bridge (DISA, Type 55M14)	52144-79
Linearizer (DISA, Type 55D10)	52149-79
DC Digital Voltmeter (DISA, Type 55D31)	47612-79
RMS Voltmeter (DISA, Type 55D35)	40338-79
Tape Recorder (Ampex, FR-1300)	44583-79
Oscilloscope (Textronix, Type 55)	25847-79
Differential Amplifier (Textronix, AM 502)	52477-79
Microphone Power Supply (B&K, Type 2807)	41966-79
X-Y Recorder (H.P., 7004B)	45008-79
Narrow Band Real Time Spectrum Analyzer (Gen-Rad, Model 2512)	
Hot-wire Calibrator (DISA, Type 55D90)	

FIGURE 4

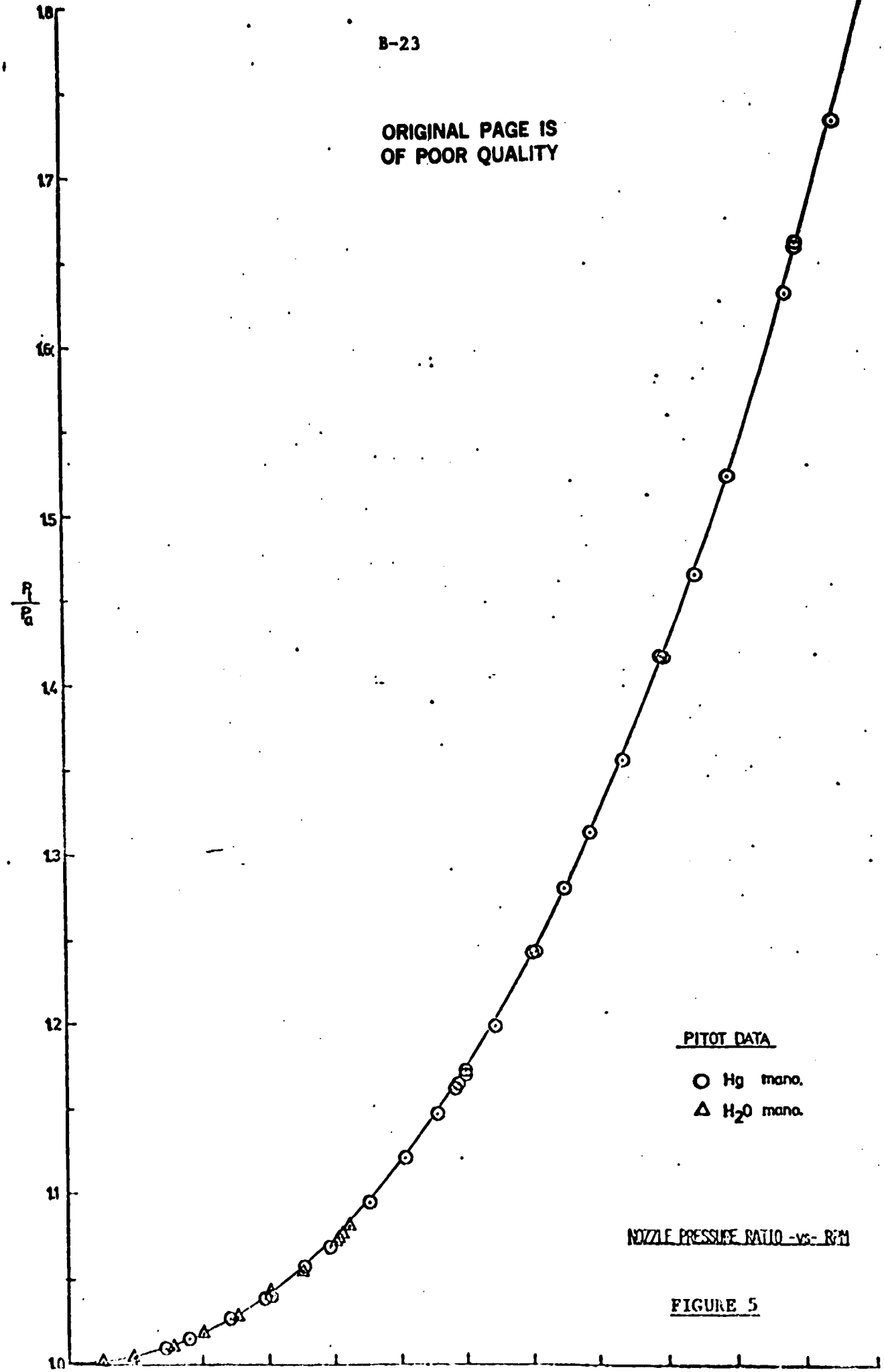

FIGURE 5

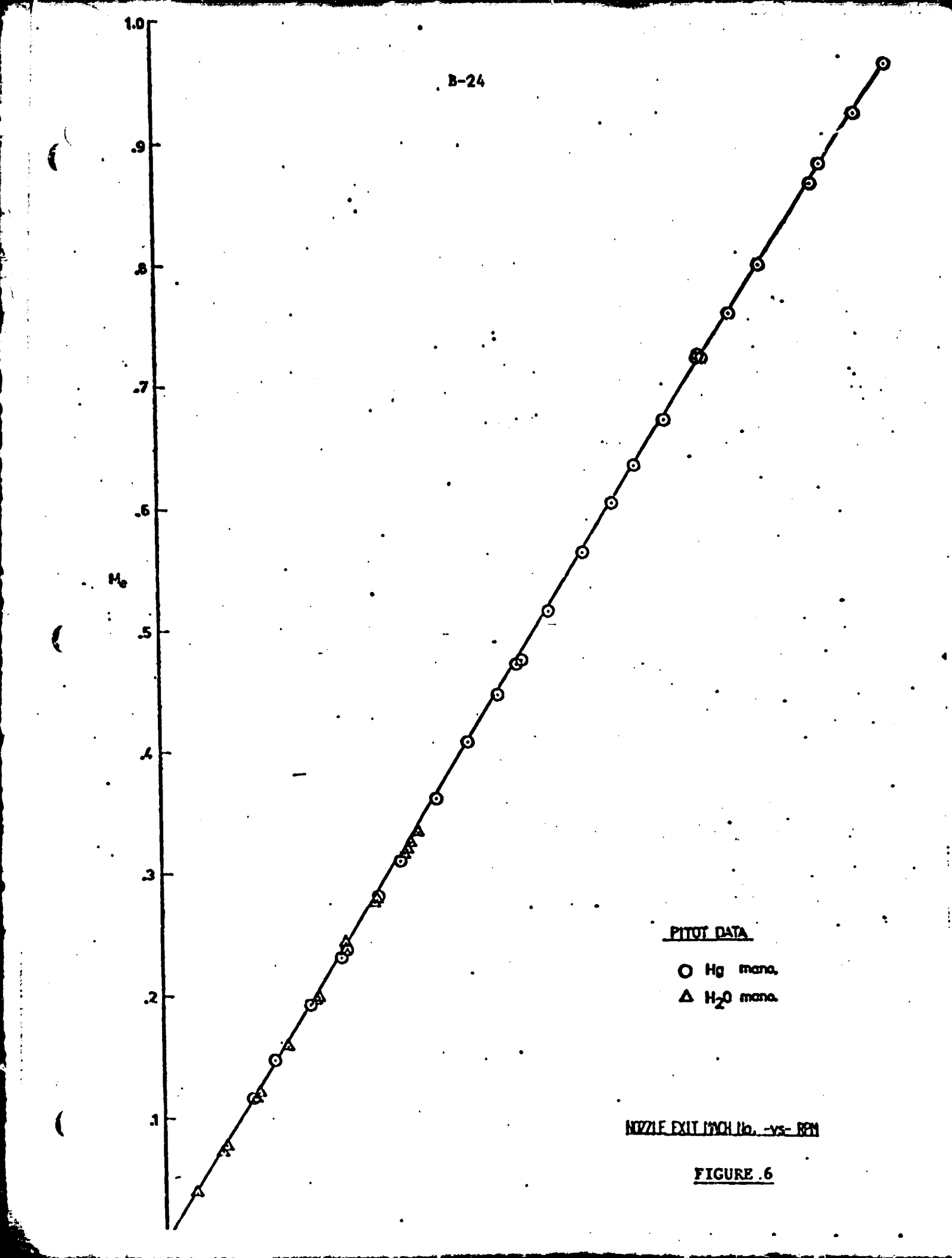

NOZZLE EXIT MACH No. -vs- RUN

FIGURE .6

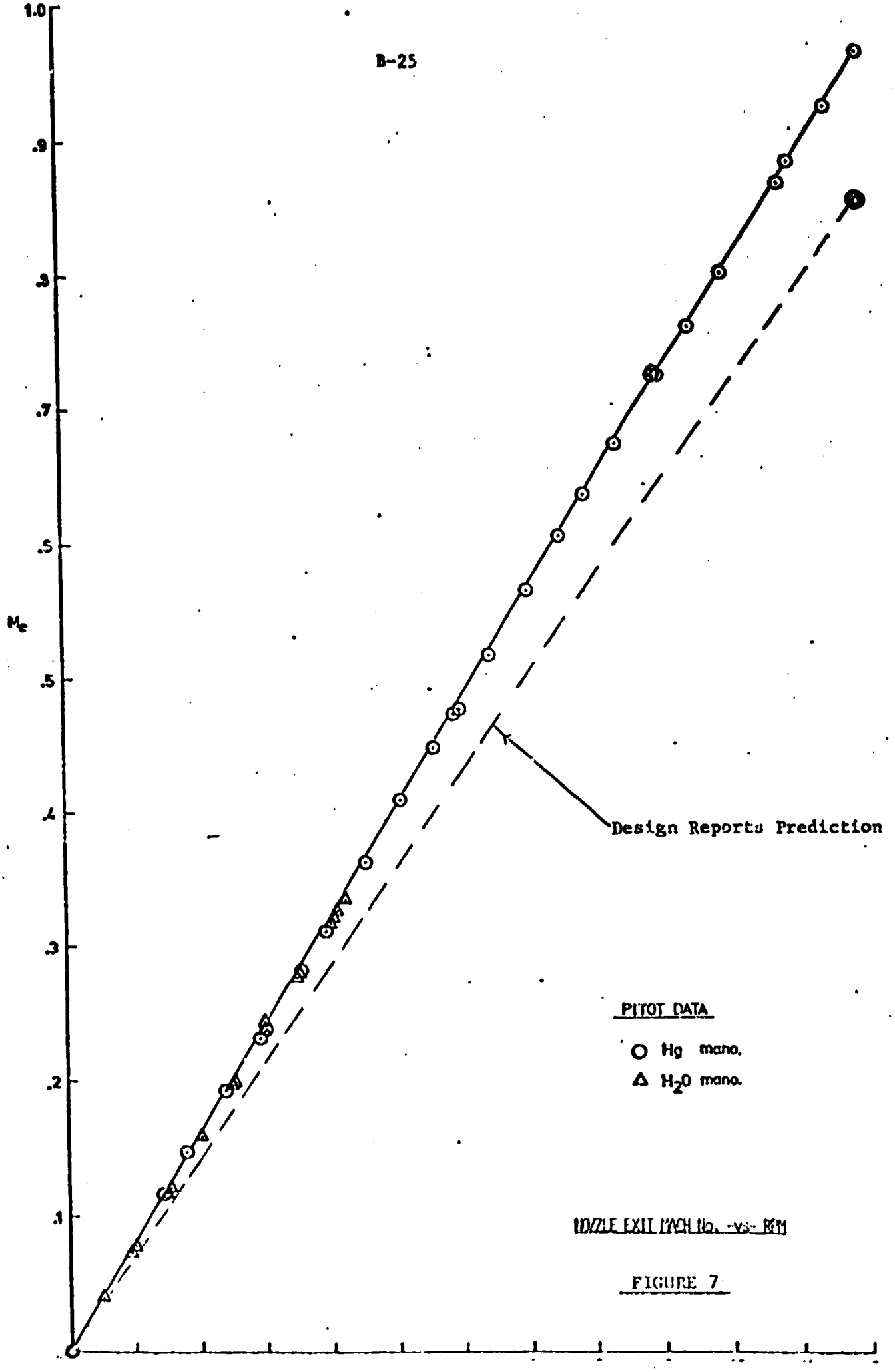

NOZZLE EXIT MACH No. -vs- RPM

FIGURE 7

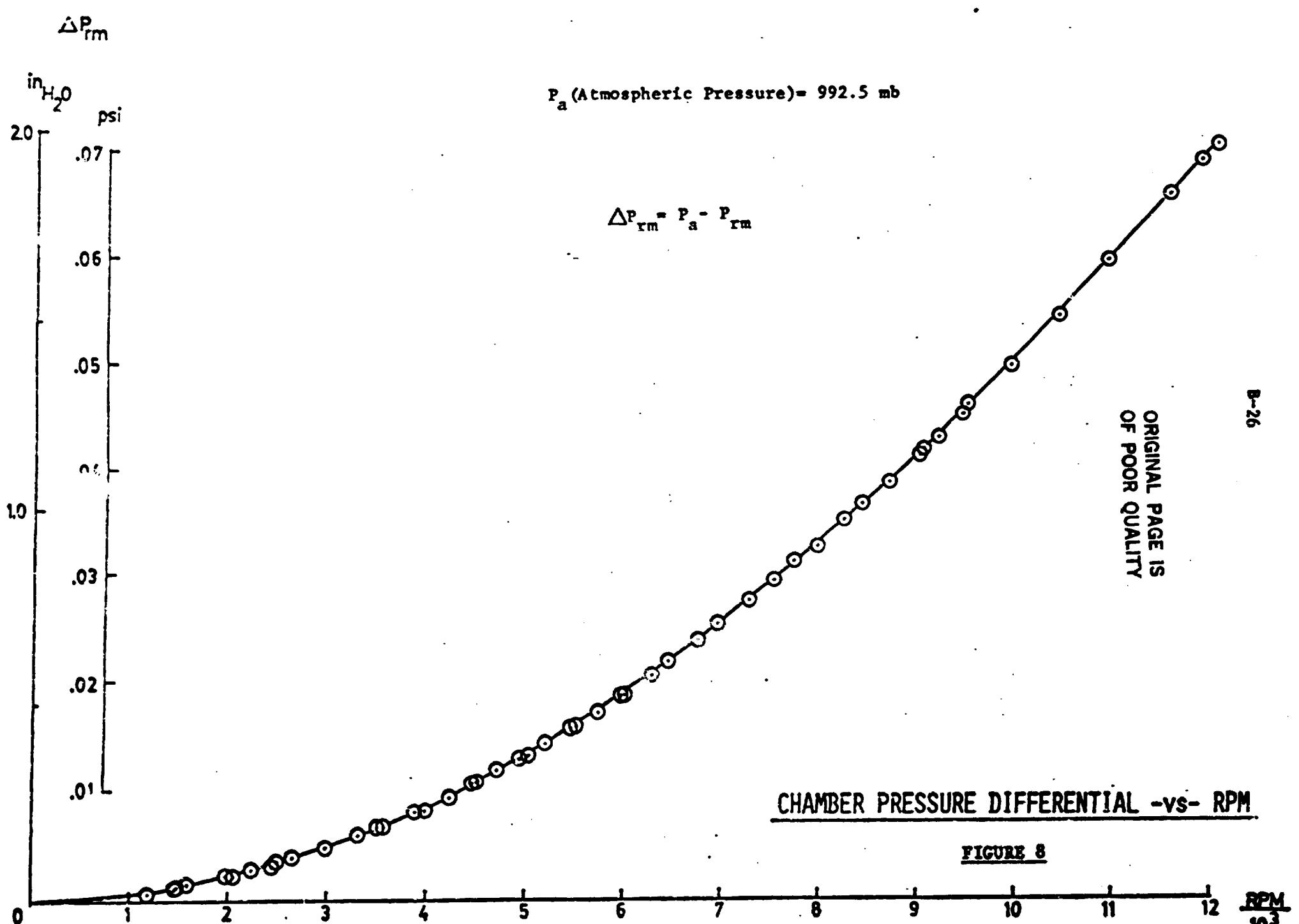

P_a (Atmospheric Pressure)= 992.5 mb

$\Delta P_{rm} = P_a - P_{rm}$

ORIGINAL PAGE IS
OF POOR QUALITY

B-26

CHAMBER PRESSURE DIFFERENTIAL -vs- RPM

FIGURE 8

EXIT VELOCITY, U_o (m/s)

RPM	Hot Wire	Calculated, Based On:	
		Mach No.	Pressure Ratio
3000	78.6	79.4	81.7
6000	166.9	158.9	171.9

FIGURE 9

NORMALIZED MEAN VELOCITY PROFILES

3000 RPM (M_E = .24)

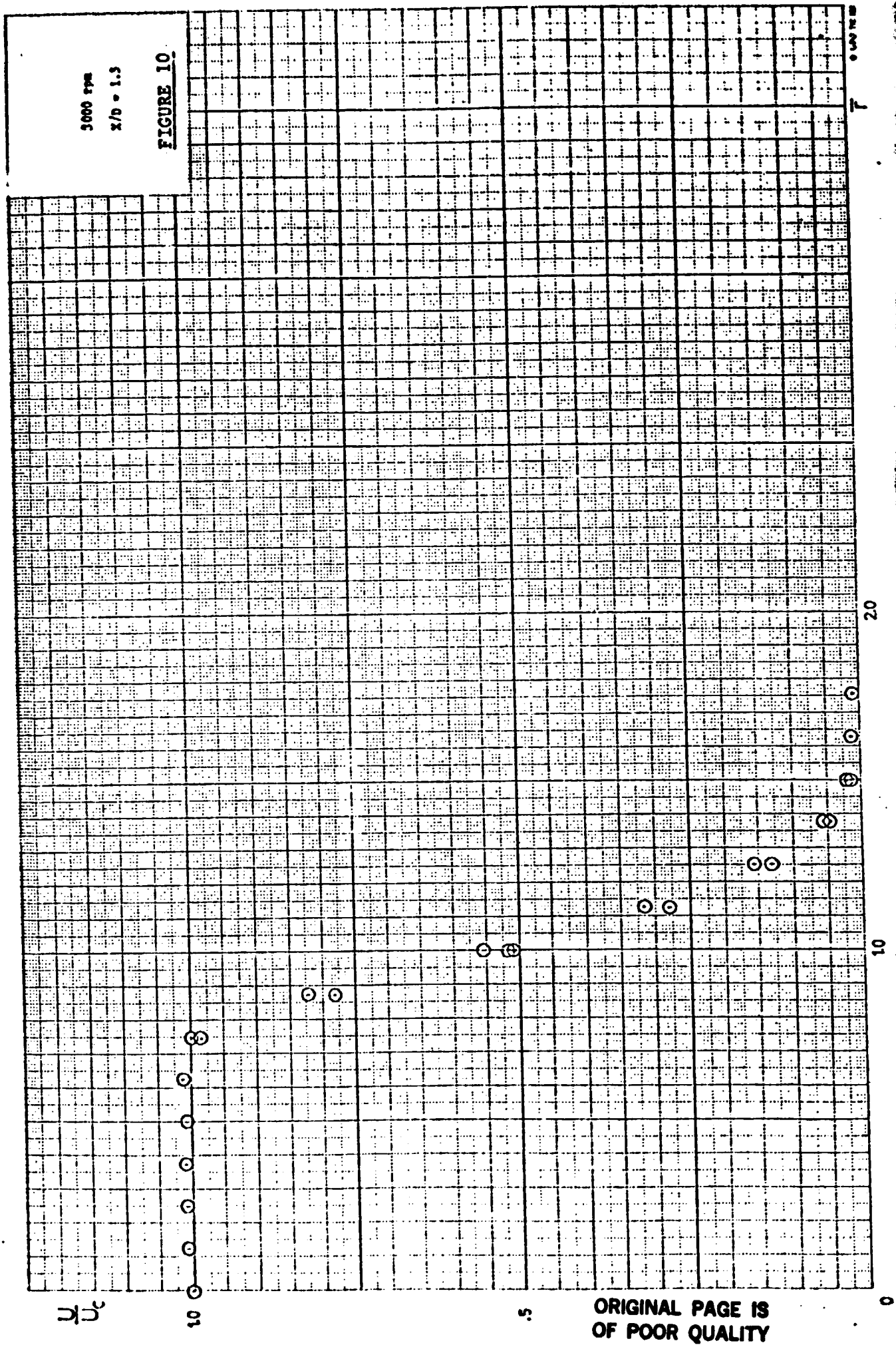

FIGURE 10

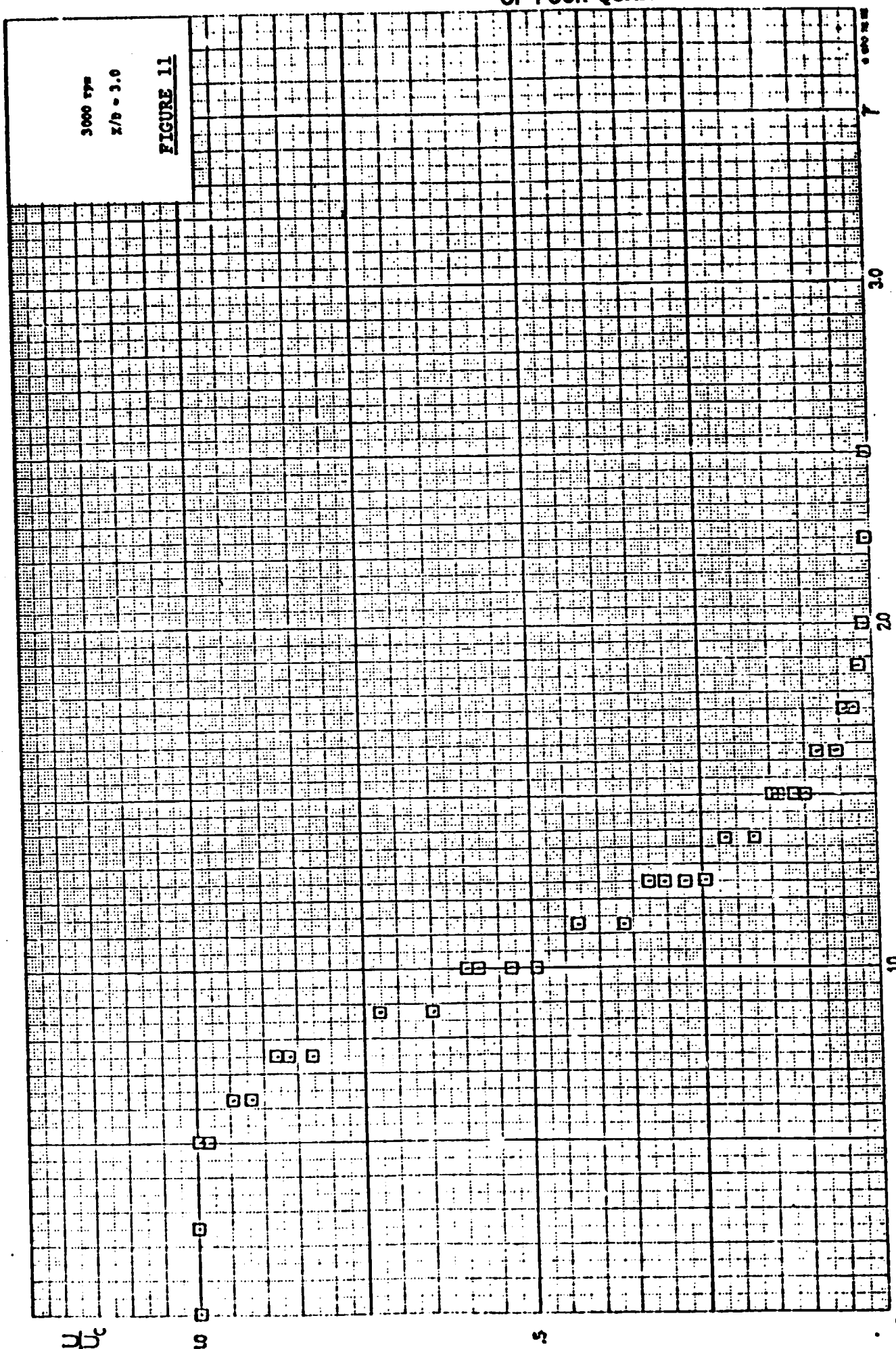

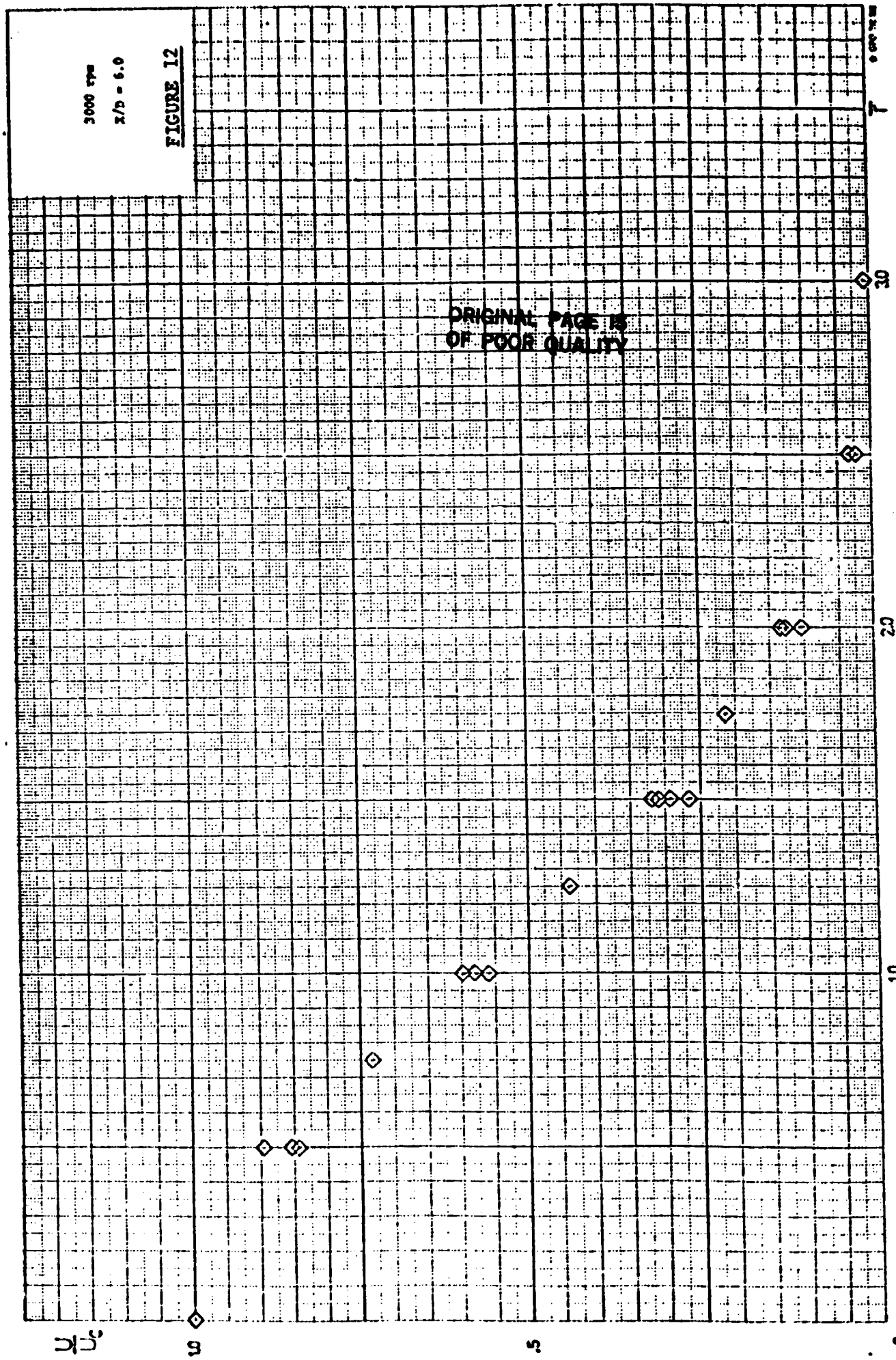

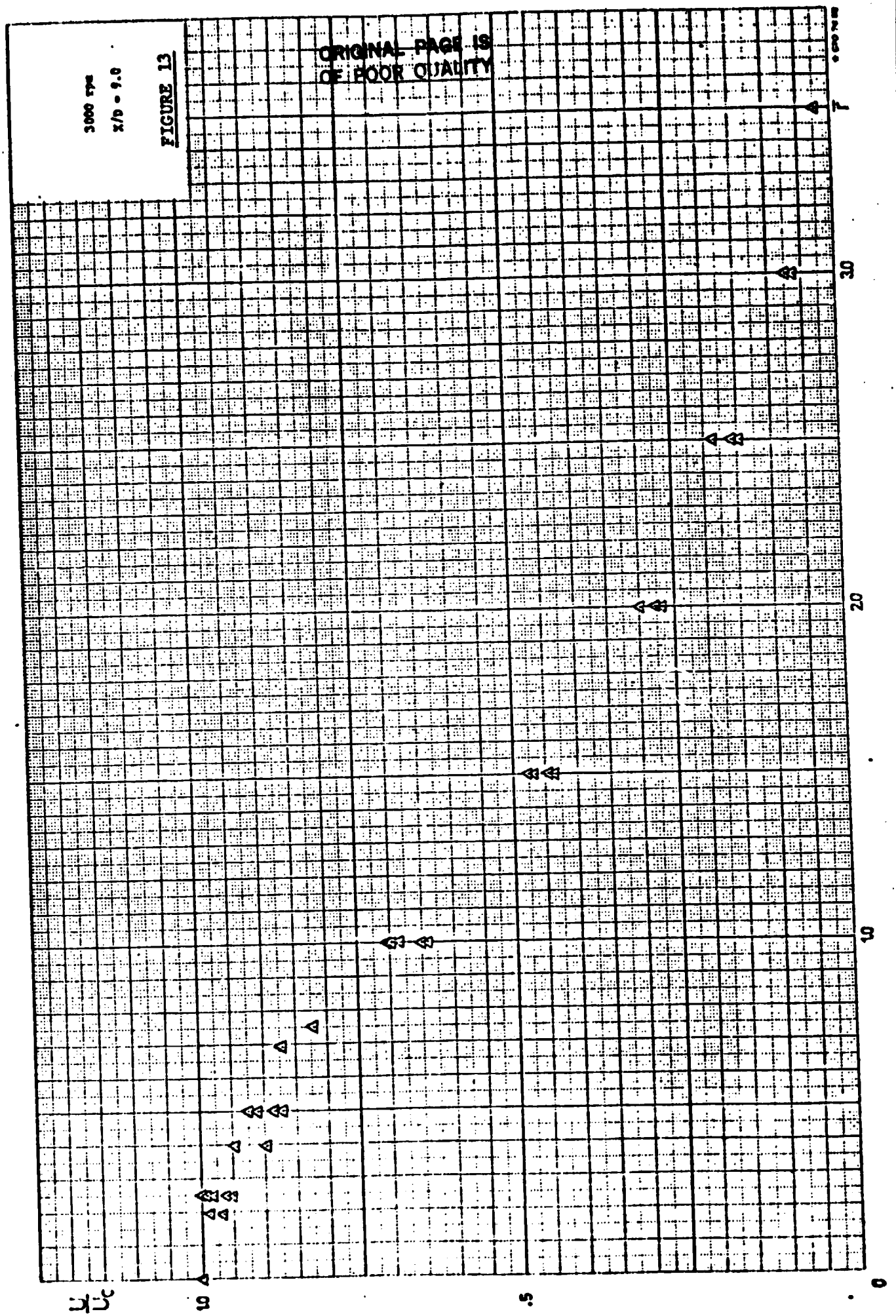

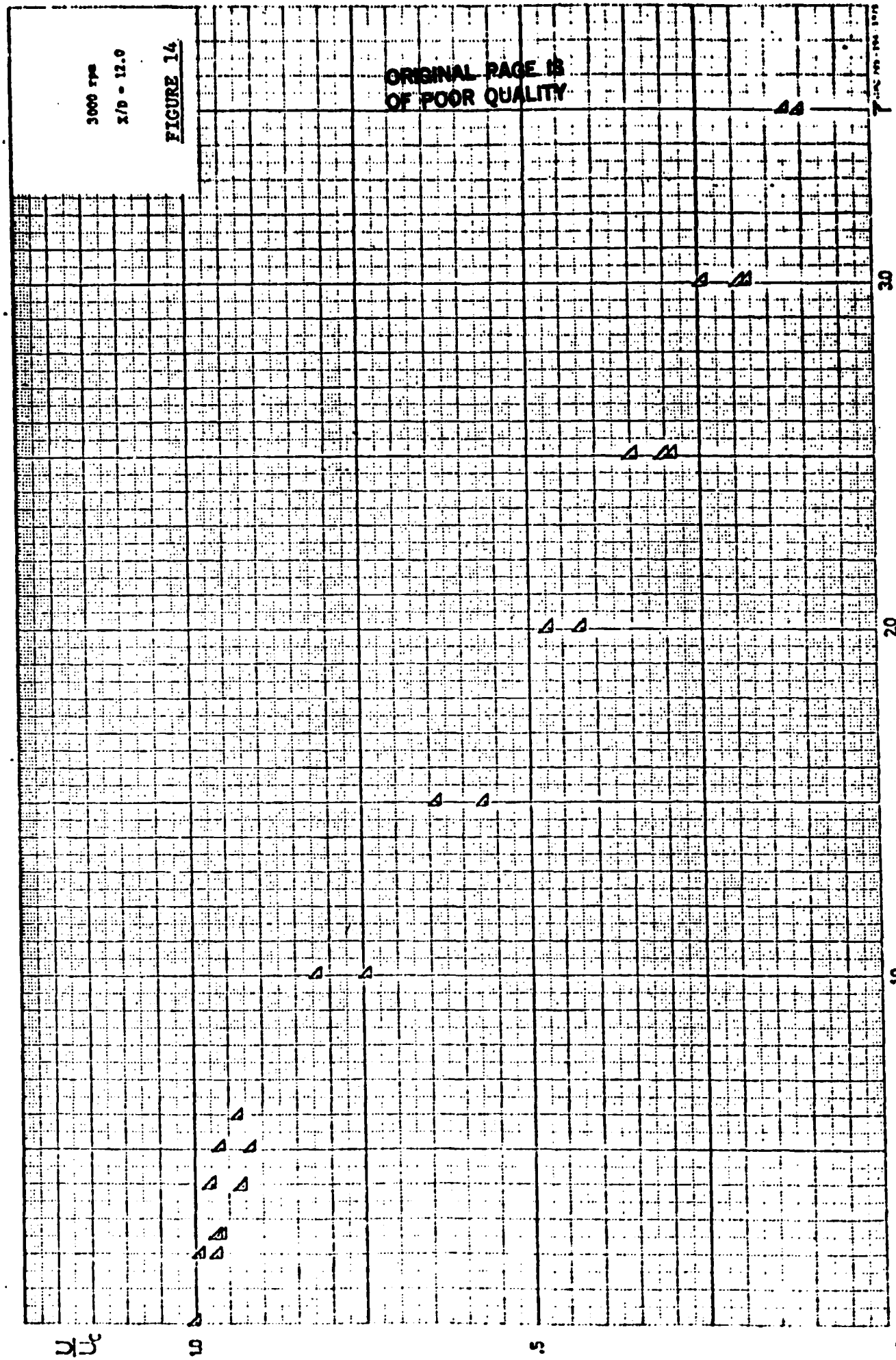

FIGURE 14

NORMALIZED MEAN VELOCITY PROFILES

3000 AND 6000 RPM (M_E = .24 AND .48)

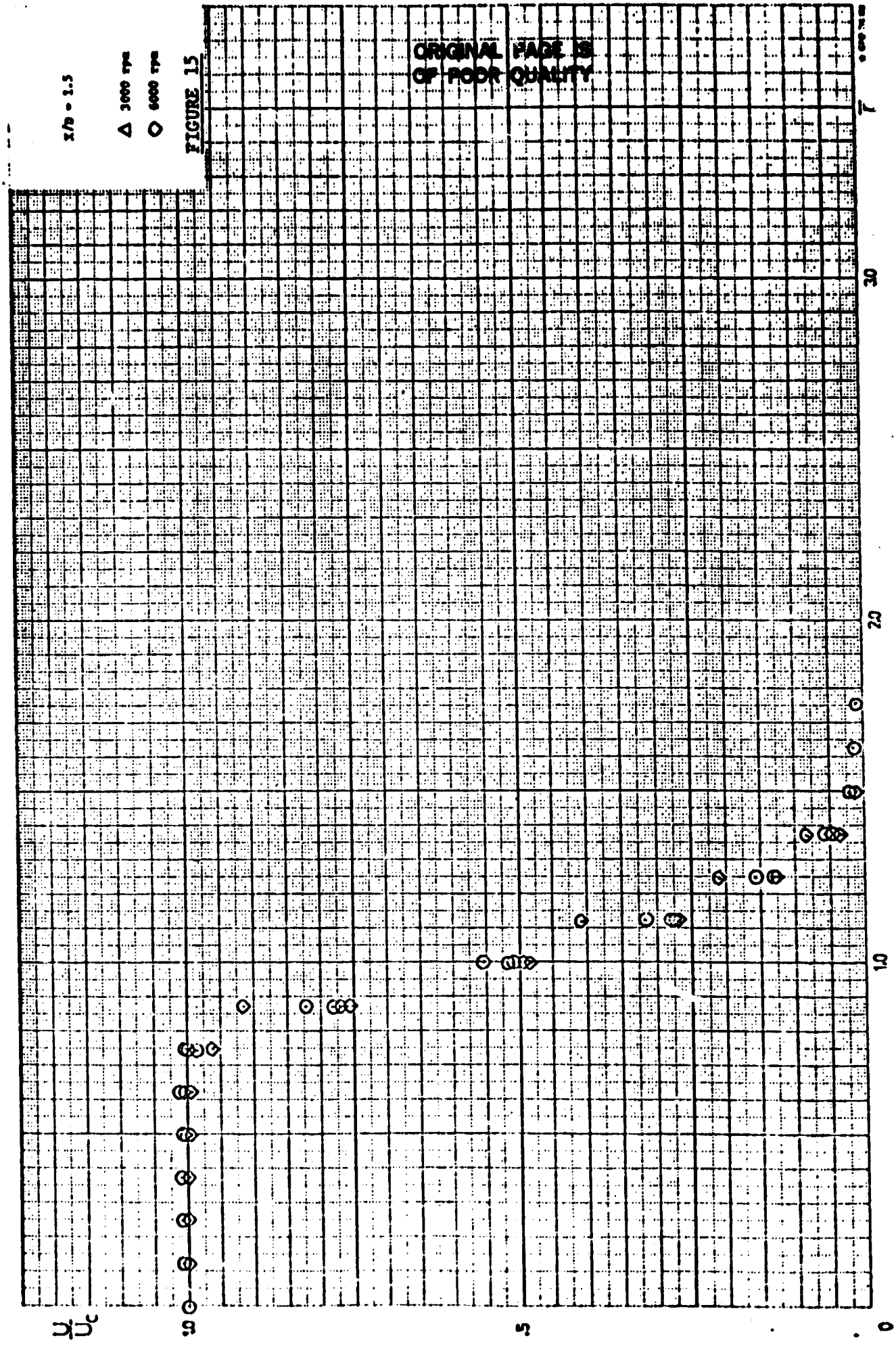
ORIGINAL PAGE IS
OF POOR QUALITY
x/b = 1.5
3000 rpm
6000 rpm
T
30
20
10
0
C_T
.15
.10
.05
0

FIGURE 15

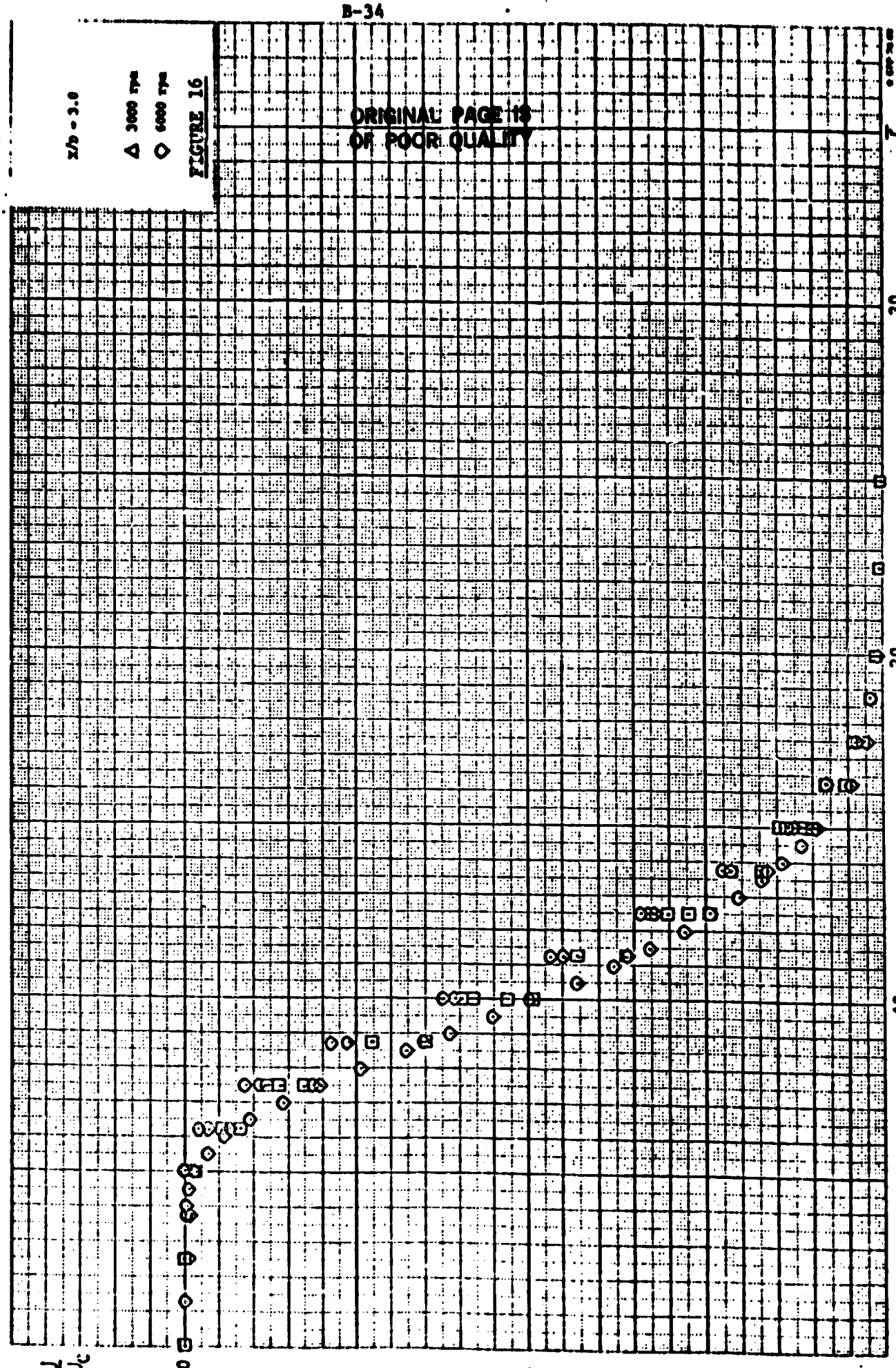

FIGURE 16

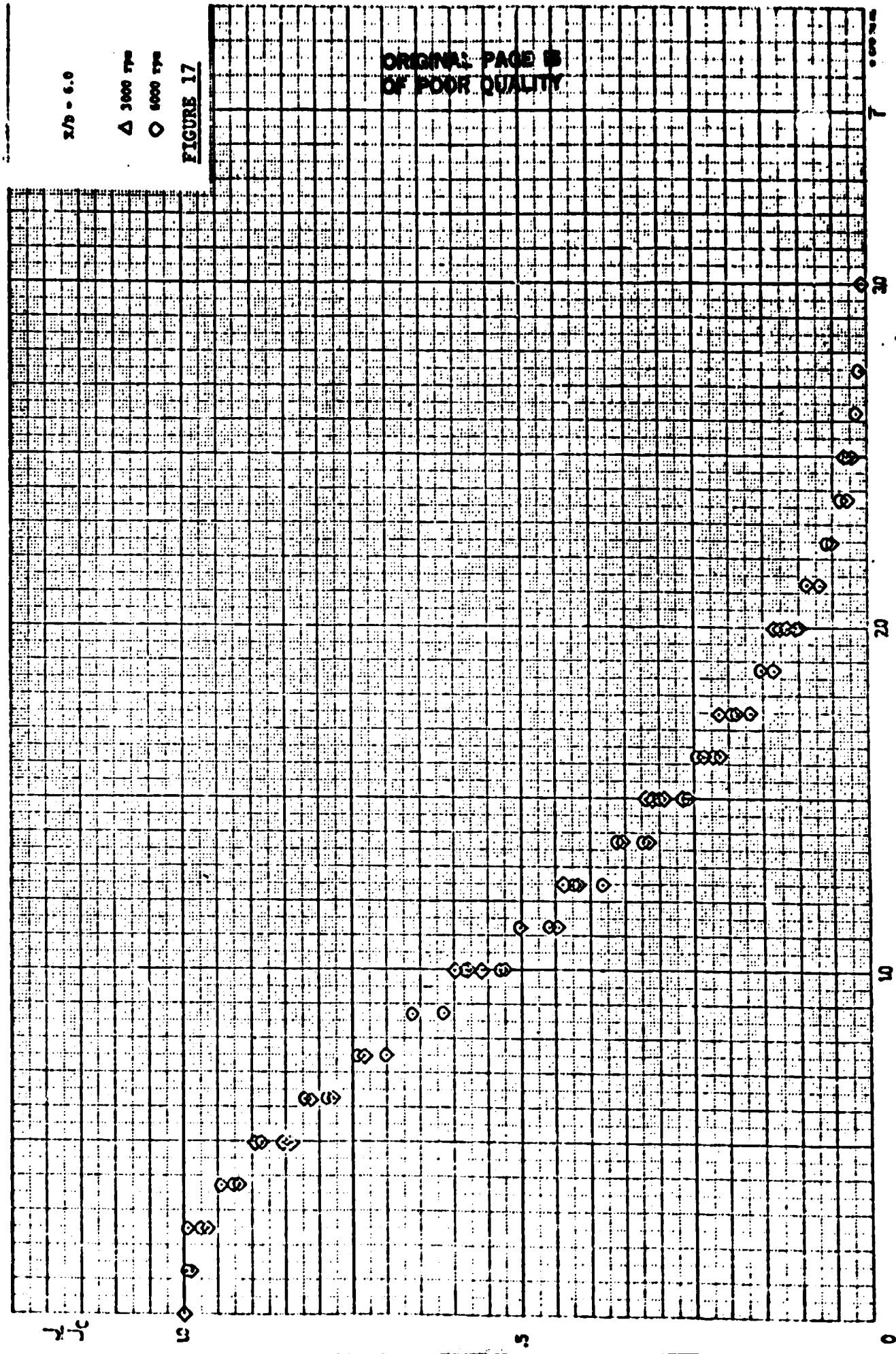

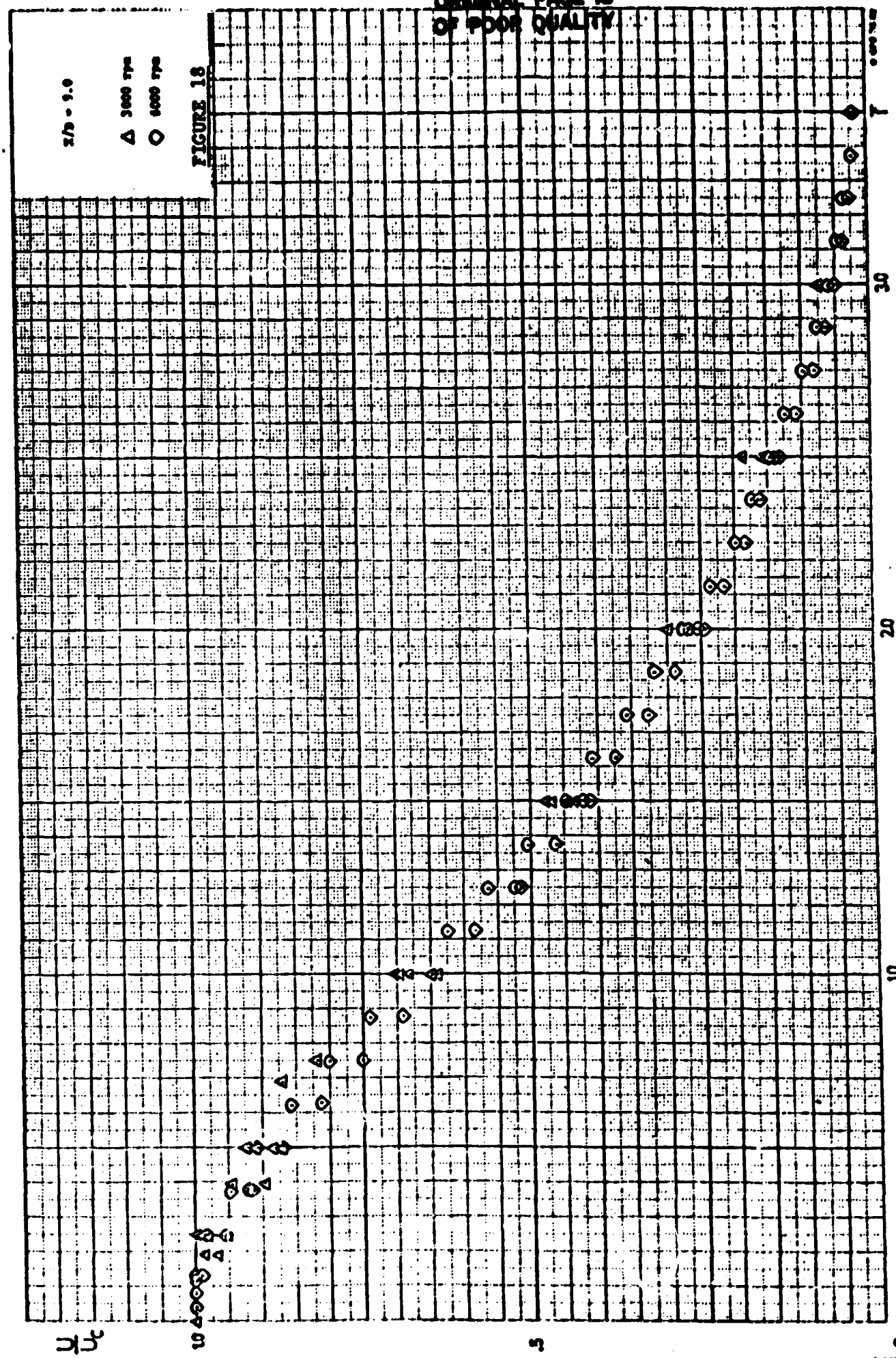

FIGURE 18

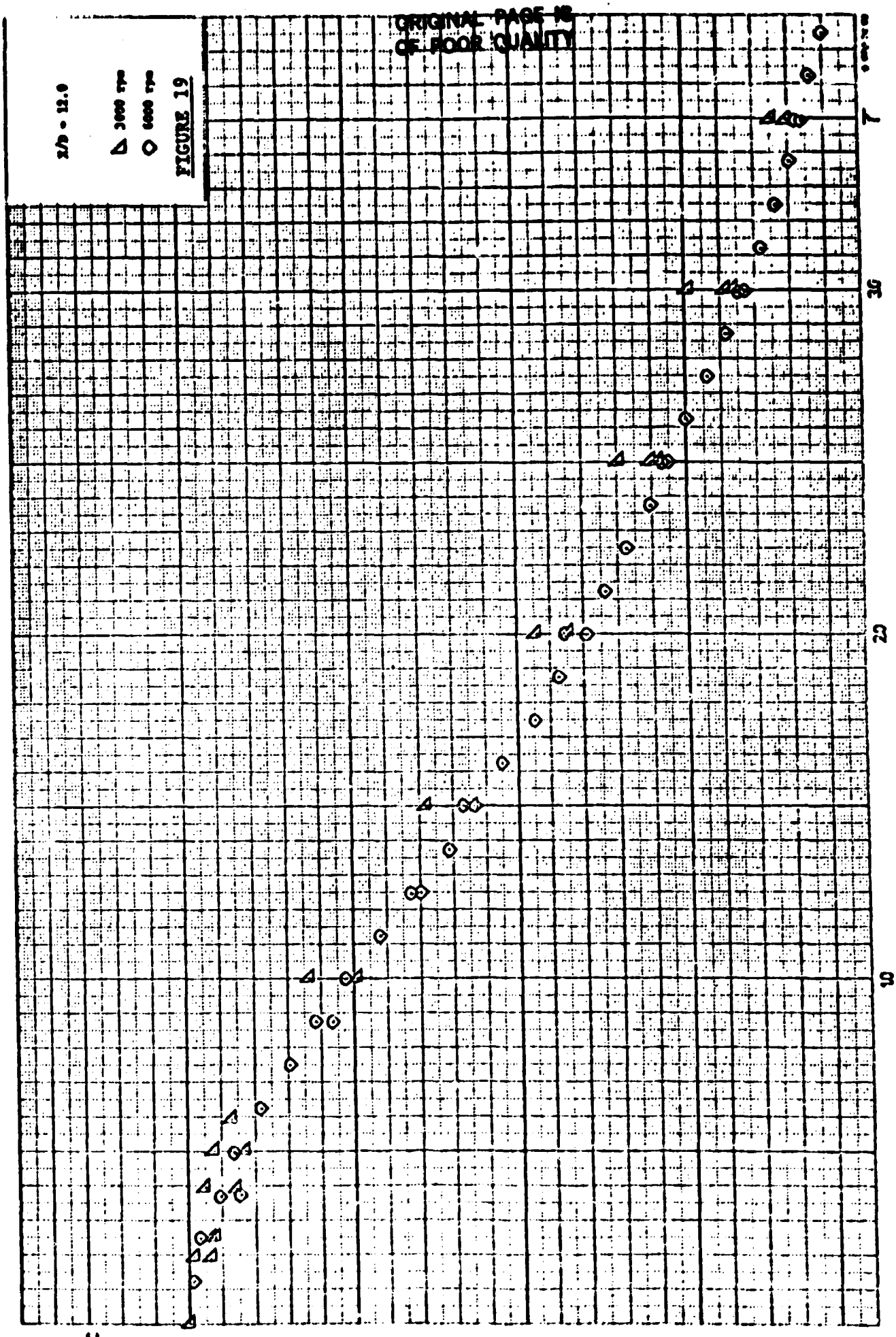

TURBULENCE INTENSITY PROFILES

3000 AND 6000 RPM (M_E = .24 AND .48)

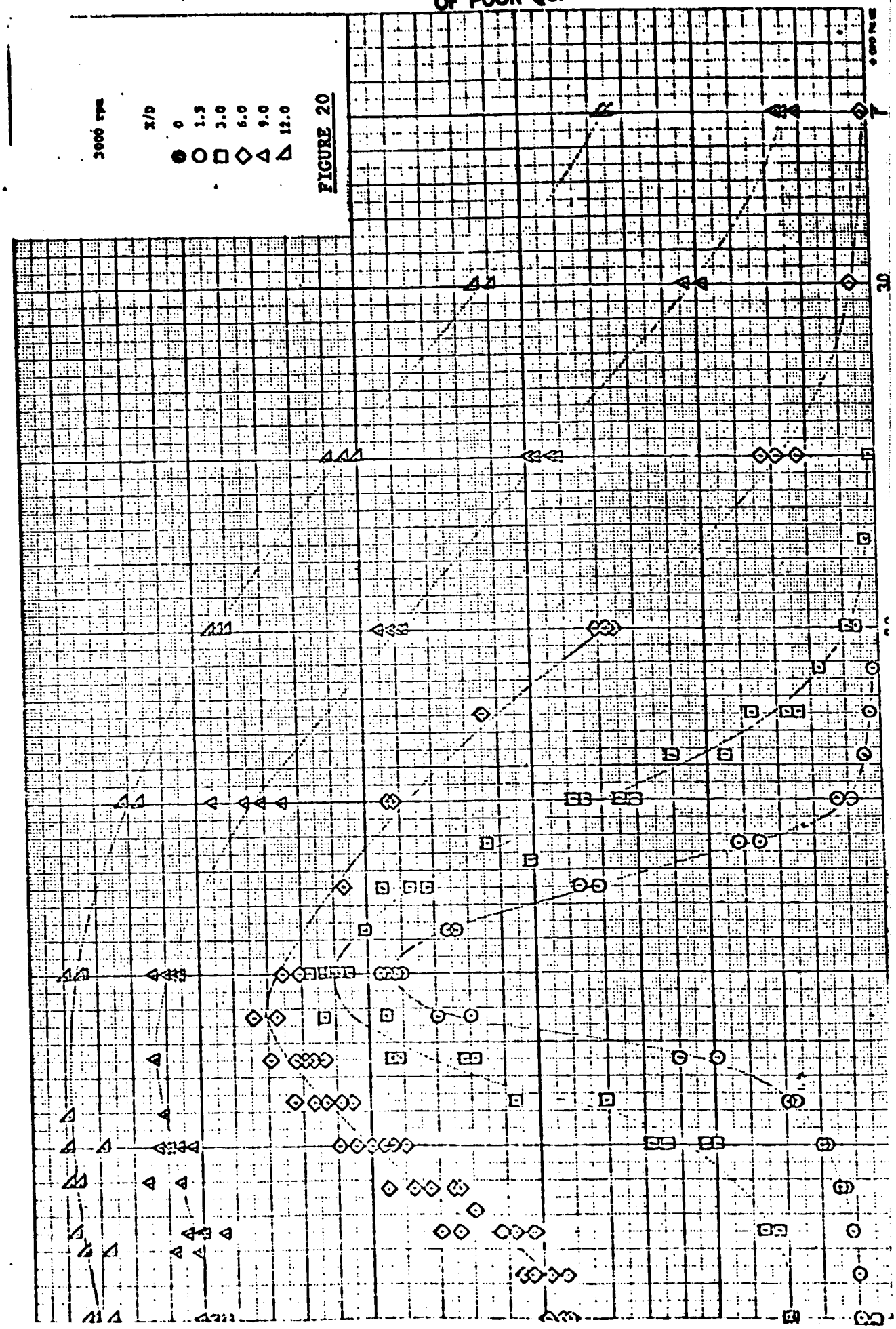

FIGURE 20

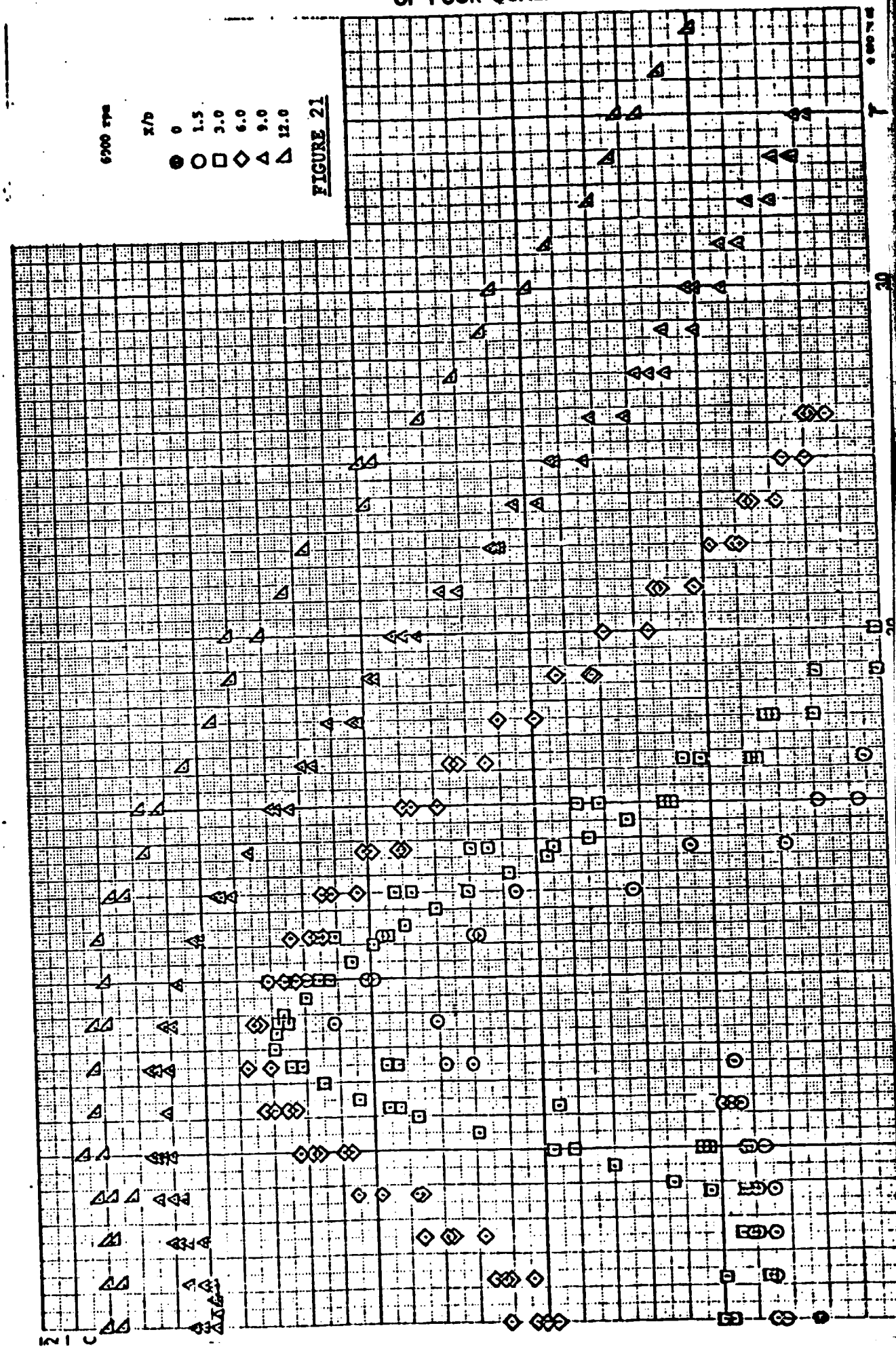

FIGURE 21

CENTERLINE ($r = 0$) NORMALIZED MEAN VELOCITY AND TURBULENCE INTENSITY PROFILES

$\bar{r} = 0$

3000 rpm

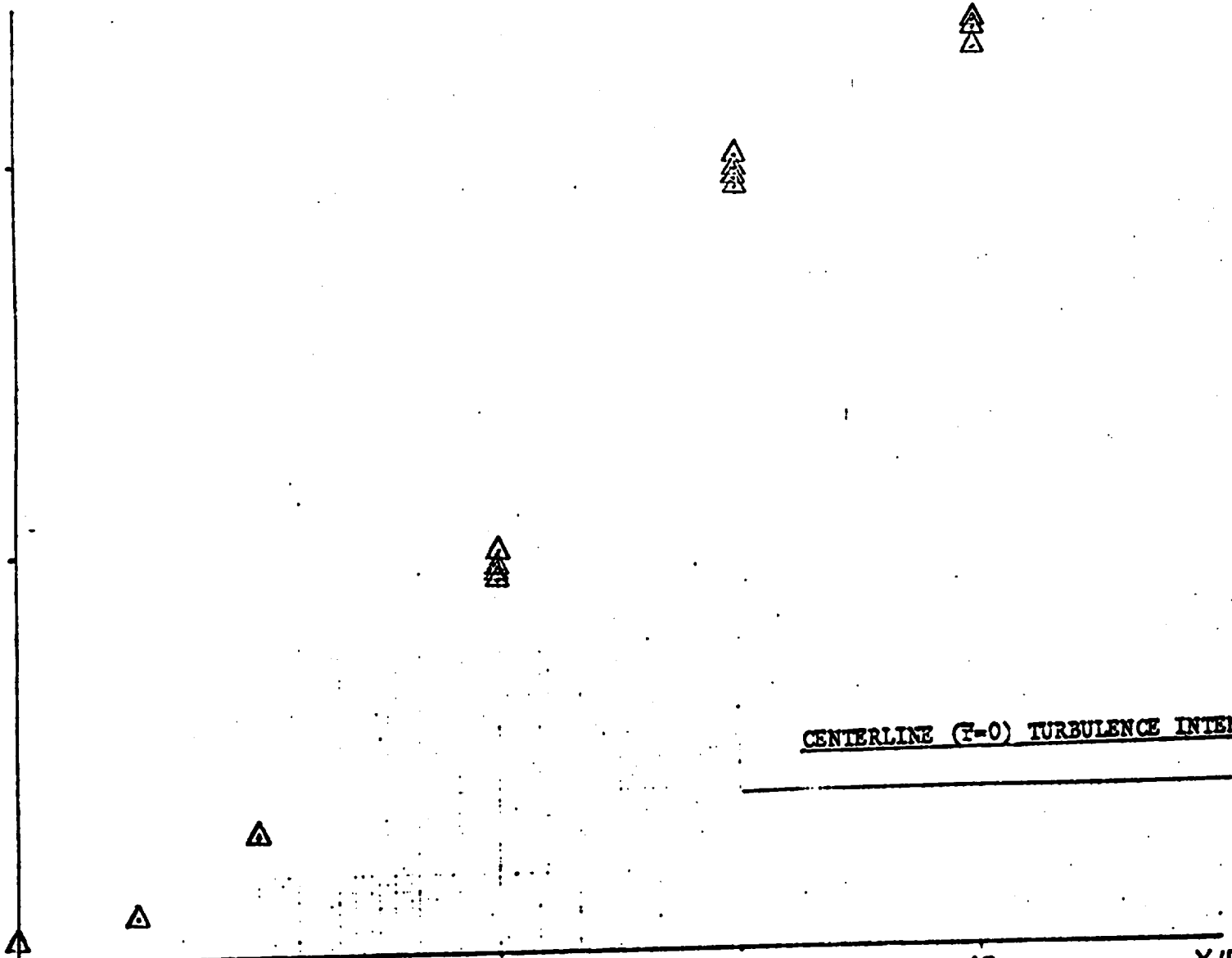

CENTERLINE ($\bar{r}$=0) TURBULENCE INTENSITY-3000 rpm

FIGURE 22

$\bar{T} = 0$

6000 rpm

CENTERLINE ($\bar{T}$=0) TURBULENCE INTENSITY-6000 rpm

FIGURE 23

X/D

3 6 9 12

ORIGINAL PAGE IS
OF POOR QUALITY

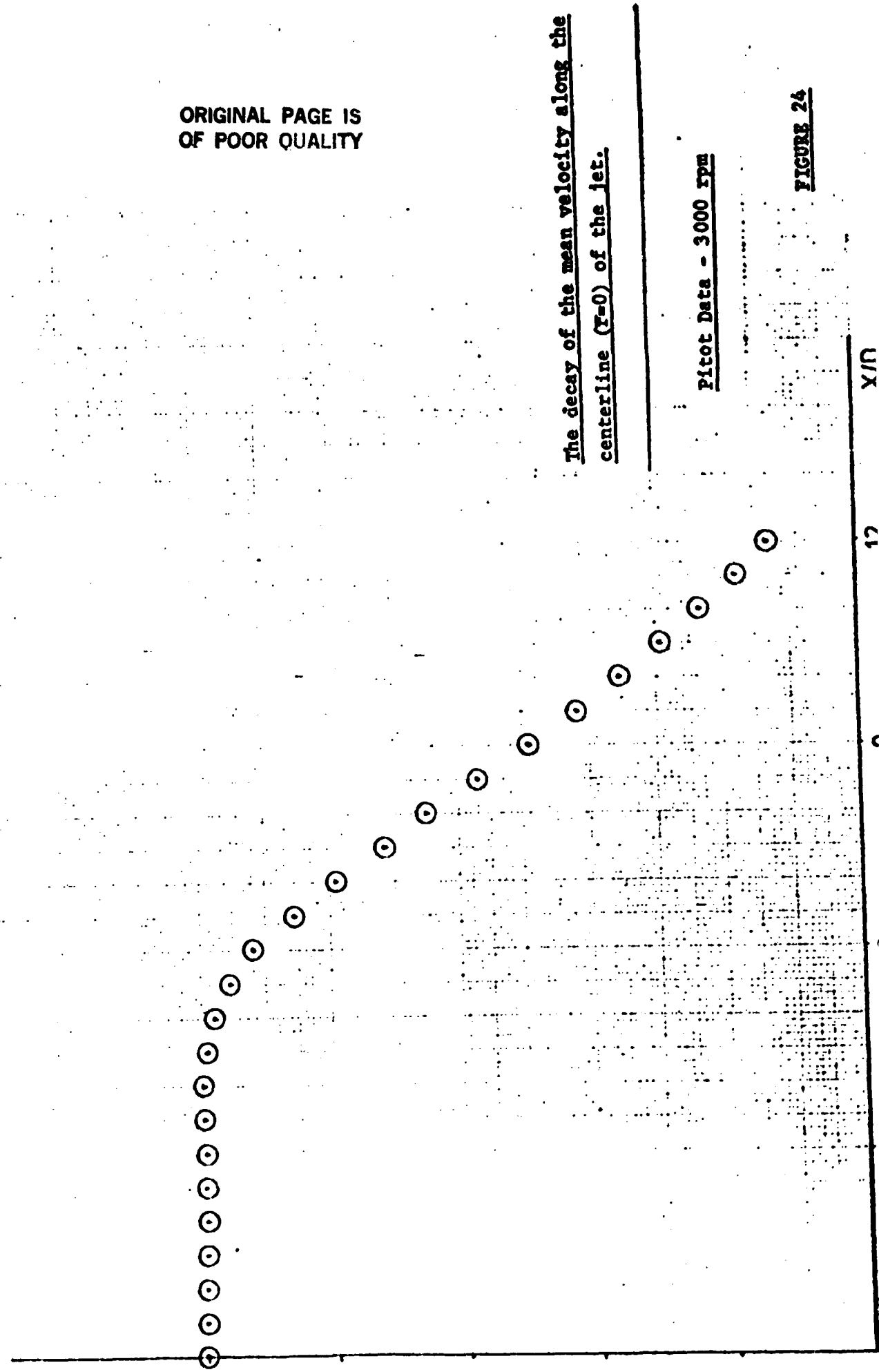

FIGURE 24

The decay of the mean velocity along the centerline (r=0) of the jet.

FIGURE 23

FREQUENCY SPECTRA OF VELOCITY FLUCTUATIONS

3000 RPM (M_E = .24)

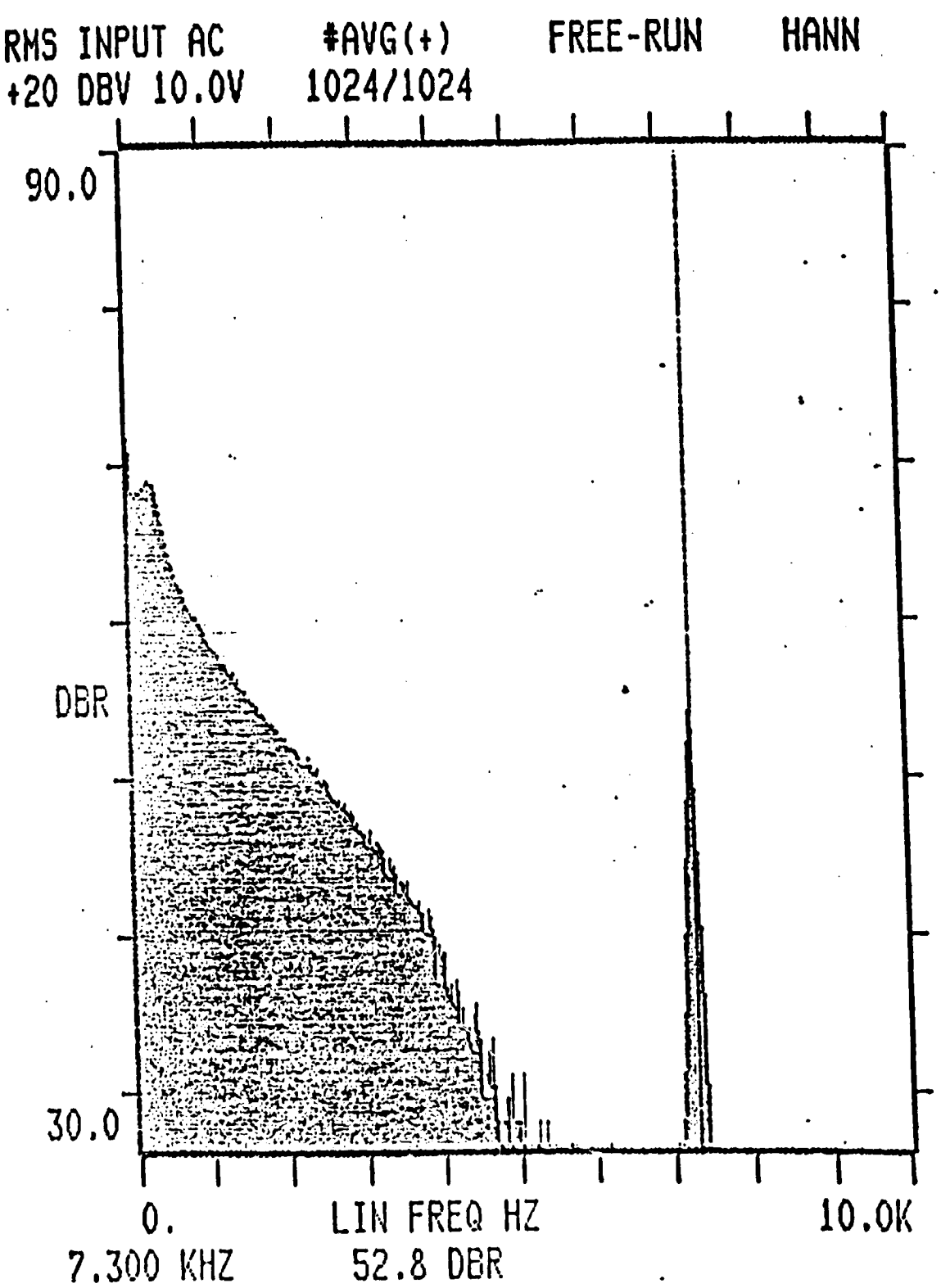

X/D = 6.0

$\bar{r}$ = 0

FIGURE 26

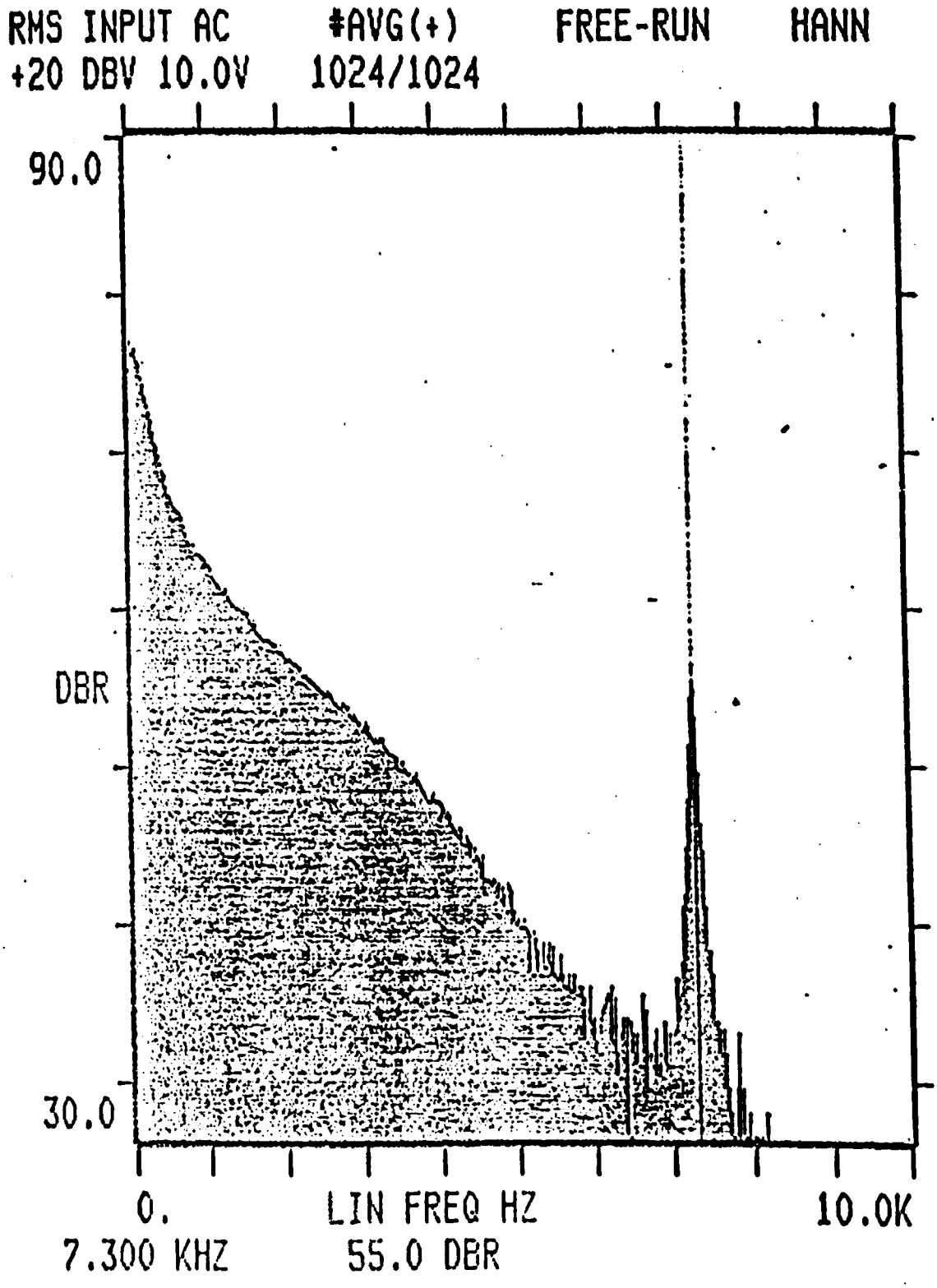

X/D = 6.0

$\bar{r}$ = 1.0

FIGURE 27

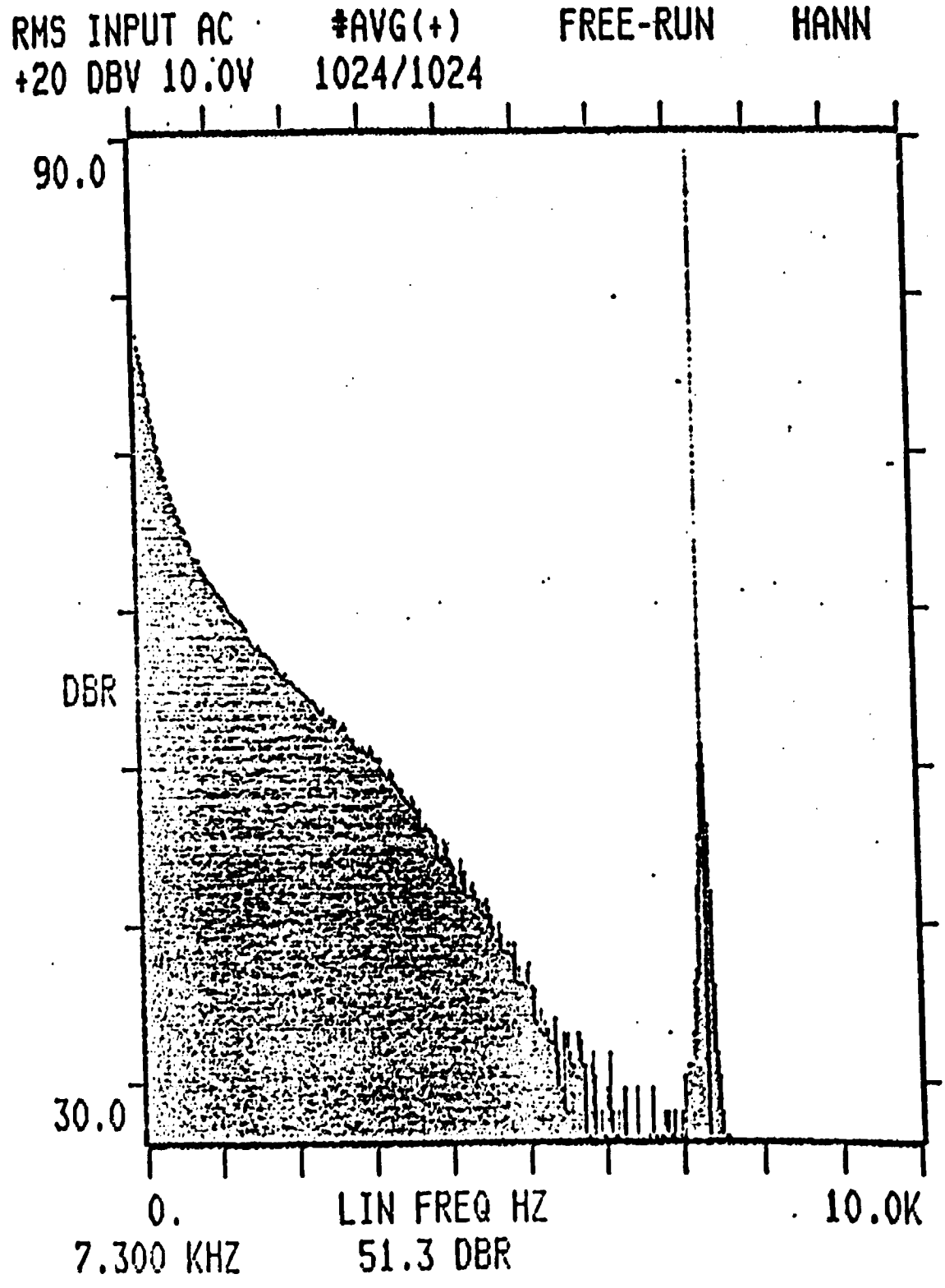

X/D = 6.0

$\bar{r}$ = 1.25

FIGURE 28

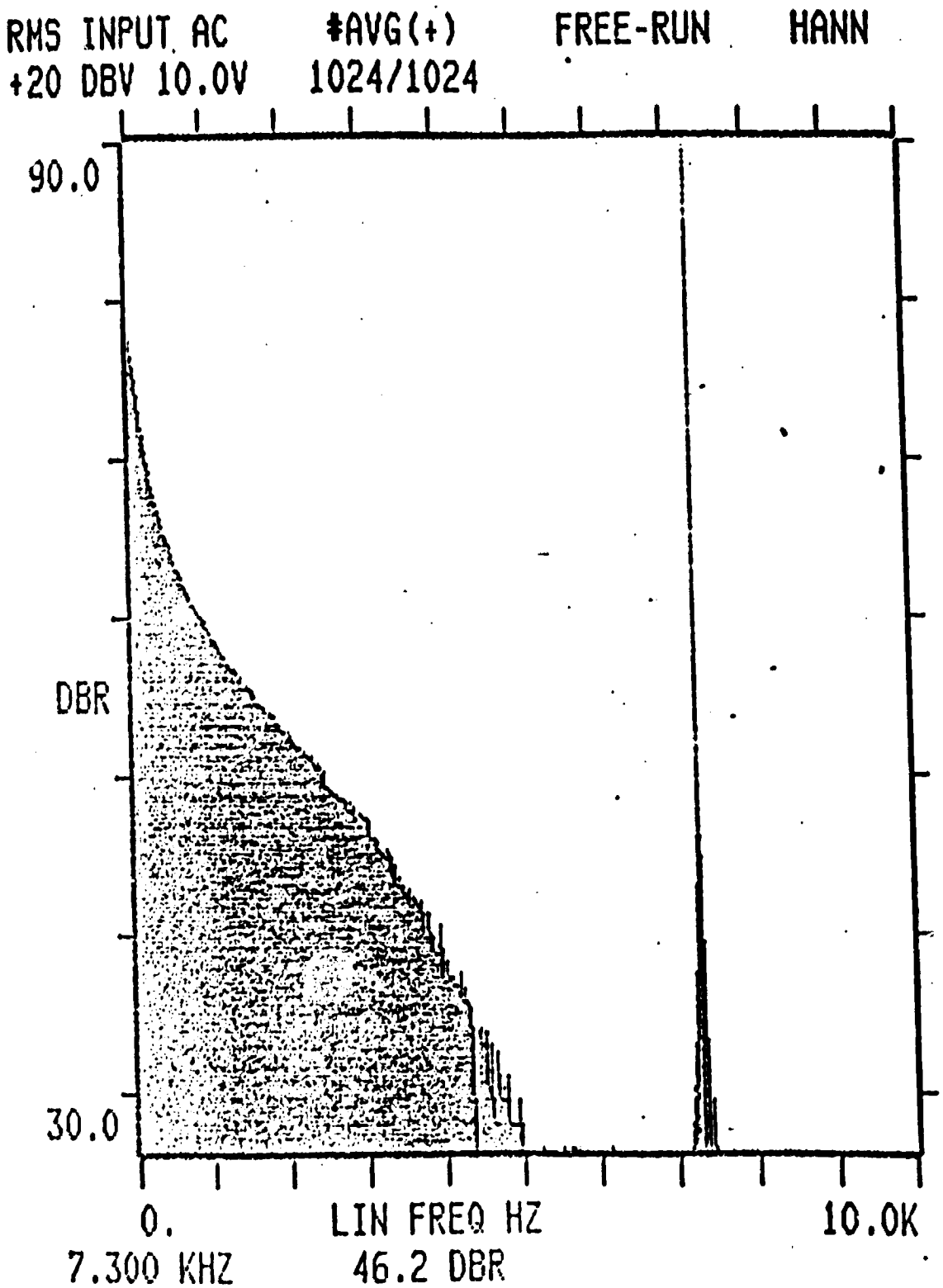

X/D = 6.0

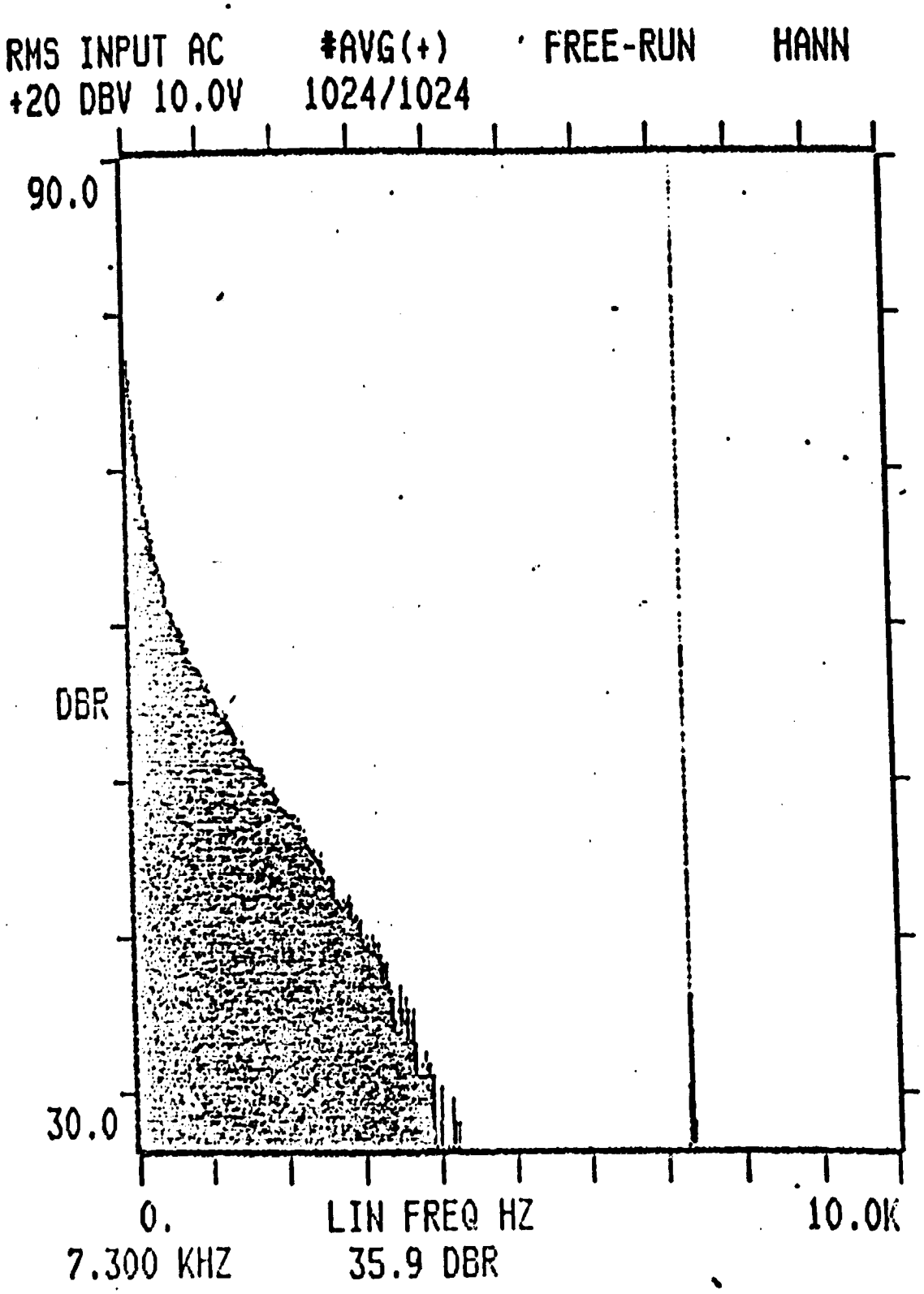

X/D = 6.0

FIGURE 30

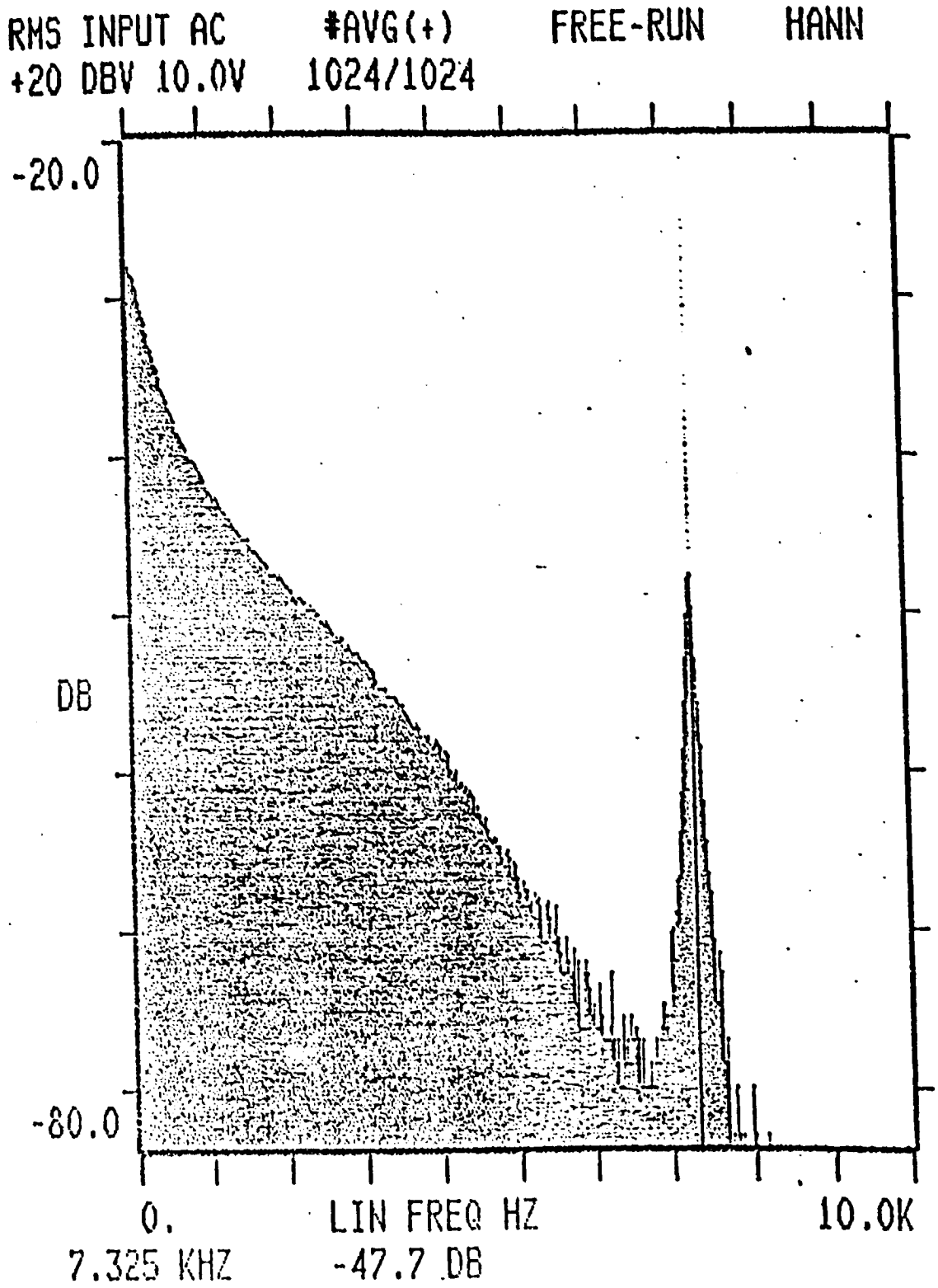

X/D = 9.0

FIGURE 31

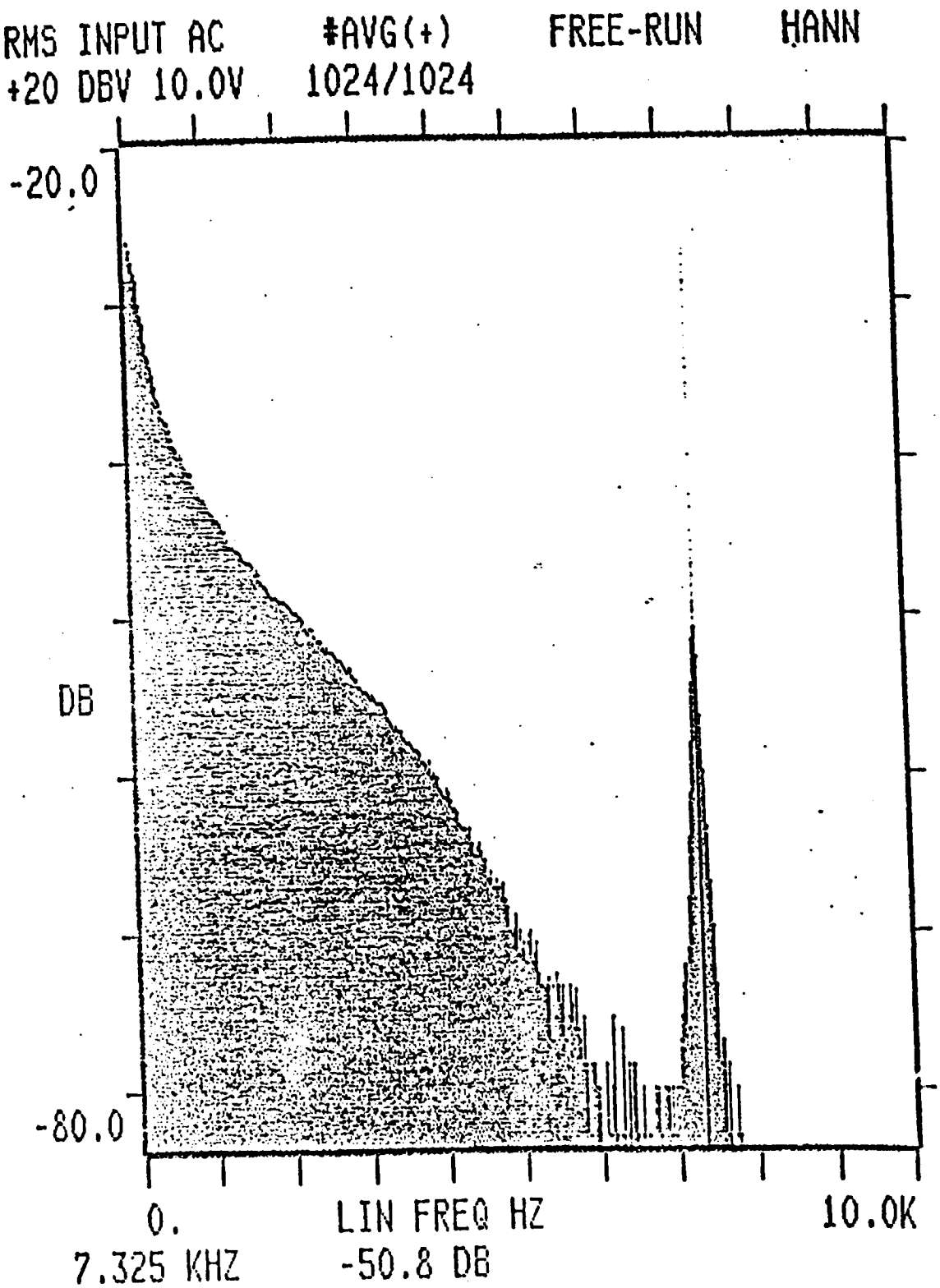

X/D = 9.0

FIGURE 32

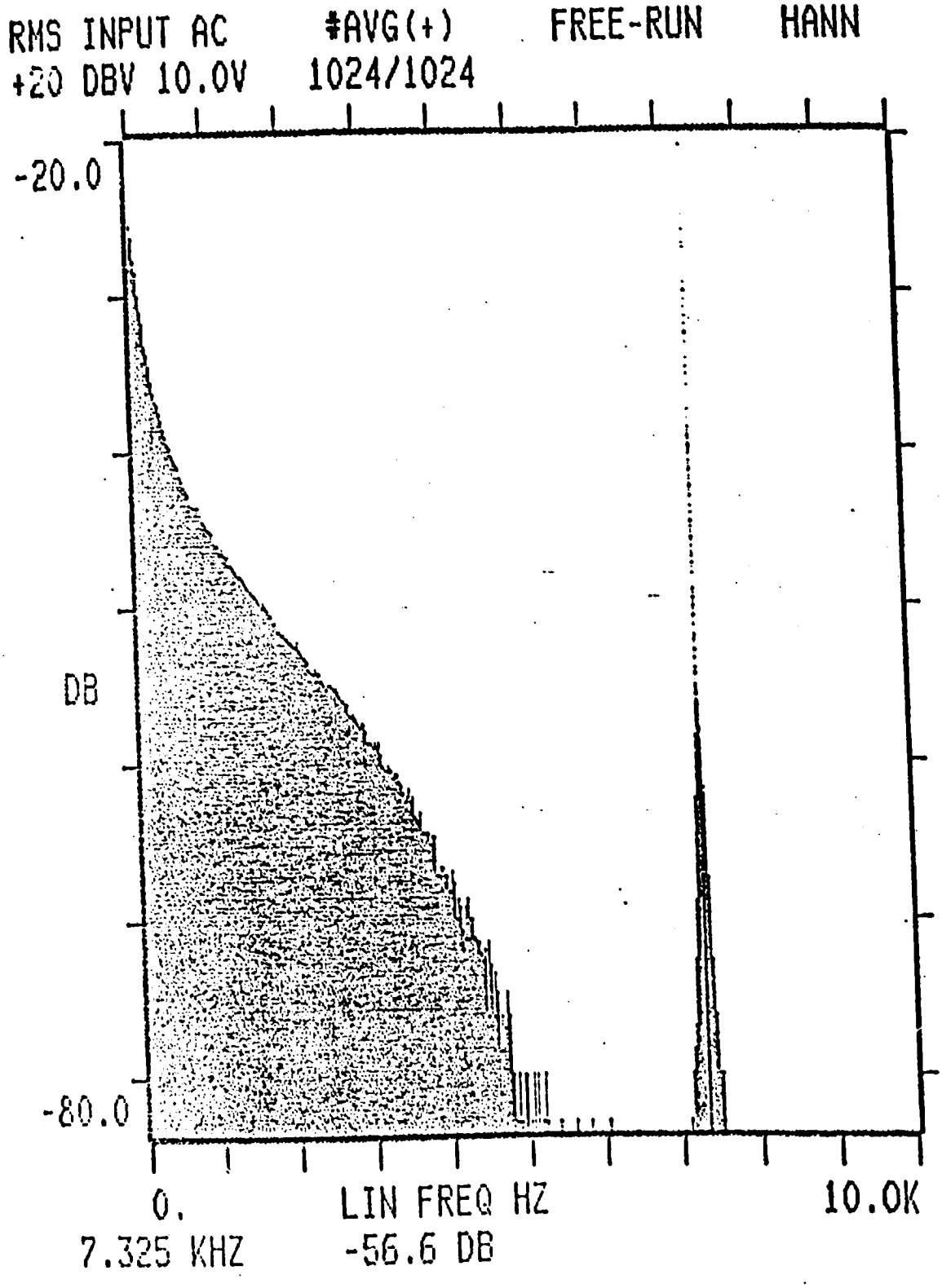

X/D = 9.0

Y = 1.5

FIGURE 33

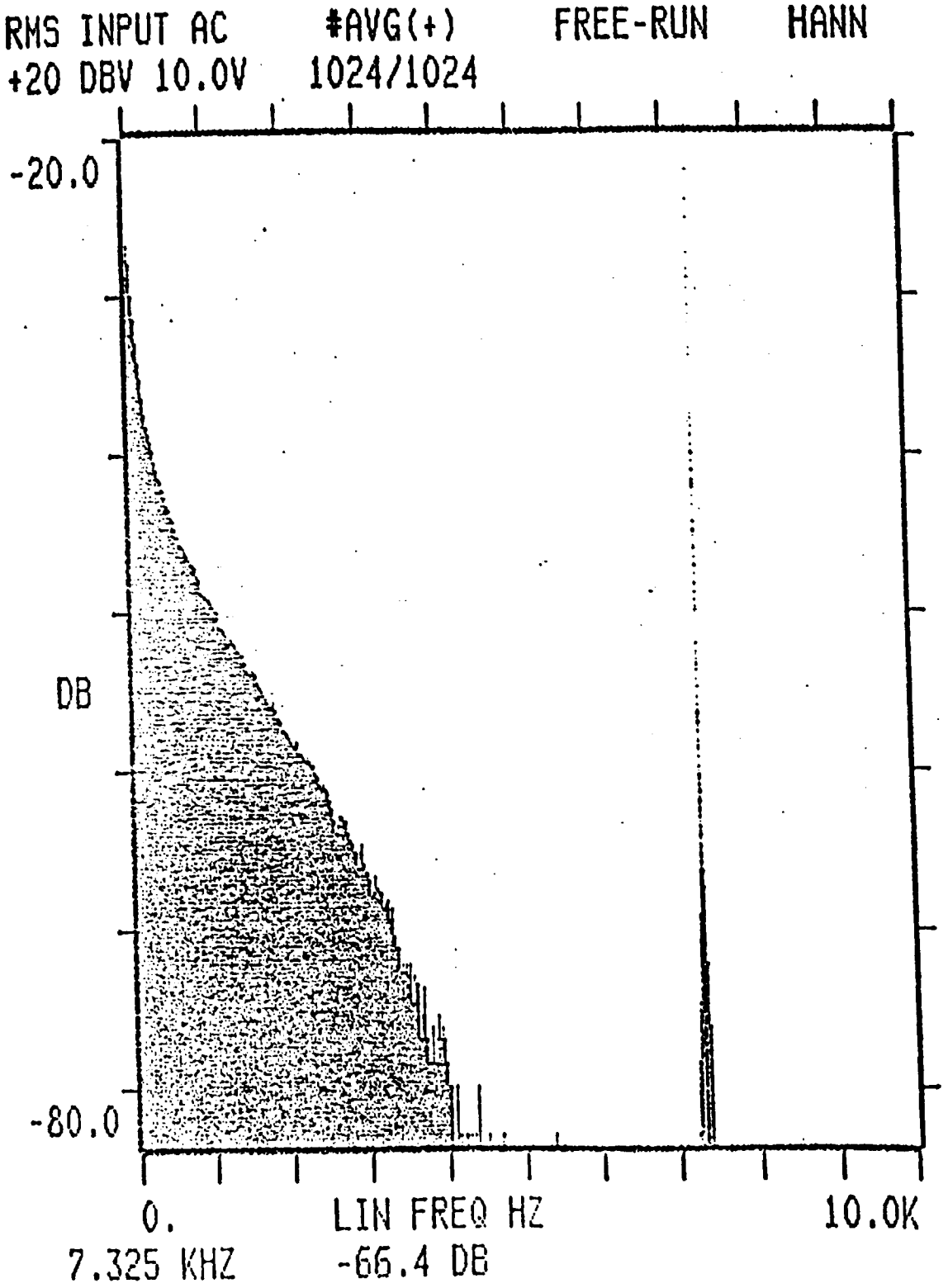

X/D = 9.0

$\bar{r}$ = 2.0

FIGURE 34

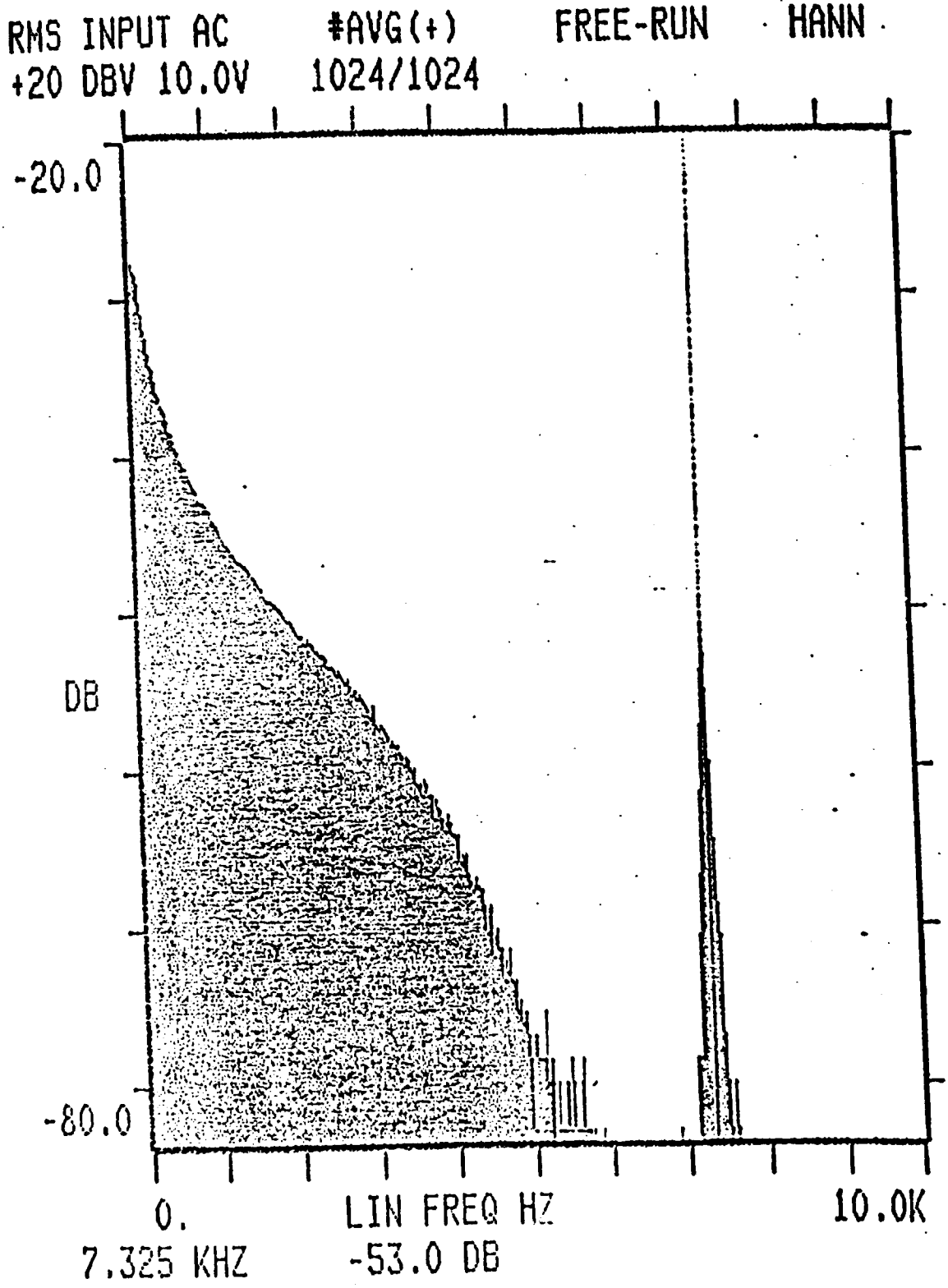

X/D = 12.0

$\bar{r}$ = 0

FIGURE 35

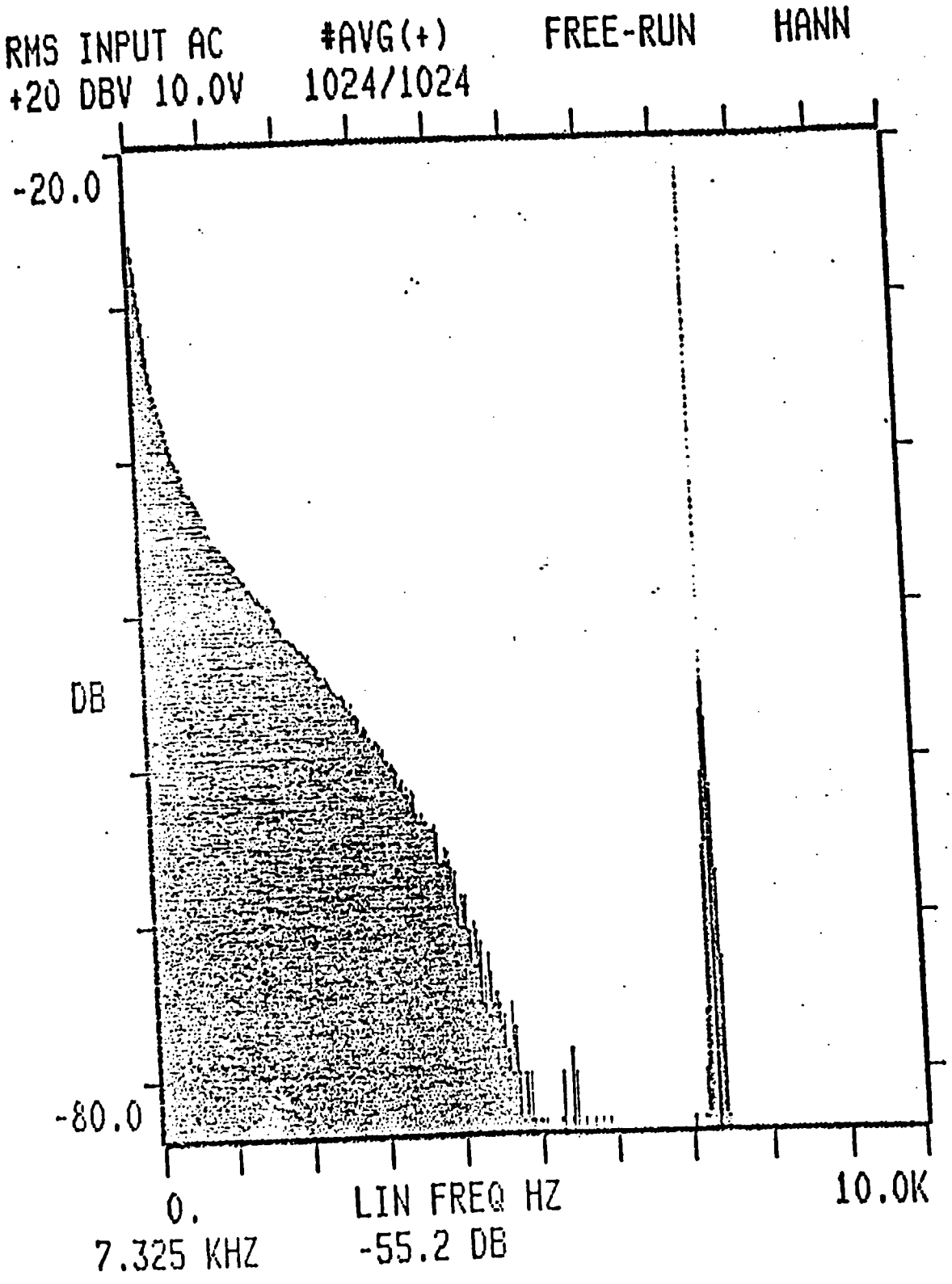

X/D = 12.0

$\bar{r}$ = 1.0

FIGURE 36

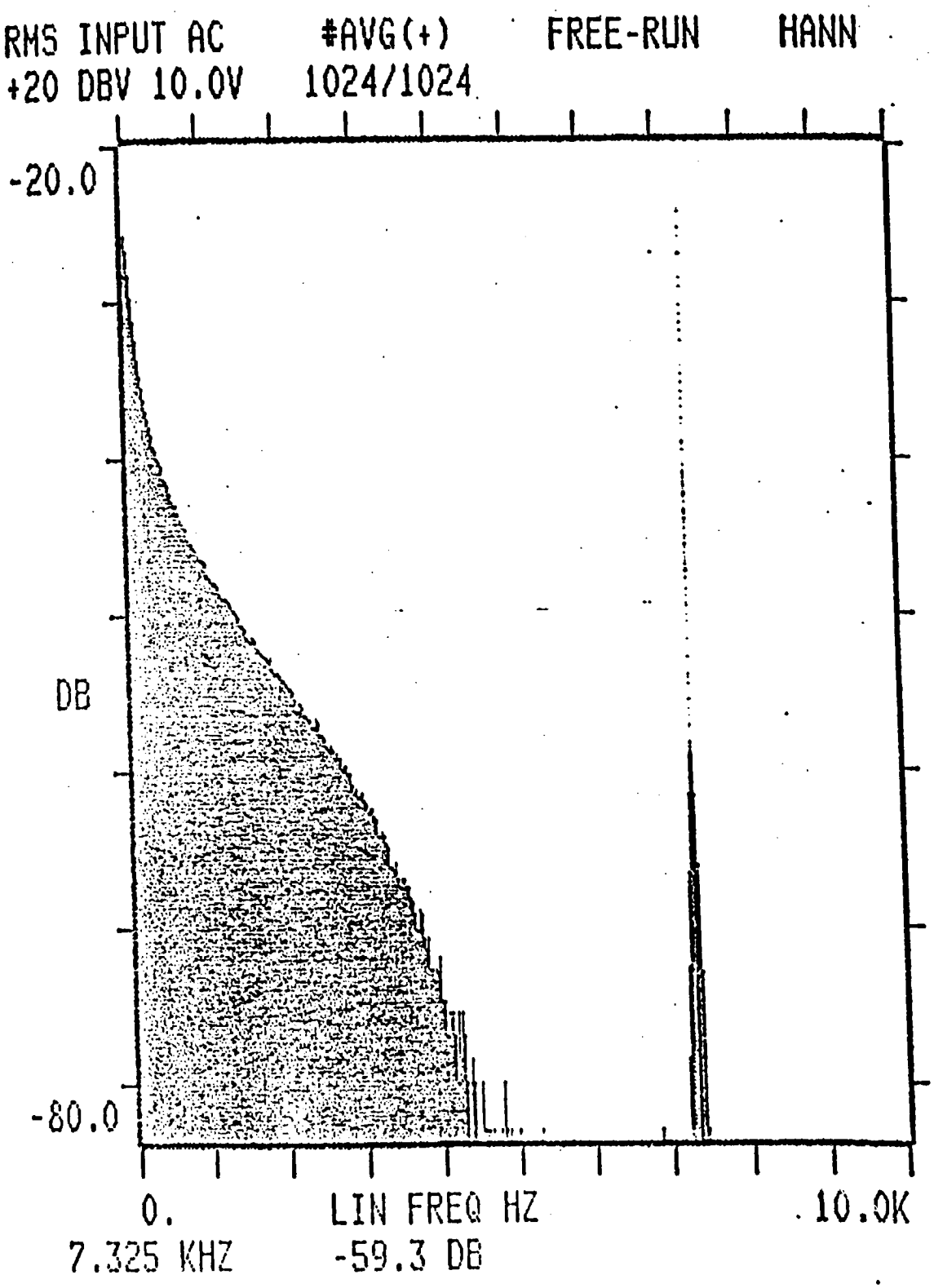

X/D = 12.0

$\bar{r}$ = 1.5

FIGURE 37

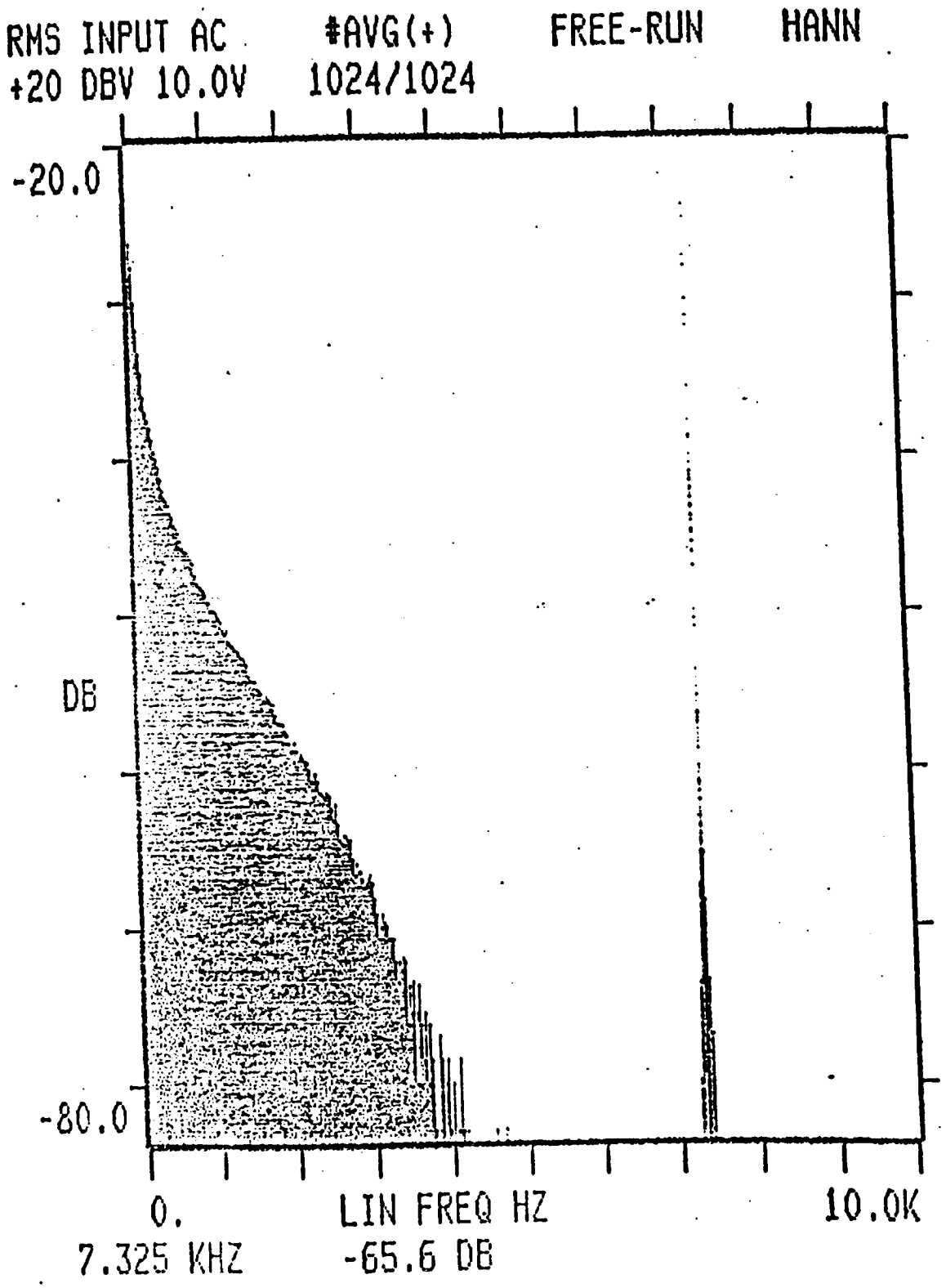

X/D = 12.0

$\bar{r}$ = 2.0

FIGURE 38

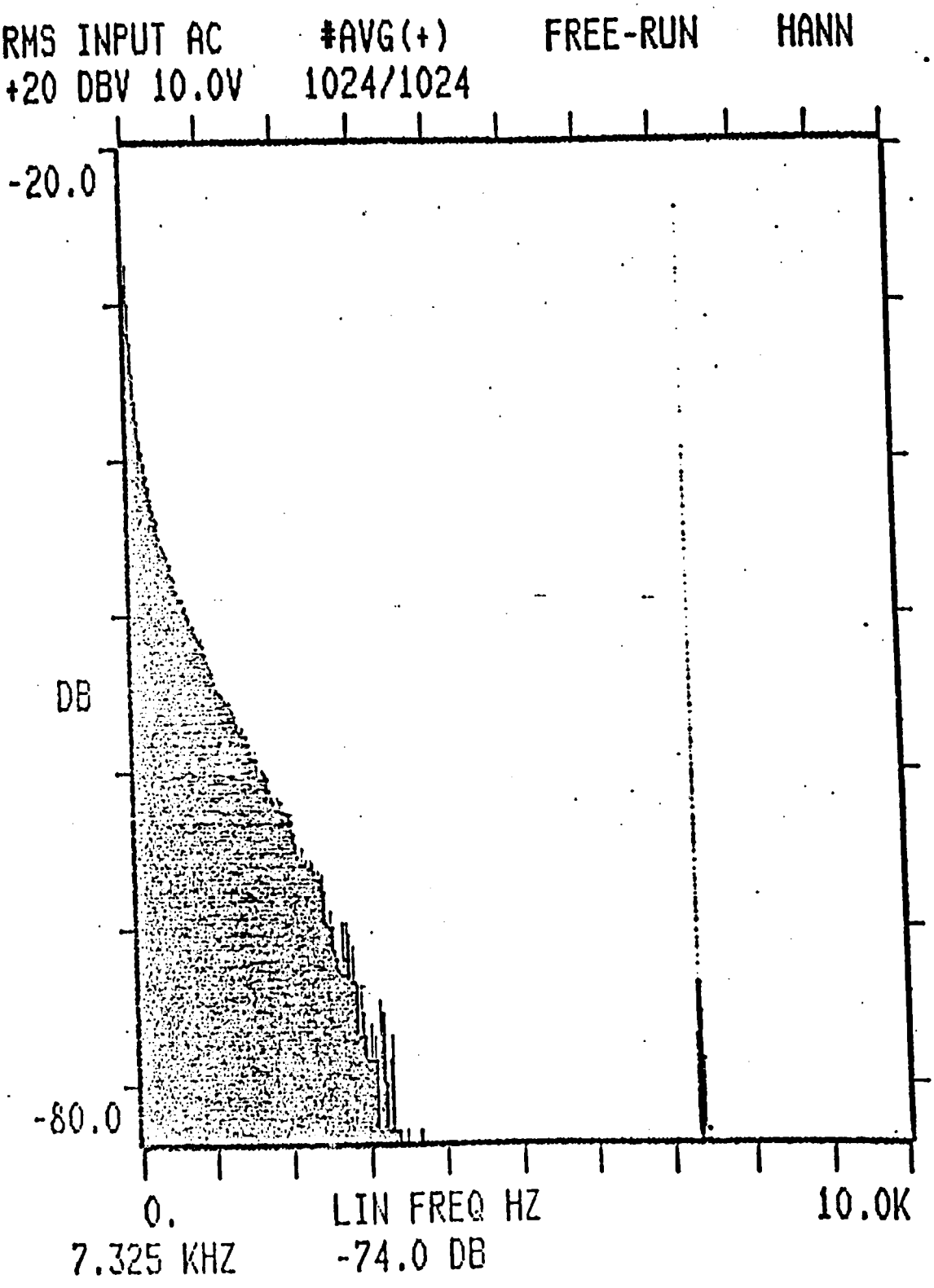

X/D = 12.0

$\bar{r}$ = 2.5

FIGURE 39

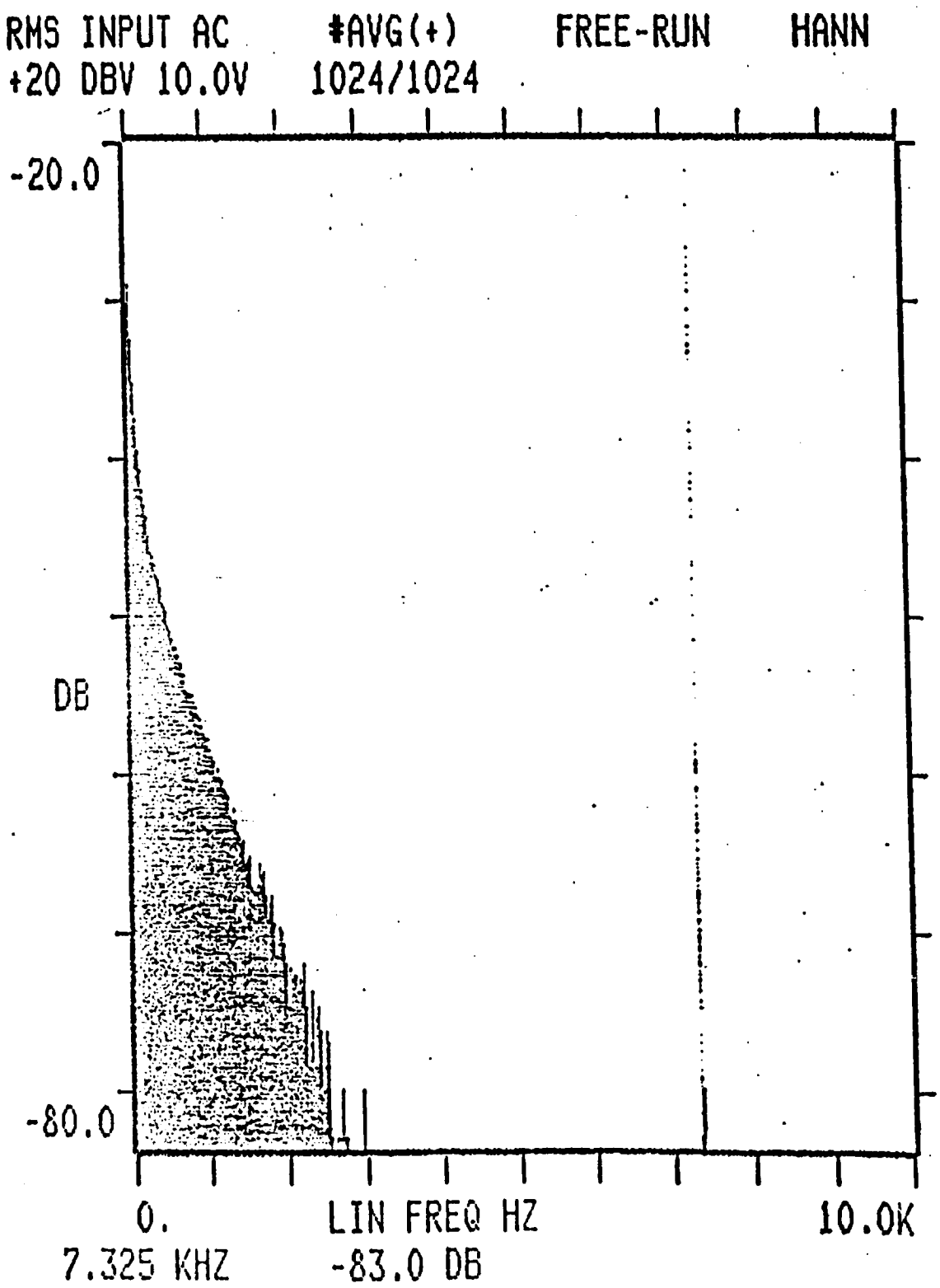

X/D = 12.0

$\bar{r}$ = 3.0

FIGURE 40

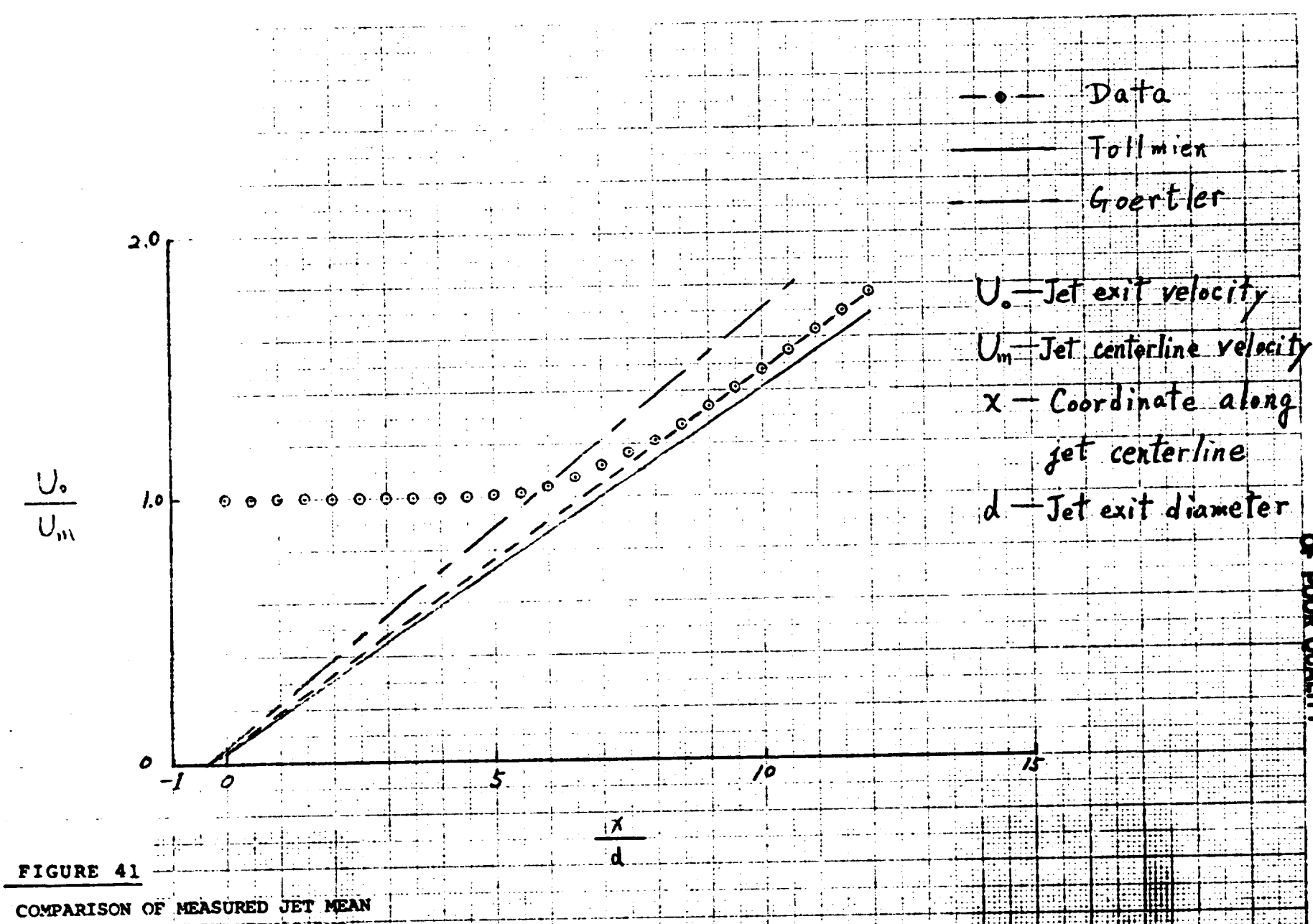

FIGURE 41

COMPARISON OF MEASURED JET MEAN VELOCITIES WITH TOLLMIEN'S AND GOERTLER'S THEORETICAL RESULTS.

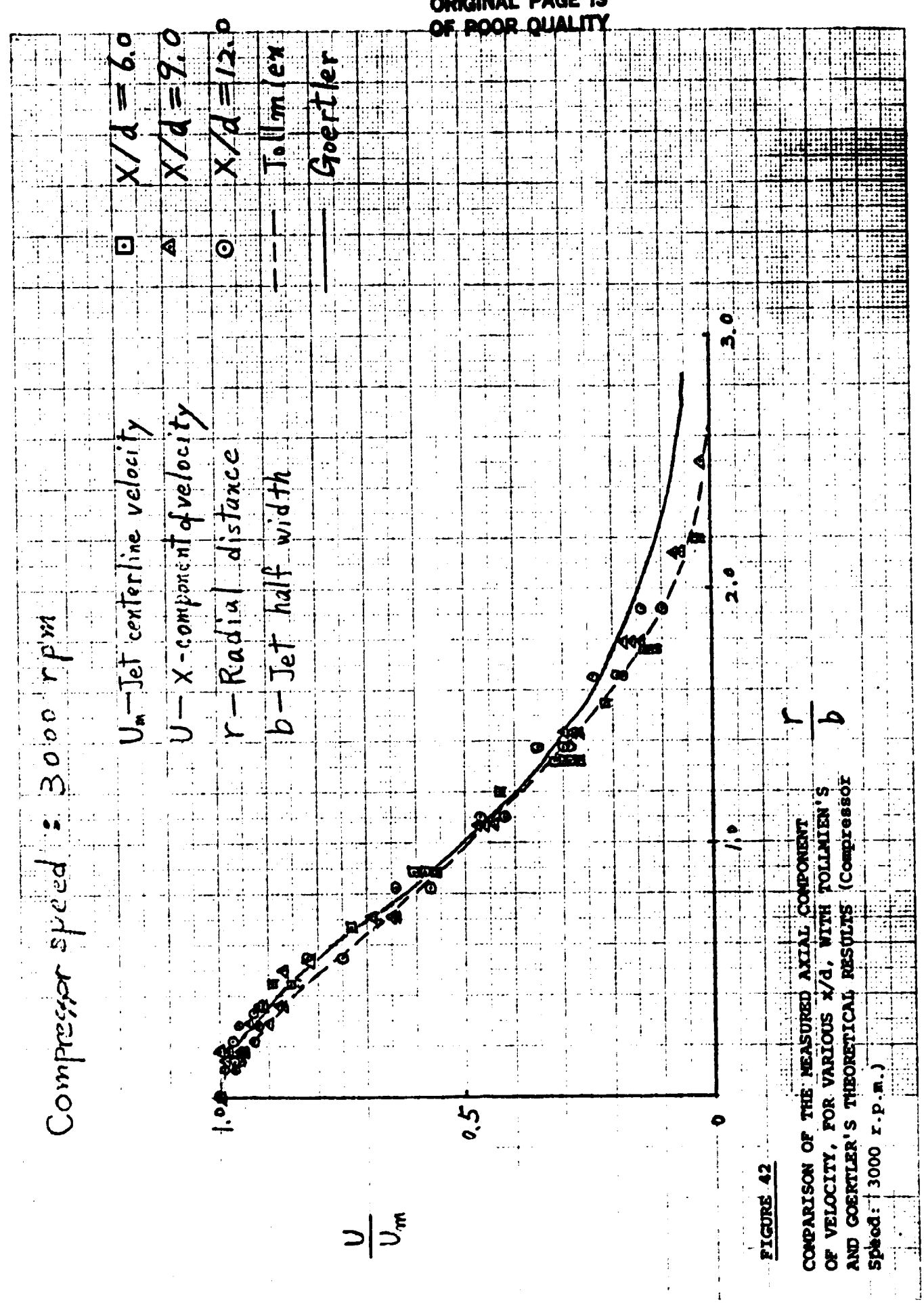

FIGURE 42

COMPARISON OF THE MEASURED AXIAL COMPONENT OF VELOCITY, FOR VARIOUS x/d, WITH TOLLMIEN'S AND GOERTLER'S THEORETICAL RESULTS (Compressor Speed: 3000 r.p.m.)

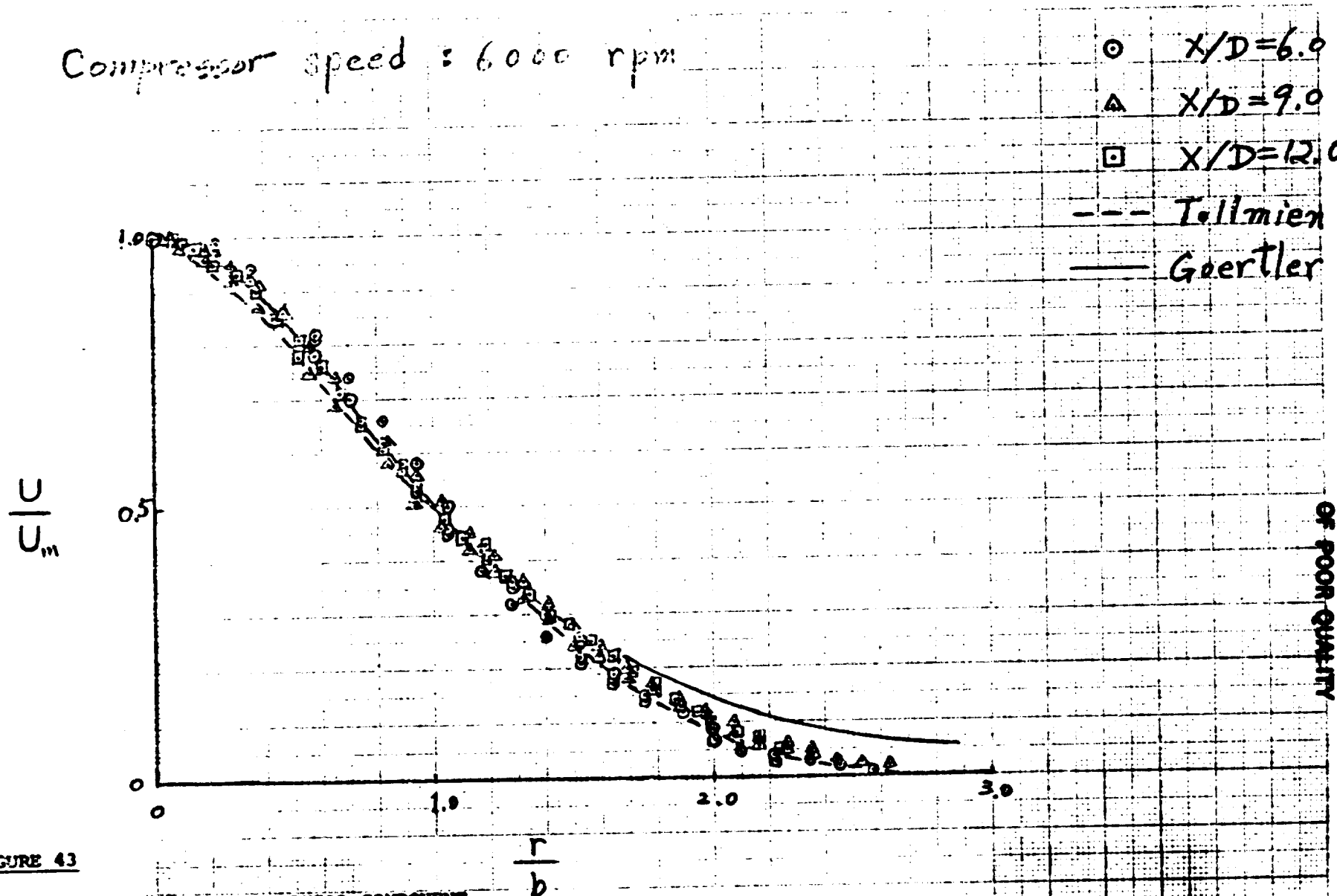

FIGURE 43

COMPARISON OF THE MEASURED AXIAL COMPONENT OF VELOCITY, FOR VARIOUS x/d, WITH TOLLMIEN'S AND GOERTLER'S THEORETICAL RESULTS (Compressor speed: 6000 r.p.m.)

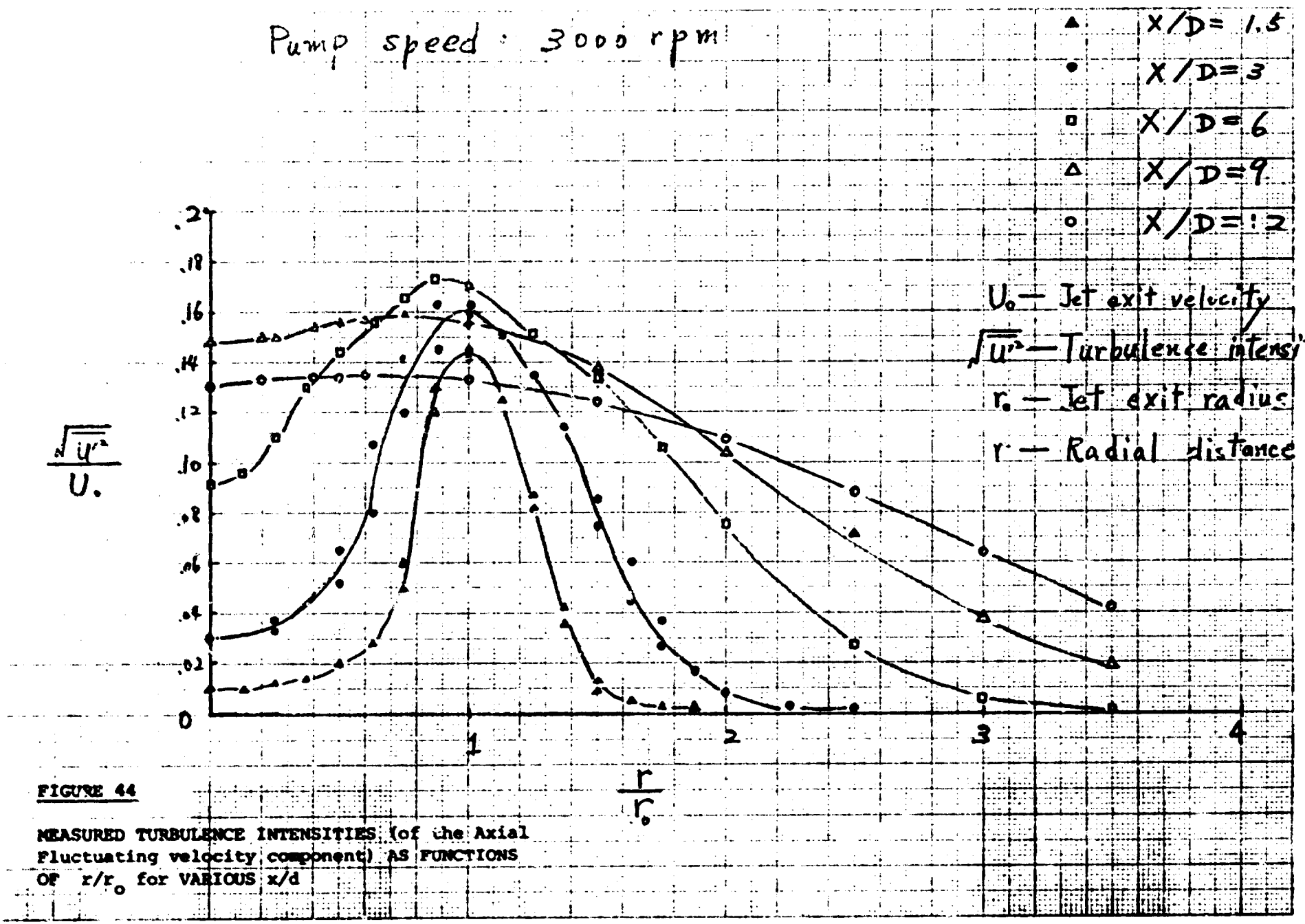

FIGURE 44

MEASURED TURBULENCE INTENSITIES (of the Axial Fluctuating velocity component) AS FUNCTIONS OF r/r_o for VARIOUS x/d

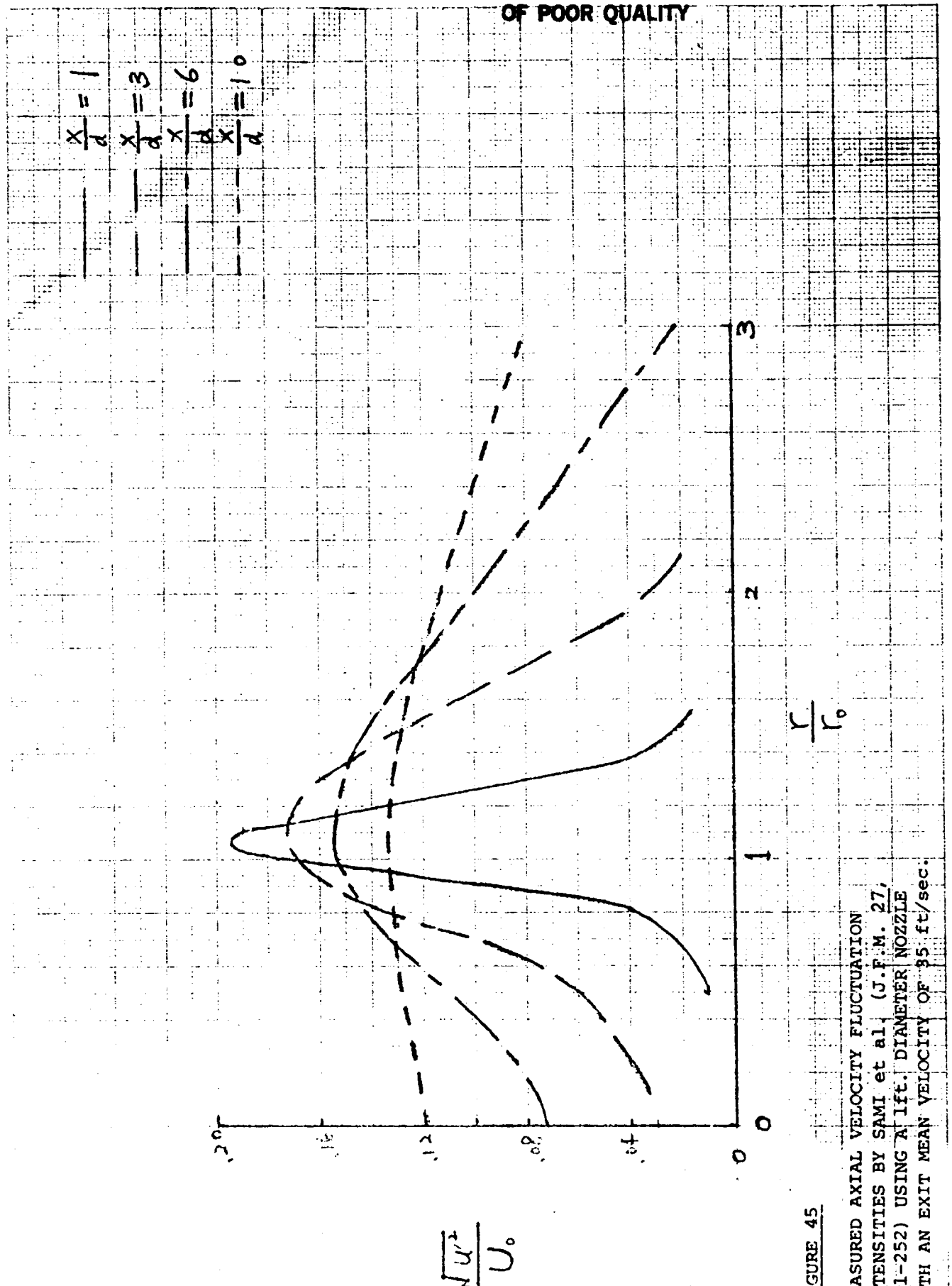

FIGURE 45

MEASURED AXIAL VELOCITY FLUCTUATION INTENSITIES BY SAMI et al, (J.F.M. 27, 231-252) USING A 1ft. DIAMETER NOZZLE WITH AN EXIT MEAN VELOCITY OF 35 ft/sec.